

See discussions, stats, and author profiles for this publication at: <https://www.researchgate.net/publication/235108904>

Fundamental Mechanism of Atomization

Article · July 1989

CITATIONS

0

READS

74

1 author:



Sung P. Lin

Clarkson University

121 PUBLICATIONS 3,474 CITATIONS

[SEE PROFILE](#)

(2)

FUNDAMENTAL MECHANISM OF ATOMIZATOIN
FINAL REPORT

AD-A213 859

S.P. Lin

July 1989

U.S. ARMY RESEARCH OFFICE

DAAL03-86-K-0072

CLARKSON UNIVERSITY

APPROVED FOR PUBLIC RELEASE

DISTRIBUTION UNLIMITED

S FIC
ELECTE
OCT 25 1989
D Cb D

89 70 93 1 170

UNCLASSIFIED

SECURITY CLASSIFICATION OF THIS PAGE (When Data Entered)

REPORT DOCUMENTATION PAGE		READ INSTRUCTIONS BEFORE COMPLETING FORM
1. REPORT NUMBER <i>ARO 23297.10-EG</i>	2. GOVT ACCESSION NO. <i>N/A</i>	3. RECIPIENT'S CATALOG NUMBER <i>N/A</i>
4. TITLE (and Subtitle) Fundamental Mechanism of Atomization		5. TYPE OF REPORT & PERIOD COVERED Final Report May 1986 - August 15, 1989
		6. PERFORMING ORG. REPORT NUMBER
7. AUTHOR(s) <i>S.P. Lin</i>		8. CONTRACT OR GRANT NUMBER(s) <i>DAAL03-86-K-0072</i>
9. PERFORMING ORGANIZATION NAME AND ADDRESS <i>Clarkson University Potsdam, N.Y. 13676</i>		10. PROGRAM ELEMENT, PROJECT, TASK AREA & WORK UNIT NUMBERS
11. CONTROLLING OFFICE NAME AND ADDRESS <i>U. S. Army Research Office Post Office Box 12211 Research Triangle Park, NC 27709</i>		12. REPORT DATE <i>July 31, 1989</i>
14. MONITORING AGENCY NAME & ADDRESS(if different from Controlling Office)		13. NUMBER OF PAGES <i>89</i>
		15. SECURITY CLASS. (of this report) <i>Unclassified</i>
		15a. DECLASSIFICATION/DOWNGRADING SCHEDULE
16. DISTRIBUTION STATEMENT (of this Report) <i>Approved for public release; distribution unlimited.</i>		
17. DISTRIBUTION STATEMENT (of the abstract entered in Block 20, if different from Report) <i>NA</i>		
18. SUPPLEMENTARY NOTES <i>The view, opinions, and/or findings contained in this report are those of the author(s) and should not be construed as an official Department of the Army position, policy, or decision, unless so designated by other documentation.</i>		
19. KEY WORDS (Continue on reverse side if necessary and identify by block number) <i>Atomization, Jet, Fuel Spray, JET fuels. JD</i>		
20. ABSTRACT (Continue on reverse side if necessary and identify by block number) <i>The physical mechanism of atomization is investigated. A problem statement is given in Section 1. The research has resulted in 6 papers. They are given in the Appendices. The results of the research are summarized in Section 2. The list of publications and the personnel involved in the research are given respectively in Section 3 and 4. The relevant bibliographies on the subject are listed in the reference section of each journal article.</i>		

UNCLASSIFIED

SECURITY CLASSIFICATION OF THIS PAGE(When Data Entered)

UNCLASSIFIED

SECURITY CLASSIFICATION OF THIS PAGE(When Data Entered)

FUNDAMENTAL MECHANISM OF ATOMIZATOIN
FINAL REPORT

S.P. Lin

July 1989

U.S. ARMY RESEARCH OFFICE

DAAL03-86-K-0072

CLARKSON UNIVERSITY

APPROVED FOR PUBLIC RELEASE

DISTRIBUTION UNLIMITED

Accesision For	
NTIS CRA&I <input checked="" type="checkbox"/>	
DTIC TAB <input type="checkbox"/>	
Unclassified <input type="checkbox"/>	
Distribution:	
By _____	
Date _____ / _____ / _____	
Availabilty Codes	
Dist	1. Legal and/or Special
A-1	

FOREWORD

The project 23297-EG "Fundamental Mechanism of Atomization" was under the directorship of Dr. David Mann of the Engineering Science Division of the Army Research Office. The period of this project is from 15 May 1986 to 30 July 1989. The grant number of this project is DAAL03-86-K-0072. During the project period, the writer also received an instrumentation grant from the Department of Defense-University Research Instrumentation Program for FY87.

TABLE OF CONTENTS

	Page
1. Problem Statement	1
2. Summary of Research Results	1
3. List of Publications	2
4. Participating Personnel	2
5. Bibliography	2
6. Appendices	3
A. Atomization of a liquid jet	
B. Absolute instability of a liquid jet in a gas	
C. Breakup of a swirling liquid jet	
D. Mechanism of the breakup of liquid jets	
E. Energy budget in atomization	
F. Navier-Stokes flow for the initial stage of atomization	
G. Toward monodispersed atomization	
H. Letters of confirmation	

1. Problem Statement

The physical mechanism of atomization is investigated. Atomization is a process of breaking up liquid jets or sheets into droplets of sizes much smaller than the jet or sheet thickness. The process is encountered in diesel engine fuel sprays and many other important industrial processes. The fundamental knowledge of the mechanism involved in the process is essential for a rational design of efficient devices which use atomization processes.

2. Summary of Research Results

A rigorous nonlinear theory of atomization is constructed. The governing equations are the Navier-Stokes equations. The boundary conditions involve the unknown boundary of an atomizing jet. This is the source of mathematical difficulty which has prevented many previous workers from obtaining rigorous theoretical results. Our new approach overcame this difficulty. The relevant system of partial differential equations are reduced to a system of nonlinear ordinary differential equations by use of the Galerkin projection and a finite difference discretization respectively in the radial and axial direction of the jet. The reduced system is solved with given initial conditions for various flow parameters. The theoretical results reveal that the origin of atomization is the pressure fluctuation at the core of the liquid jet. This pressure fluctuation resonates subharmonically the interfacial capillary waves which led to the formation of ligaments which are the precursors of the atomized droplets. These processes are depicted in detail in Appendices F and E. It is also shown that an external forcing with a frequency much smaller than the capillary wave frequency cannot alter the most popular droplet size but tends to increase the number of larger droplets which scale with the wave packet length shown in figure 5 of Appendix F. However, when the external forcing frequency is fine-tuned to the capillary wave frequency (Appendices A and D), a narrow size distribution of droplets may be obtained. This idea led to an exploratory project of monodispersed droplet generation which is now funded by NSF. The demonstration of this idea by use of the Aerometric Particle Analyzer, which was purchased with the aid of a DoD instrumentation grant, is given in Appendix G. The results given in Appendix B imply that in order to avoid extinction of combustion processes in internal combustion engines, one must operate at a Weber number much smaller than the critical Weber number which is a function of the Reynolds number and the gas to liquid density ratio. The results in Appendix C show that adding swirl to liquid jets may result in a wider size distribution which may be exploited for more efficient use of fuel.

3. List of Publications

Six journal publications have resulted from this research project. The following three articles have already appeared.

- a. Lin, S.P. and Kang, D.J., "Atomization of a Liquid Jet," *Physics of Fluids*, **30**, 2000, 1987.
- b. Lin, S.P. and Lian, Z.W., "Absolute Instability of a Liquid Jet in Gas," *Physics of Fluids*, **A, 1**, 490, 1989.
- c. Kang, D.J. and Lin, S.P., "Breakup of a Swirling Liquid Jet," *Int. J. of Eng. Fluid Mech.*, **2**, 47, 1989.

The following three papers have been accepted for publication. The letters of acceptance are given in Appendix H.

- d. Lin, S.P. and Lian, Z.W., "Mechanisms of the Breakup of Liquid Jets," AIAA Journal.
- e. Lin, S.P. and Creighton, B.J., "Energy Budget in Atomization," *Aerosol Science and Technology*.
- f. Kang, D.J. and Lin, S.P., "Navier-Stokes Flow for the Initial Stage of Atomization," *J. Colloid and Interface Science*.

4. Participating Personnel

The following individuals have participated in the undertaking of this project.

- a. Dr. S.P. Lin, Professor, Principal Investigator
- b. Dr. D.J. Kang, Graduate Research Assistant. Completed Ph.D. degree 29 September 1988. Thesis title: "Fundamental Mechanism of Liquid Jet Atomization".
- c. Mr. B.J. Creighton, Graduate Research Assistant. Completed M.S. degree. May 1989. Thesis title: "Energy Balance in Breakup of Liquid Jets and Curtains"
- d. Mr. D. Woods, Graduate Research Assistant.
- e. Mr. E. Ibrahim, Graduate Research Assistant.
- f. Mr. Z.W. Lian, Graduate Teaching Assistant.

5. Bibliographies

Relevant bibliographies are cited in the references sections of the articles included in the appendices.

6. Appendices

Atomization of a liquid jet

S. P. Lin and D. J. Kang

Department of Mechanical and Industrial Engineering, Clarkson University, Potsdam, New York 13676

(Received 30 October 1986; accepted 3 April 1987)

Generation of ripples by wind blowing over a viscous fluid was investigated by G. I. Taylor [*The Scientific Papers of G. I. Taylor* (Cambridge U. P., Cambridge, 1963), Vol. 3, No. 25] with linear stability analysis. Taylor considered the case of temporally growing disturbances in a low density gas and applied his results to explain the process of atomization of a liquid jet injected into a low density gas. Taylor's analysis is extended here to investigate the case of a spatially growing disturbance in a dense gas. Taylor showed that temporal disturbances of wavelength shorter than the capillary length are stable. The same is found for the spatial disturbances. Each type of disturbance possesses a maximum growth rate with a specific wavelength and frequency. The atomized droplet size corresponding to the maximum growth rate is shown in both theories to decrease inversely as the square of the jet velocity. While the maximum growth rate increases as the square root of the gas-to-liquid density ratio when A^2 exceeds 1 for the temporal disturbances, the same dependence on the density ratio does not hold for spatial disturbances until A^2 exceeds 100, where A^2 is a flow parameter representing the ratio of surface force to the viscous force. When A^2 exceeds 100 the growth rates predicted by two theories deviate significantly only at air pressure higher than 10 atm for most liquids at room temperature. However, for all parameters, the spray angle changes along the jet axis according to the spatial theory, but remains constant according to the temporal theory. It is shown that the viscous force in the liquid may be increased relative to the surface tension force to the point that no discernable spray angle may be observed in practice. Then an intact jet without atomization may result. It is shown that the onset of atomization is primarily caused by the pressure fluctuation which resonates the capillary waves. The results on the interfacial amplification rate suggest that a sufficiently large initial amplitude at the nozzle exit is essential for the onset of atomization.

I. INTRODUCTION

The process of breaking up a liquid jet into droplets of diameters much smaller than the jet diameter is called jet atomization. This process has various applications, including the liquid fuel injection in internal combustion engines, spray coatings of protective materials on surfaces, and sprays of pesticides. Despite its practical importance, the mechanism of atomization is not yet well understood. A concise review of works in this area is included in a recent article by Reitz and Bracco.¹ In contrast to the breakup of ink jets at small Reynolds numbers into droplets of sizes comparable with the jet diameter,²⁻⁴ the atomization of jets takes place at large Reynolds numbers. While the seeds of atomization may be already sowed in the flow inside of the jet nozzle, the atomization site is actually at the liquid-gas interface. The most cultivated theory of atomization postulates that the aerodynamic interaction at the liquid-gas interface creates the unstable wave growth which eventually leads to the formation of small droplets.^{1,5-8} One of the most serious weaknesses in the existing aerodynamic interaction theory is that the disturbance is assumed to be temporally growing everywhere in the jet at the same rate, while the observed disturbance actually grows spatially along the jet. The importance of this distinction has already been demonstrated by Keller *et al.*⁹ for the case of low speed jet breakup. Moreover, it is known^{10,11} that flow which is stable with respect to temporally varying disturbances may actually become unstable with respect to spatially varying disturbance. In this work,

we investigate the stability of a liquid jet issued into an ambient gas with respect to spatially growing disturbances. The results are used to explain the existence of the intact length, the formation of spray angle, and some aspects of the mechanism of atomization.

II. STABILITY ANALYSIS

Consider the axisymmetric liquid jet injected into an unbounded gas, as shown in Fig. 1. The liquid is an incompressible Newtonian fluid and the gas is assumed to be an incompressible inviscid fluid. The governing differential equations are

$$\partial_t \mathbf{V}_i + \mathbf{V}_i \cdot \nabla \mathbf{V}_i = -(\frac{1}{\rho_i}) \nabla P_i + \nu_i \nabla^2 \mathbf{V}_i, \quad (1)$$

$$\nabla \cdot \mathbf{V}_i = 0 \quad (i = 1, 2),$$

where $i = 1$ denotes the liquid and $i = 2$ denotes the gas, \mathbf{V} is the velocity, ∇ is the gradient operator, ρ is the density, t is the time, P is the pressure, ν is the kinematic viscosity, and ∇^2 is the Laplacian. Note that in order to focus our attention of the aerodynamic interaction between liquid and gas, we have neglected the gravitational force in (1). Note that $\nu_2 = 0$. The boundary conditions at the interface $r = \eta$ are the kinematic boundary condition¹²

$$\mathbf{V}_{ir} = \partial_r \eta + \mathbf{V}_{ir} \partial_r \eta \quad (2)$$

and the dynamic boundary condition¹²

$$\tau_1 \cdot \mathbf{n} - \tau_2 \cdot \mathbf{n} - \sigma \mathbf{n} (1/R_1 + 1/R_2) = 0, \quad (3)$$

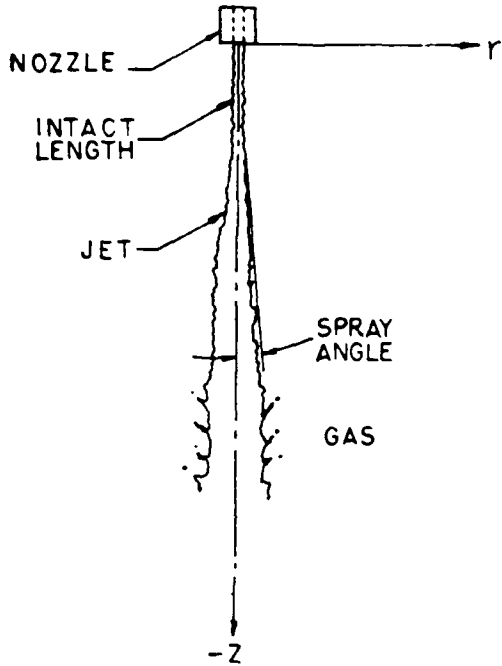


FIG. 1. Definition sketch.

\mathbf{n} is a unit normal vector pointing into the liquid; the subscripts r and z denote, respectively, the r and z components of the velocity in the cylindrical coordinate system; τ is the stress tensor; σ is the constant surface tension; and R_1 and R_2 are the principal radii of the interface. Here R_1 and R_2 are positive if measured from the center of curvature in the direction of \mathbf{n} . There exists a basic state

$$\mathbf{V}_1 = -\mathbf{i}_z U_0, \quad \mathbf{V}_2 = 0, \quad \bar{P}_1 - \bar{P}_2 = \sigma/a, \quad \eta = a, \quad (4)$$

which satisfies (1) and its boundary conditions. This basic state represents an axisymmetric cylindrical jet of radius a injecting at a constant speed U_0 into an unbounded quiescent gas. To investigate the manner in which this basic state becomes unstable, we perturb the flow with disturbances

$$\mathbf{V}_i = \bar{\mathbf{V}}_i + \mathbf{V}'_i, \quad P_i = \bar{P}_i + P'_i, \quad \eta = a + \zeta. \quad (5)$$

Substituting (5) into (1), canceling out the basic state part, neglecting the nonlinear term, and expressing the resulting equations in terms of the dimensionless variables

$$(x, y, d) = (r, z, \zeta)/a, \quad \tau = t/(a/U_0), \\ \mathbf{v}_i = (u_i, v_i) = (V'_u, V'_z)/U_0, \quad p_i = P_i/\rho_1 U_0^2,$$

we have

$$(\partial_r - \delta_{11} \partial_z) \mathbf{v}_i = -(\rho_1/\rho_2) \nabla p_i + (\delta_{11}/R) \nabla^2 \mathbf{v}_i, \quad (6)$$

$$\nabla \cdot \mathbf{v}_i = 0, \quad (7)$$

where $R \equiv$ Reynolds number $\equiv U_0 a / v_1$, and δ_{11} is the Kronecker delta function. Here we consider only the axisymmetric disturbance. The corresponding linearized boundary conditions are

$$v_i = d_r - \delta_{11} d_z, \quad v_1 = v_2, \quad u_{1x} + v_{1y} = 0,$$

$$p_2 - p_1 + 2v_{1x}/R - \text{We}(d + d_{yy}) = 0,$$

where subscripts x and y denote partial differentiation and We is the Weber number defined by

$$\text{We} = \sigma/\rho_1 U_0^2 a.$$

Equation (7) is the necessary and sufficient condition for the existence of a streamfunction ψ such that

$$xv_i = \psi_{yy}, \quad xu_i = -\psi_{xx},$$

where subscripts x and y denote partial differentiation. Taking the curl of (6) and expressing the resulting equation in terms of ψ , we have

$$[\partial_r - (\delta_{11} E^2/R)] E^2 \psi_{yy} - \delta_{11} E^2 \psi_{yy} = 0, \quad (8)$$

where

$$E^2 = \partial_{xx} - (1/x) \partial_x + \partial_{yy}. \quad (9)$$

The corresponding linearized boundary conditions at $x = 1$ in terms of ψ are

$$\psi_{yy}/x = d_r - d_z, \quad (10)$$

$$-(\psi_{1x}/x)_x + (\psi_{1y}/x)_y = 0, \quad (11)$$

$$p_2 - p_1 + 2(\psi_{1yx}/x - \psi_{1y}/x^2)/R - \text{We}(d + d_{yy}) = 0. \quad (12)$$

The normal mode solutions of (8) are given by

$$d = C_0 \exp(iky + \omega\tau), \\ \psi_1 = x \exp(iky + \omega\tau) \{C_1 J_1(\lambda x) + C_2 K_1(\lambda x) \\ + [C_3 J_1(kx) + C_4 K_1(kx)]\}, \quad (13)$$

$$\psi_2 = -ix \exp(iky + \omega\tau) [B_1 J_1(kx) - B_2 K_1(kx)],$$

where k is the wavenumber, ω is the wave frequency, K 's and J 's denote the modified Bessel functions, C 's and B 's are the integration constants, and

$$\bar{\lambda}^2 = R(\omega - ik), \quad \lambda^2 = k^2 + \bar{\lambda}^2.$$

For boundness of the solution, we require $B_1 = C_2 = C_4 = 0$. Upon substitution of the above general solution into (6), we find

$$p_1 = -i(\omega - ik) C_3 J_0(kx) \exp(iky + \omega\tau), \quad (14) \\ p_2 = -(\rho_2/\rho_1) \omega B_1 K_0(kx) \exp(iky + \omega\tau).$$

The constants C_0 , C_1 , C_3 , and B_1 in the solution can be determined by use of the four boundary conditions (10)–(12). The nontrivial solution of this system exists if the determinant of the coefficient matrix vanishes. This condition leads to the following characteristic equation:

$$(\omega - ik)^2 + \frac{2k^2}{R} \left(\frac{I_1'(k)}{I_0(k)} - \frac{2kl}{\lambda^2 + k^2} \frac{I_1(k) I_2(\lambda)}{I_0(k) I_1(\lambda)} \right) \\ \times (\omega - ik) + \omega^2 \frac{\rho_2}{\rho_1} \frac{\lambda^2 - k^2}{\lambda + k^2} \frac{K_0(k) I_1(k)}{K_1(k) I_0(k)} \\ - W_c \cdot k (1 - k^2) \frac{\lambda^2 - k^2}{\lambda^2 + k^2} \frac{I_1(k)}{I_0(k)} = 0. \quad (15)$$

In the limiting case of $\rho_2 = \mu_1 = 0$, (15) reduces to

$$(\omega - ik)^2 = \text{We} k (1 - k^2) I_1(k) / I_0(k),$$

which is the axisymmetric result of Rayleigh for a low speed inviscid jet modified by Keller *et al.*⁹ in their study of spatially growing long wave disturbances.

Jet atomization produces droplets of diameters much smaller than the jet diameter. The appropriate limiting case is therefore $k = Ka$ as $a \rightarrow \infty$, where K is the dimensional wavenumber. In the limit of $k \rightarrow \infty$, (15) reduces to

$$[R(\omega - ik) + 2k^2]^2 + R^2 \text{We} k^3 + (\rho_2/\rho_1)R^2 \omega^2 - 4k^3 \lambda = 0.$$

In dimensional form this equation becomes

$$\rho_1(\Omega - iKU_0 + 2\nu_1 K^2)^2 + \sigma K^3 + \rho_2 \Omega^2 - 4K^3 \rho_1 \nu_1 (K^2 \nu_1^2 + \Omega - iKU_0)^{1/2} = 0, \quad (16)$$

where $\Omega = \omega(U_0/a)$. Equation (16) reduces to the characteristic equation obtained by Taylor¹³ in his study of the generation of ripples by wind over a viscous fluid when $(\Omega - iKU_0)$ is replaced by his complex wave frequency α . This is as it should be since in the limit of $a \rightarrow \infty$ the present problem is identical to Taylor's problem if we view the temporally growing ripples in a reference frame traveling at a velocity $-i_z U_0$. While the complex wave frequency viewed in an inertial frame is Ω , the frequency viewed in a frame moving with $-i_z U_0$ is $\Omega - iKU_0$. In fact, the same transformation reduces (15) to Eq. (5) of Reitz and Bracco.¹ However, it should be emphasized that this argument is valid only for temporally growing disturbances in which K is real. For such disturbances, the imaginary part of Ω , i.e., Ω_i , gives the wave frequency and the real part Ω_r , gives the amplification rate. It is seen from (13) that the growth rate of temporally growing disturbances is the same everywhere regardless of the values of x and y . This is contrary to what is observed in an atomizing jet in which the disturbance grows spatially from a zero displacement at the nozzle exit. For such disturbances, $K = K_r + iK_i$ is complex, but $\Omega = i\Omega_i$ is purely imaginary. Here K_i is the spatial growth rate of a disturbance of wavenumber K , with a frequency Ω_i . Hence, the spatially growing wave phenomenon is not invariant with respect to a Galilean transformation. Consequently, to be consistent with the observation that the interfacial displacement is zero for all time at the nozzle exit, we must place the origin of the coordinate at the nozzle exit, as shown in Fig. 1.

In the limiting case of $a \rightarrow \infty$, a can no longer be used as the characteristic length. Let the characteristic length and time be, respectively,

$$a = \sigma/\rho_2 U_0^2, \quad a^2/\nu_1$$

and define the dimensionless frequency and wavenumber, respectively, by

$$i\omega_r = \Omega/(a^2), \quad k = Ka.$$

Then (16) can be rewritten in a dimensionless form as

$$[i(\omega_r - kA/\rho) + 2k^2]^2 + A^2 k^3 - \rho^2 \omega_r^2 - 4k^3 [k^2 + i(\omega_r - kA/\rho)]^{1/2} = 0, \quad (17)$$

where

$$\rho = (\rho_2/\rho_1)^{1/2}, \quad A = (\sigma/\rho_1 \nu_1 U_0)/\rho.$$

For a given set of parameters ρ , A , (17) can be solved for the spatial amplification rate k_r and the oscillation frequency ω_r , for various values of k_i .

It is easily verified that (17) has the following two neutral solutions for all A and ρ :

$$(a) \quad k_r = k_i = \omega_r = 0$$

and

$$(b) \quad k_r = 1, \quad k_i = 0, \quad \omega_r = A/\rho.$$

Near the first neutral solution (a), we have

$$k_r = 0 + \Delta k_r, \quad k_i = 0 + \Delta k_i, \quad \omega_r = 0 + \Delta \omega_r.$$

Substituting these into (17) and retaining only the first-order terms, we have

$$i[\Delta \omega_r - A(\Delta k_r + i\Delta k_i)/\rho] = \rho \Delta \omega_r.$$

The solution of this equation gives

$$\Delta k_r = \rho \Delta \omega_r/A, \quad \Delta k_i = \rho^2 \Delta \omega_r/A = \rho \Delta k_r.$$

Thus as k_r increases from 0 to Δk_r , k_r becomes positive. It follows from (13) and the fact that the jet is issued into the negative y direction that the unperturbed surface implied by (a) is unstable. Similarly, substituting the expansion near the point specified by (b), i.e.,

$$k_r = 1 + \Delta k_r, \quad k_i = \Delta k_i, \quad \omega_r = (A/\rho) + \Delta \omega_r,$$

into (17) and retaining only the first-order terms we have from the real and imaginary parts,

$$-2\Delta \omega_r + 2\Delta k_r/\rho^2 + 3A\Delta k_r/\rho = 0,$$

$$2\Delta \omega_r + 3A^2 \Delta k_r - 2A\Delta k_r/\rho = 0.$$

Elimination of $\Delta \omega_r$ between these two equations gives

$$\Delta k_r = -[A/\rho/(2\rho^{-2} + 3A^2)]\Delta k_i.$$

Thus as k_r decreases from $k_r > 1$ to $k_r < 1$, k_r changes from negative to positive at $k_r = 1$ for all A and ρ . Hence, the jet is always unstable for all relevant parameters, for all $k_r < 1$. The growth rate k_r of the disturbance increases as k_r is decreased from 1 and then decreases again near $k_r = 0$ to zero. Thus there is a maximum growth rate k_{rm} between $k_r = 1$ and $k_r = 0$ for any given A and ρ . In order to determine the wavelength corresponding to the maximum spatial growth rate, we must solve (17) numerically. To do this, we solve simultaneously the following two equations obtained from the real and imaginary parts of (17):

$$\begin{aligned} & [2(1 - Z^2) + BZ]^2 - (Y - B + 4Z)^2 \\ & + (A^2/k_r)(1 - 3Z^2) \\ & - \rho^2 Y^2 - 4(1 - 3Z^2)F^{1/2} \cos(\phi/2) \\ & + 4(3Z - Z^3)F^{1/2} \sin(\phi/2) = 0, \end{aligned} \quad (18)$$

$$\begin{aligned} & 2[2(1 - Z^2) + BZ](Y - B + 4Z) \\ & + (A^2/k_r)(3Z - Z^3) \\ & - 4(1 - 3Z^2)F^{1/2} \sin(\phi/2) \\ & - 4(3Z - Z^3)F^{1/2} \cos(\phi/2) = 0, \end{aligned} \quad (19)$$

where

$$Z = k_r/k_i, \quad Y = \omega_r/k_r^2, \quad B = A/\rho k_r,$$

$$F = \{(1 - Z^2) + BZ\}^2 + (2Z + Y - B)^2\}^{1/2},$$

$$\phi = \tan^{-1}[(2Z + Y - B)/(1 - Z^2 + BZ)].$$

Equations (18) and (19) have been solved numerically by use of the modified Newton method¹⁴ to find k_r and ω_r , corresponding to a given set of k_i for various values of A and ρ .

Before giving the numerical results, some comments on the relation between the temporal and spatial disturbances will be made. Assuming the wave frequency to be negligibly small, Taylor¹³ obtained numerically the following dimensional temporal growth rate from a characteristic equation related to (16), which was explained earlier:

$$\Omega = (2/a) U_0 \rho (Sk^2/A), \quad (20)$$

where S is the real part of Taylor's dimensionless complex frequency. To compare with our results, we normalize the above frequency with our characteristic time, i.e., a^2/v_1 and obtain

$$\omega_r(T) = (a^2/v_1)\Omega = (a^2/v_1)(2U_0\rho/a)(Sk^2/A) = 2Sk^2, \quad (21)$$

where T in parentheses denotes the temporal case. According to the Gaster theorem¹⁵ we have the following relations, near $k_1 = 0$, between the temporal and spatial disturbances:

$$\omega_r = \omega_r(T), \quad (22)$$

$$k_r = \frac{\omega_r(T)}{\partial\omega_r(T)/\partial k}, \quad (23)$$

Note that when $\omega_r - kA/\rho$ in (17) is replaced by ω_{r0} and k is regarded as real, (17) is reduced to the characteristic equation of Taylor.¹³ Thus $\omega_r(T)$ in the present inertial frame is related to that in Taylor's¹³ moving frame by

$$\omega_r(T) = \omega_{r0}(T) + k_r A/\rho. \quad (24)$$

Taylor¹³ assumed $\omega_{r0}(T)$ to be negligibly small. In order to better compare Taylor's¹³ results with ours, we solved his characteristic equation without putting $\omega_{r0}(T) = 0$. Our numerical results confirm Gaster's theory (22) and (23) for small amplification rates $k_r \rightarrow 0$, but not for general values of k_r .

Equation (21) was also used by various authors^{1,7,8} to estimate the spray angle. It was assumed that the spray angle can be estimated by the ratio of the disturbance amplitude increase to the distance traveled by the fluid particle in the same time period τ . It then follows from (13) and (21) that to first-order approximation, the tangent of the spray angle β is

$$\begin{aligned} \tan \beta &= \frac{d(a\zeta)}{d\tau} \frac{\tau}{U_0 \tau} \\ &= \frac{2\pi}{M} a \frac{[(d/d\tau) \exp(\Omega\tau)]_{\tau=0}}{\tau_0} = \frac{4\pi\rho}{M} \frac{(Sk^2)_m}{A}, \end{aligned} \quad (25)$$

where $4\pi/M$ is the dimensionless wave amplitude remaining arbitrary within the framework of linear theory and $(Sk^2)_m/A$ is the maximum temporal amplification rate obtained by Taylor.¹³ The above argument (25) assumed that the disturbance travels with the jet velocity and that the absolute instability and convective instability are simply related by the Gaster¹⁵ theorem. The first assumption is valid only when $\rho \ll 1$. Since the second assumption is valid only for a spatially homogeneous system near $k_1 = 0$, it results in a less realistic modeling of a jet breakup. Note that β in (25) is independent of y . The spatially growing disturbance theory does not require these assumptions. The tangent of the spray angle in our coordinate system is simply

$$\tan \beta = -\frac{d}{dy}(\text{envelope of } d) = C_0 k_1 \exp(-k_1 y).$$

For small k_1 , we have approximately

$$\tan \beta = C_0 k_1 (1 - k_1 y + \dots). \quad (26)$$

Hence, unless $C_0 k_1$ is sufficiently large, a discernable β may not appear until some distance downstream in the $-y$ direction. This may be the origin of the so-called intact length over which the jet does not appear to diverge.

III. RESULTS

The relation between the spatial amplification rate and the wavelength is shown in Fig. 2 for the case of $A^2 = 100$ and three different values of ρ . If the gas is air at room temperature, then for most liquids $P = 800\rho^2$ atm. Therefore, the approximate pressure of the three curves in Fig. 2 are 1, 10, and 200 atm. It is seen that waves of length shorter than the capillary length $\sigma/\rho_2 U_0^2$ are stable ($k_1 < 0$); otherwise, they are unstable. Moreover, there is a prominent maximum amplification rate for each ρ at a "resonant" frequency with a critical wavelength of the same order as the capillary length. As ρ is increased, both the amplification rate and the critical wavelength are increased, signifying the increased inertial effect of air on the unstable capillary waves. The amplification curves for other values of A and ρ behave similarly.

The numerical results of the spatial amplification rate for $A^2 = 100$ and $\rho^2 = 0.24$ are given in Table I. The corresponding results for the temporal case are given in Table II, where the calculation is based on Taylor's characteristic equation obtained in a frame moving with the wind speed. However, $\omega_{r0}(T)$ was not assumed to be negligible compared with $\omega_r(T)$. It is seen from Table II that $\omega_{r0}(T)$ is indeed not negligible for this particular relatively large value of $\rho^2 = 0.24$. For much smaller values of ρ , of order 0.01, our numerical results (which are not presented) showed that Taylor's¹³ assumption was correct. The air pressure corresponding to this density ratio for most liquids is approximately 10 atm at room temperature. It is easily verified from

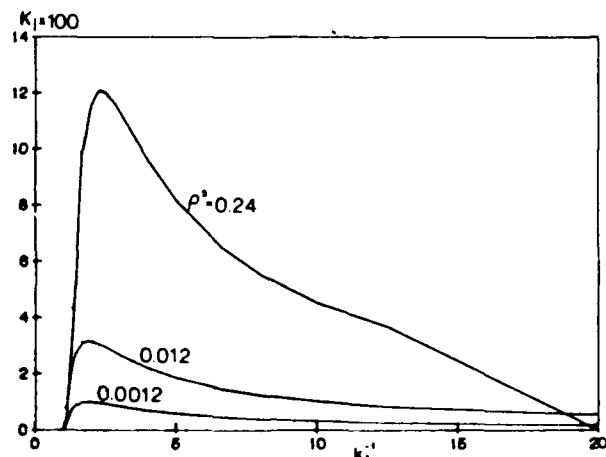


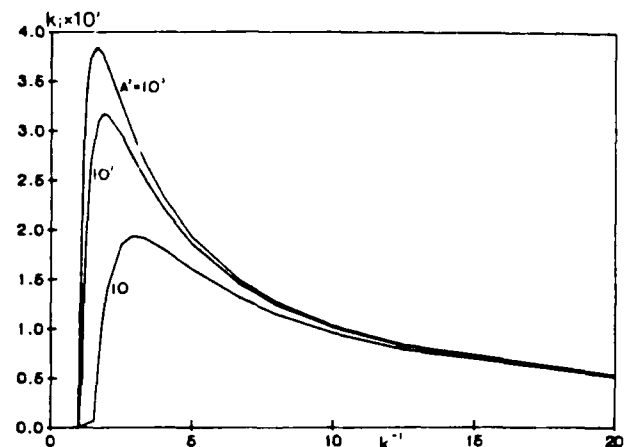
FIG. 2. Variation of growth rate with wavenumber; $A^2 = 100$.

TABLE I. Spatial growth rate; $A^2 = 100$, $\rho^2 = 0.24$.

k_x	k_y	ω_i
0	0	0
0.05	0.02357	0.99857
0.10	0.04518	1.95328
0.20	0.08165	3.73680
0.30	0.10748	5.37111
0.40	0.12006	6.89835
0.44	0.12062	7.49629
0.43	0.12075	7.34676
0.42	0.12069	7.19739
0.45	0.12032	7.64612
0.50	0.11585	8.40641
0.60	0.09872	10.10190
0.70	0.05143	12.39342
0.80	0.02315	15.20356
0.90	0.00504	18.09900
1.0	0.0	20.41241
1.1	-0.00589	23.40714
1.2	-0.01169	26.39107

Tables I and II that the Gaster theorem (22) and (23) together with (24), is indeed valid for smaller values of k . However, for the values of k , near the maximum value, the agreement is not as good as expected since the Gaster theorem is intended for $k \rightarrow 0$. The disagreement becomes worse as ρ is further increased. Note that the wave frequencies in Table II are all negative, but they are all positive in Table I. Since the phase of the waves is given by $i(ky + \omega\tau)$, the spatially growing waves travel downstream in a fixed frame and the temporally growing disturbances propagate upstream in a frame moving with the jet. However, these two waves have the same wave speed ω/k , given by (22) and (24) in the inertial frame for those waves having $k \rightarrow 0$. This can be easily verified using the data in Tables I and II. Figure 3 shows that the spatial amplification rate increases with A for a given value of $\rho^2 = 0.012$.

In order to compare the spray angle predicted by (26) with experiments, we plot k_x/ρ against A^2 in Fig. 4. Note that k_x is a function of ρ and A . Some of the spray angles measured by Reitz and Bracco¹ with their number IX nozzle are given in Fig. 4 and Table III together with other relevant

FIG. 3. Variation of growth rate with wavenumber; $\rho^2 = 0.012$.

data. The numbers in the first column of Table III are the test series numbers used by Reitz and Bracco. The corresponding values of ρ , A ; the intact length x , divided by the jet diameter d_0 ; and $\tan \beta$ are calculated from Reitz and Bracco's Table I.¹ For each set of ρ and A , the maximum values of k , and the corresponding values of k_x , are numerically determined from the solution of (18) and (19). The characteristic length a for each test is also given in Table III. These values are given in the last four columns. Note that the different values of the characteristic length a in Table III are all, indeed, several orders smaller than the nozzle diameter $d_0 = 0.034$ cm. Therefore, the asymptotic analysis for $Kd_0 \rightarrow \infty$ used here is relevant. The curve of the spray angle against A^2 obtained from the temporal theory is also given in Fig. 4 for comparison. Note that the spatial theory predicts larger spray angles than that predicted by the temporal theory when $A^2 > 100$, but the converse is true when $A^2 < 100$. Note that this curve becomes almost horizontal when $A^2 > 100$. However, it descends almost parabolically to $k_x/\rho = 0$ near $A^2 \rightarrow 0$. This shows that the spray angle increases as constant $\times \rho$ at large values of A , but as $k_x \sim A\rho = \sigma/\rho_1 v_1 U_0$ for A smaller than 10. The theoretical

TABLE II. Temporal growth rate; $A^2 = 100$, $\rho^2 = 0.24$.

k_x^{-1}	$2Spk_x^2/A$	$\omega_0(T)$
5.84816	0.05730	-11.07224
4.62384	0.06874	-8.62971
2.93428	0.09104	-5.21004
2.46530	0.09673	-4.22662
2.23597	0.09798	-3.72915
2.01183	0.09683	-3.22202
1.90228	0.09477	-2.96150
1.68932	0.08583	-2.41080
1.48289	0.06683	-1.76242
1.32974	0.04433	-1.14328
1.22169	0.02626	-0.64746
1.15417	0.01471	-0.34078

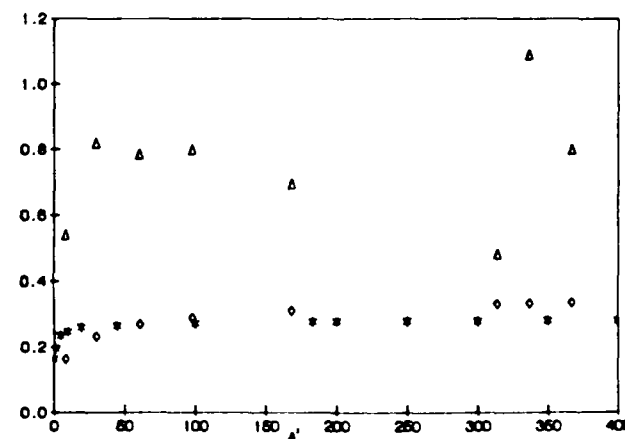
FIG. 4. Variation of spray angles with A^2 and ρ ; Δ , experiments $\rho^{-1} \tan \beta$, \diamond , spatial theory $\rho^{-1} k_x$, $*$, temporal theory $(Sk_x)_m/A$.

TABLE III. Experimental and theoretical data.

Series	$\rho^2 \times 10^3$	A^2	$\tan \beta$	x_i/d_0	C_0	$a \times 10^4 \text{ cm}$	k_i	k_{rm}	ω_i	$a \times 10^4 \text{ cm}$
22	1.3	337	0.0393	2.0	3.29	15.2	0.01194	0.60	305.13466	4.628
23	1.3	314	0.0175	20.0	1.47	6.3	0.01188	0.59	289.63321	4.309
24	7.7	168	0.0612	15.0	2.26	5.2	0.02713	0.56	82.18053	2.308
25	8.6	367	0.0743	1.5	2.40	1.2	0.03075	0.59	120.95915	5.036
26	12.9	61	0.0892	0.2	2.93	2.5	0.03045	0.50	34.03625	8.393
28	17.2	98	0.1051	0	2.79	0	0.03766	0.52	38.71045	1.350
30	25.8	30	0.1317	0	3.54	0	0.03716	0.43	14.38934	0.410
34	20.4	2.2×10^{-4}	0	>40	0	0	0.00097	0.07	0.00726	0.613
35	51.5	8.5	0.1228	0	3.33	0	0.03684	0.30359	3.76927	0.117

curve in Fig. 3 was obtained with $C_0 = 1$. The predicted spray angles are uniformly smaller than the experimental values. If we wish to bring up the calculated spray angle to agree with the measured ones, we may use the values C_0 given in Table III. This amounts to assigning different values for the height of the first wave rest at the nozzle exit. Although the dimensional wave amplitude $C_0 a$ of these initial waves are all smaller than 10^{-4} cm , which is two orders of magnitude smaller than the nozzle diameter $d_0 = 0.034 \text{ cm}$, and different initial wave amplitudes $C_0 a$ for the same nozzle may be actually encountered in experiments, we are actually not entitled to speak of any finite wave amplitude in the linear theory. Thus although the practice of adjusting the value of C_0 for the best fit with experiments may be physically reasonable, it remains problematic. The matter can be settled only by use of nonlinear theory.

When the viscosity of the jet liquid is increased with all other physical quantities fixed, A decreases. It follows from the results in Fig. 4 that the amplification rate and the spray angle decrease as the viscosity is increased. The effect is very dramatic when A is very small. The series number 34 test in Table III is a case in point. In this test the liquid is glycerol. Because of its high viscosity the amplification rate k_i is only 0.00097. It follows from (14) that even if the largest initial amplitude of $C_0 = 3.54$ in Table III is used, the distance required to amplify the spray angle to a mere 1° is

$$y = 10\ 022.9.$$

The dimensional distance is therefore

$$ya = 0.6144 \text{ cm},$$

which is 18 diam of the nozzle. This length is of the same order of magnitude as the intact length of 40 diam reported by Reitz and Bracco.¹ Recall that the jet was predicted to be unstable if it is subjected to disturbances of all wavelength, including those shorter than a . It appears that the intact portion of jet is actually also unstable, but the amplification rate of the disturbance is so small that the spray angle has not yet been amplified to the observable value. This view can be further supported by the observation that capillary waves are usually observed in the intact portion of the jet. These waves seem to be the unstable infinitesimal waves which are amplified to small finite amplitudes. These finite amplitude waves owe their existence to nonlinear stability, which is possible because of the small amplification rate. The nonlinear stability will reduce the spray angle predicted by linear

theory and lengthen the intact portion of jets. Thus the linear theory probably will give a better prediction of the spray angle when nonlinear stability is absent. Note that the jets start to diverge to the extent consistent with the measured values given in Table III only when the initial amplitudes are increased to the values $C_0 a$. Nonlinear stability is usually not attainable when the disturbance amplitude exceeds a threshold amplitude. Thus $C_0 a$ can be identified as the threshold amplitude a_c . It appears that in order for the atomization to start right at the nozzle exit, the disturbance amplitude must exceed a_c there. The a_c are listed in Table III for each test series. It cannot be overemphasized that the above arguments on nonlinear effects remain conjectural until a full nonlinear analysis is carried out to confirm them. These arguments are offered here merely as targets for future nonlinear analysis.

IV. DISCUSSION

Taylor's¹³ major results are as follows. A high speed jet is unstable with respect to temporally growing disturbance of wavelength longer than the capillary length $\sigma/\rho_2 U_0^2$. There exists at a specific wavelength a maximum growth rate among unstable disturbances for any given A and $\rho \ll 1$. The growth rate increases as A is increased with fixed $\rho \ll 1$. The droplet size corresponding to the maximum growth rate decreases inversely as the square of the jet velocity. These findings were based on linear stability analysis of temporally growing disturbances in a gas of low density such that $\rho \ll 1$. The present analysis of spatially growing disturbances for arbitrary values of ρ led to the same conclusion on the qualitative effects of the various physical factors mentioned above. Significant quantitative differences on the maximum growth rate were found when ρ exceeds 0.01 for A in the range of 10–1000. This value of ρ corresponds to air pressure of approximately 10 atm for most liquids at room temperature. The present theory predicts that the maximum growth rate increases and peaks sharply about a given wavelength as ρ is increased with A fixed. The practical implication is that a larger gas-to-liquid density ratio may be more favorable for atomizing a liquid jet into a narrower size distribution about the most popular drop size corresponding to the maximum growth rate. Numerical results reveal that the maximum growth rates for a wide range of ρ and A all occur at a dimensionless wavelength of order 1, with little deviation. The length was normalized with the capillary length $\sigma/\rho_2 U_0^2$.

Hence, finer droplets may be produced by use of smaller surface tension with given ρ_2 and U_0 . While the temporal theory yields a constant spray angle independent of the axial location, the spatial theory gives a spray angle which varies along the jet axis. Moreover, the former theory predicts that the spray angles increases with ρ when A exceeds 1, but the latter theory does not give the same dependence on the density ratio until A^2 exceeds 100. This can be seen easily from Fig. 4. When $A^2 \ll 1$, both theories give $\beta = B\sigma/\rho_1 v_1 U_0$. However, the constant of proportionality B is much larger for the temporal case. The present theory showed that β also depends on the initial wave amplitude $C_0 a$. A large value of $C_0 a$ will give a better head start for the development of the spray angle, which increases in the direction of the jet flow according to (26). Thus if a nozzle is so designed that the initial wave amplitude is exceedingly small and if the atomization takes place at a very small A (which may occur, for example, when the viscosity is exceedingly large), then a measurable spray angle may not be observed until a finite intact length is exceeded.

It was assumed that the viscosity of the gas phase is of secondary importance in jet atomization. This assumption must be evaluated. The viscosity of the gas and the high speed of the jet result in the formation of a thin boundary layer at the interface. The boundary layer may become unstable and generate shear waves¹⁶ (Tollmein-Schlichting waves). The shear waves may extract kinetic energy from the main flow and amplify. Thus in addition to the air pressure fluctuation, the shear waves may cause the onset of atomization. The size of droplets caused by shear waves may be estimated with the critical shear wavelength at the onset of the boundary layer instability. Assume that the velocity distribution in the gas boundary layer flow is given by the Blasius¹⁶ profile. Then the critical Reynolds number and the critical wavelength are given, respectively, by¹⁷

$$R_c = U_0 \delta / \nu_2 = 400, \quad \lambda_c = (2\pi/0.3)(\delta/0.32),$$

where δ is the momentum thickness.¹⁶ Using the maximum jet velocity of $U_0 = 1.11 \times 10^4$ cm/sec which occurs in test 23 in Table III, and using the air kinematic viscosity of 0.15 cm²/sec at room temperature, we find from the definition of the critical Reynolds number,

$$\delta = 5.5 \times 10^{-3} \text{ cm.}$$

It follows from the expression of λ_c that

$$\lambda_c = 3.5 \times 10^{-1} \text{ cm.}$$

This length is at least two orders of magnitude larger than the capillary length. On the other hand, most of the droplets from atomizing jets possess diameters smaller than or comparable to the capillary length.^{7,8} It appears that the viscosity effect of the gas is of secondary importance in an atomizing jet.

Without having rigorously analyzed the effects of gas viscosity and the finite amplitude nonlinear effects, we can offer only the following tentative statement concerning the mechanism of jet atomization. The onset of atomization is due to the pressure fluctuation which causes the resonant oscillation of capillary waves at the liquid-gas interface. The initial disturbance amplitude at the nozzle exit must be larger than a threshold amplitude for the atomization to take place immediately at the nozzle exit. Otherwise, atomization will occur only downstream of a finite intact length. Atomization may also be caused by shear waves, which tend to produce droplets of size several orders larger than the capillary length.

ACKNOWLEDGMENT

This work was supported in part by Grant No. DAAL03-86-K-0072 of the Army Research Office.

- ¹R. D. Reitz and F. V. Bracco, *Phys. Fluids* **25**, 1730 (1982).
- ²D. B. Bogay, *Annu. Rev. Fluid Mech.* **11**, 207 (1979).
- ³M. J. McCarthy and N. A. Molloy, *Chem. Eng. J.* **7**, 1 (1974).
- ⁴A. M. Sterling and C. A. Sleicher, *J. Fluid Mech.* **68**, 477 (1975).
- ⁵R. A. Castlman, *NACA Rep. No. 440*, 1932.
- ⁶V. G. Levich, *Physicochemical Hydrodynamics* (Prentice-Hall, Englewood Cliffs, NJ, 1962).
- ⁷W. E. Ranze, *Can. J. Chem. Eng.* **36**, 175 (1958).
- ⁸W. E. Ranze and W. M. Dreier, *Ind. Eng. Chem. Fund.* **3**, 53 (1964).
- ⁹J. B. Keller, S. I. Rubinow, and Y. O. Tu, *Phys. Fluids* **16**, 2052 (1973).
- ¹⁰S. P. Lin, *J. Fluid Mech.* **104**, 111 (1981).
- ¹¹S. P. Lin, *J. Fluid Mech.* **112**, 443 (1981).
- ¹²S. P. Lin and C. Y. Wang, in *Encyclopedia of Fluid Mechanics*, edited by N. P. Cherevinskoff (Gulf, Houston, TX, 1986), Chap. 28.
- ¹³G. I. Taylor, *The Scientific Papers of G. I. Taylor* (Cambridge U. P., Cambridge, 1963), Vol. 3, No. 25.
- ¹⁴C. F. Gerald, *Applied Numerical Analysis* (Addison-Wesley, Reading, MA, 1980), pp. 122-128.
- ¹⁵M. Gaster, *J. Fluid Mech.* **14**, 222 (1962).
- ¹⁶H. Schlichting, *Boundary-Layer Theory* (McGraw-Hill, New York, 1968), pp. 447-463.
- ¹⁷P. G. Drazin and W. H. Reid, *Hydrodynamic Stability* (Cambridge U. P., Cambridge, 1981), pp. 224-229.

Absolute instability of a liquid jet in a gas

S. P. Lin and Z. W. Lian

Department of Mechanical and Industrial Engineering, Clarkson University, Potsdam, New York 13676

(Received 15 September 1988; accepted 8 November 1988)

The effect of the ambient gas density on the onset of absolute instability in a viscous liquid jet is examined. The critical Weber number, above which the instability is convective and below which the instability is absolute, is determined as a function of Reynolds number and the density ratio of gas to liquid. It is shown that the gas density has the effect of raising the critical Weber number. It also raises the cutoff wavenumber below which disturbances are spatially amplified and above which they are damped.

I. INTRODUCTION

The capillary instability of an infinitely long jet with respect to temporally growing disturbances was analyzed by Rayleigh.¹ Keller² *et al.* examined the capillary instability of a semi-infinite jet with respect to spatially growing disturbances. They found that the temporal and spatial disturbances are analytically related if the Weber number is sufficiently large. For sufficiently small Weber numbers, Leib and Goldstein³ found that the state of convective instability obtained by Keller *et al.* actually cannot be reached by a given initial disturbance in the sense of Briggs⁴ and Bers.⁵ Leib and Goldstein demonstrated, for the first time, the existence of the absolute instability in an inviscid jet. Recently, they⁶ determined from Chandrasekhar's⁷ dispersion equation the critical Weber number below which a viscous jet is absolutely unstable as a function of Reynolds number. They also found that the cutoff wavenumber, above which the disturbance is spatially damped, is one independent of the Weber number.

Here, we examine the effect of the ambient gas density on the absolute instability discovered by Leib and Goldstein. It is shown that the gas density has the effect of enlarging the domain of absolute instability in the Reynolds–Weber number space. Moreover, it raises the cutoff wavenumber below which the jet is convectively unstable, and also raises the amplification rate of the spatially growing disturbances when the absolute instability is absent.

II. FORMULATION

Consider a circular cylindrical jet of an incompressible viscous Newtonian liquid issued from a nozzle into an unbounded inviscid gas. The governing dynamic equations of motion in the liquid and the gas phases are, respectively, the Navier–Stokes and Euler equations. The boundary conditions are the vanishing of the net force per unit area of the interface, and the equality of radial fluid velocity in each phase with the total time rate of change of the interfacial position. A uniform velocity distribution U in a circular jet of radius r_0 in a quiescent gas is an exact solution to this set of differential equations in the absence of gravity. This exact mathematical solution representing a possible basic state is physically unstable. The stability analysis of this basic state with respect to any Fourier component of the disturbances

of the form $C_0 \exp(\omega\tau + iky)$ led to the characteristic equation (1) when viewed in a reference frame with its origin fixed at the nozzle exit,^{8,9}

$$(\omega - ik)^2 + \frac{2k^2}{R} \left(\frac{I'_1(k)}{I_0(k)} - \frac{2kl}{\lambda^2 + k^2} \frac{I_1(k)I'_1(\lambda)}{I_0(k)I_1(\lambda)} \right) \\ \times (\omega - ik) + \omega^2 \frac{\rho_2}{\rho_1} \frac{\lambda^2 - k^2}{\lambda^2 + k^2} \frac{K_0(k)I_1(k)}{K_1(k)I_0(k)} \\ - \frac{1}{\beta} k(1 - k^2) \frac{\lambda^2 - k^2}{\lambda^2 + k^2} \frac{I_1(k)}{I_0(k)} = 0, \quad (1)$$

where C_0 is the wave amplitude, ω is the complex wave frequency (the real part of which gives the exponential temporal growth rate, and imaginary part of which gives the wave frequency of disturbances), k is the complex wavenumber [the real part of which is equal to $2\pi r_0$ /(wavelength) and the imaginary part of which gives the spatial amplification rate], τ is time normalized with r_0/U , y is the axial distance measured in the unit of r_0 in the opposite direction of the jet flow, I and K are, respectively, the modified Bessel functions of the first and second kind, their subscripts denote the order of the functions, and λ is defined by

$$\lambda^2 = k^2 + R(\omega - ik).$$

The three independent flow parameters in (1) are Reynolds number R , Weber number β , and the density ratio Q defined, respectively, by

$$R = Ur_0/\nu_1, \quad \beta = \rho_1 U^2 r_0/\sigma, \quad Q = \rho_2/\rho_1,$$

where ν is kinematic viscosity, ρ is density, σ is surface tension, and the subscripts 1 and 2 denote, respectively, the liquid and gas phases. Note that the above nondimensionalization of time implies that the dimensional frequency is given by $\omega U/r_0$.

III. RESULTS

Figure 1 shows the loci of the two characteristic roots obtained when a given set of flow parameters as the temporal growth rate ω , varies for a number of values of the wave frequency ω_1 . As the ω_1 is reduced from a finite positive value to zero, these loci approach toward two different branches of amplification curves $\omega_1 = 0$ for the spatially growing disturbances. Note that $k > 0$ gives the spatial instability because the y axis is chosen to be negative in the flow direction. It can be seen that two of the loci with

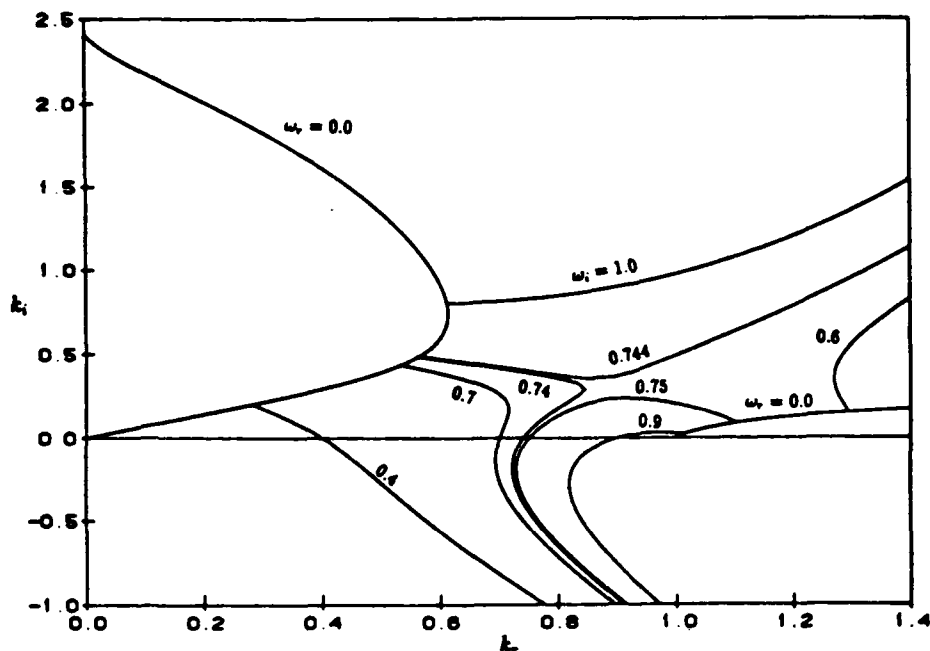


FIG. 1. Absolute instability: $Q = 0.0013$, $\beta = 1$, $R = 20$.

$0.74 < \omega_r < 0.75$ will intersect in the upper half-plane at a saddle point.⁵ A similar situation has already been shown by Leib and Goldstein³ for the case of negligible gas density. As the Weber number is increased, with the values of Q and R given in Fig. 1 being fixed, this saddle point moves closer to the pure spatial amplification curve for disturbances with a "group velocity" in the direction of jet flow. Note that the amplification curve, which does not originate from $k_r = 0$, is for the disturbances with upstream propagating "group velocity." Following Leib and Goldstein, the minimum value of β for which the saddle point of Eq. (1) lies in the upper half-plane is defined as the critical Weber number. Figure 2

gives the dependence of the critical Weber number on R for three values of Q . Here, $Q = 0.0013$ corresponds to the air to water density ratio in one atmospheric pressure in room temperature. The curve $Q = 0$ was obtained by Leib and Goldstein. In the parameter range below the curves, the jet is absolutely unstable. The dashed line indicates the inviscid limit obtained by Leib and Goldstein for the case of $Q = 0$. It is seen that the gas density has the effect of enlarging the domain of absolute instability for the β - R plane.

Above these curves, the jet is convectively unstable. Figures 3 and 4 give a few typical amplification curves for convectively unstable disturbances. Leib and Goldstein showed

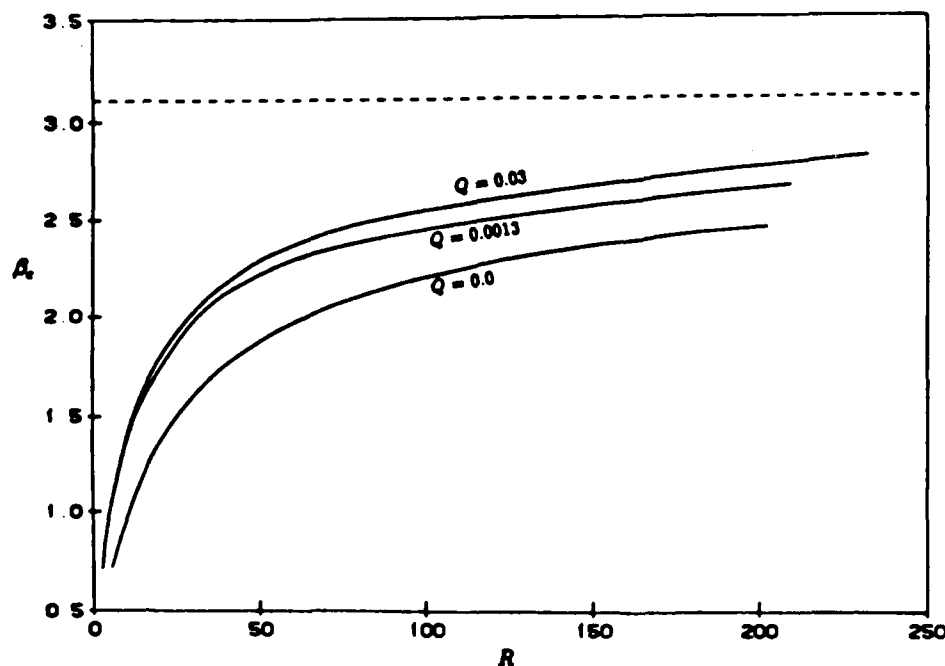


FIG. 2. The critical Weber number versus Reynolds number.

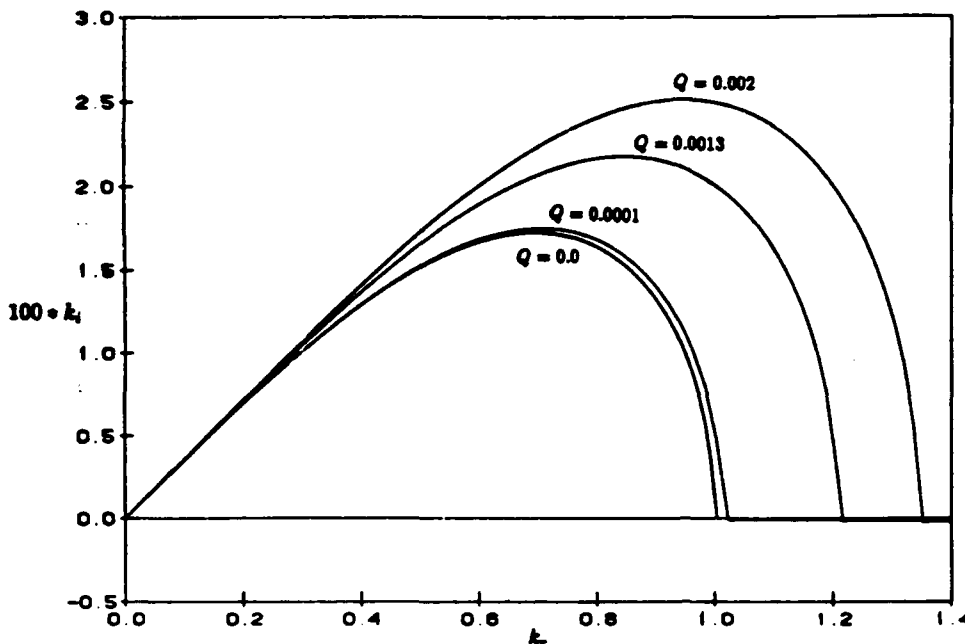


FIG. 3. The growth rate for convectively unstable disturbances: $R = 20\,000, \beta = 400$.

that the cutoff wavenumber, above which the disturbance is damped, is one independent of β for the case of $Q = 0$. It is seen from Figs. 3 and 4 that the gas density tends to raise the cutoff wavenumber very significantly. This has a practical significance of producing smaller droplets by use of larger ambient gas density.⁹

It is very hard to resist the temptation of speculating that the absolute instability may correspond to the dripping mode of the jet instability. When a saddle point of the eigenvalue exists at a certain frequency and there exist both upstream and downstream propagating convectively unstable branches, a disturbance with this certain frequency may be alternatively attracted toward these two branches as time

evolves. The simultaneous spatial and temporal growth alternating in the upstream and downstream directions with a regular frequency casually observed in a dripping jet seems to correspond to the mathematical picture of absolute instability. This speculation is even more tempting when one realizes that the absolute instability is predicted only for a small Weber number, which is the ratio of the inertial force to the surface tension force. However, the argument remains speculative, since the dripping phenomenon involves a highly nonlinear finite amplitude of disturbances that cannot be accounted for in the present linear theory. However, Leib and Goldstein³ suggested that the absolutely unstable disturbance may grow nonlinearly by the mechanism of direct res-

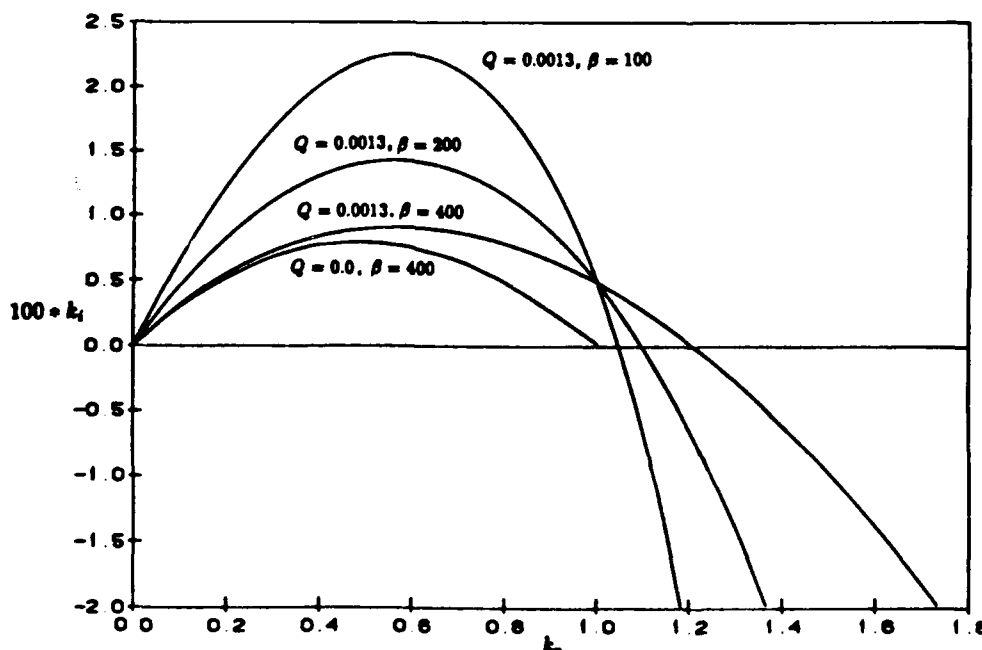


FIG. 4. The growth rate for convectively unstable disturbances, $R = 34.5$.

onance advanced by Akylas and Benney.¹⁰ The physical significance of the absolute instability in the context of nonlinear theories remains to be explored.

ACKNOWLEDGMENTS

This work was supported in part by Grant No. DAALO-386-K-0072 of the Army Research Office, Grant No. MSM-8817372 of the National Science Foundation, and a New York State Science and Technology Grant. The computation was carried out with the Cornell National Supercomputer Facility, which is funded in part by the NSF, the State of New York and the IBM Corporation.

- ¹Lord W. S. Rayleigh, Proc. London Math. Soc. **10**, 4 (1879).
- ²J. B. Keller, S. I. Rubinow, and Y. O. Tu, Phys. Fluids **16**, 2052 (1973).
- ³S. J. Leib and M. E. Goldstein, J. Fluid Mech. **168**, 479 (1986).
- ⁴R. J. Briggs, *Electron Stream Interaction with Plasmas* (MIT Press, Cambridge, MA, 1964).
- ⁵A. Bers, *Handbook of Plasma Physics* (North-Holland, Amsterdam, 1983), Vol. 1, pp. 452-516.
- ⁶S. J. Leib and M. E. Goldstein, Phys. Fluids **29**, 952 (1986).
- ⁷S. Chandrasekhar, *Hydrodynamic and Hydromagnetic Stability* (Dover, New York, 1961).
- ⁸A. M. Sterling and C. A. Sleicher, J. Fluid Mech. **68**, 477 (1975).
- ⁹S. P. Lin and D. J. Kang, Phys. Fluids **30**, 2000 (1987).
- ¹⁰T. R. Akylas and D. J. Benney, Stud. Appl. Math. **63**, 209 (1980).

APPENDIX C

Breakup of a Swirling Liquid Jet

D. J. Kang and S. P. Lin
Department of Mechanical and Industrial Engineering
Clarkson University
Potsdam, New York, USA

ABSTRACT

The phenomenon of breakup of a liquid jet is of fundamental concern in various industrial processes, including atomization, jet cutting, and ink jet printing. The breakup is due to flow instability in the jet and the ambient gas. Lin and Kang [5] recently showed that the fundamental mechanism of atomization is the resonance of capillary waves by the pressure fluctuation in the flows of liquid and gas. Their conclusion was based on the stability analysis of a liquid jet with respect to spatially growing axisymmetric disturbances. Their work is here extended to include the nonaxisymmetric disturbances and the effect of swirl frequently encountered in practice. The stability of an inviscid jet issued into an unbounded ambient gas with respect to spatially growing disturbances is analyzed. The numerical results demonstrate that the breakup process may be enhanced by use of a larger gas-to-liquid density ratio and/or a larger swirl imparted on the jet. This enhancement is at the expense of a broader size distribution of the droplets. On the other hand, suppression of swirl and smaller gas-to-liquid density ratio produce longer intact lengths of the jets, which is desirable in the applications of jet cutting and ink printing. A smaller ratio of inertial force to surface tension force is shown to favor smaller droplets. The present findings, together with those found previously by the authors, are offered as a partial guide for a rational design of the processes involving jet breakup phenomena.

INTRODUCTION

The phenomenon of disintegration of a liquid jet is relevant to the processes encountered in ink jet printing, atomization, and other industrial practices. The possibility of refining the jet breakup process for produc-

ing monodispersive ceramic particles is currently being explored. While the ink jet may breakup into droplets of size comparable to the jet diameter at low jet speeds, an atomization jet usually produces droplets of sizes much smaller than their diameter at relatively high speed. Atomization processes have been used widely in liquid fuel injection, spray coating, pesticide application, and aerosol generation. A concise review of the works related to atomization was given by Reitz and Bracco [10]. The works on the jet breakup at low speed are reviewed by many authors, including Bogy [1] and McCarthy and Molloy [7].

The classical work of Rayleigh on the breakup of a liquid jet is well known. He studied the stability of an inviscid jet issued into a vacuum with respect to temporally growing disturbances. Keller et al. [2] pointed out that the observed disturbances in a liquid jet actually grow spatially rather than temporally everywhere at the same rate. In particular, the disturbance at the nozzle exit is incapable of growing due to the no-slip condition. They found that the spatially growing disturbances in an inviscid jet injecting into vacuum behave differently from the temporal ones only when the jet speed is sufficiently low. They found that the jet is more unstable with respect to axisymmetric disturbances than to nonaxisymmetric ones. Taylor [11] investigated the formation of temporally growing ripples at the interface between a viscous jet of infinitely large radius and an inviscid gas of small density. His work was recently extended by Lin and Kang [5], who investigated the spatially growing disturbances in a viscous jet emanating from a nozzle into an inviscid dense gas. They obtained numerical results only for the limiting case of infinitely large radius. As a consequence, they could treat only axisymmetric disturbances. Their results differ significantly from that of Taylor's when the gas-to-liquid density ratio is large. Their theory allows them to give a better explanation of the spray angle and the existence of intact lengths. They compared their theoretical results with the experimental results of Reitz and Bracco, and came to the conclusion that the basic cause of atomization is the pressure fluctuation at the liquid-air interface which resonates the capillary waves. The viscous force plays only a secondary role in comparison with the inertial force associated with the gas-to-liquid density ratio. Because of this we will, in this work, neglect the viscosities, but take up the effects of the disturbance nonaxisymmetry and the inertial force associated with the swirl often encountered in practice. This same problem was considered by Ponstein [9] except he treated the disturbances as temporally growing. The significant difference between the temporal and spatial disturbances has already been demonstrated by Keller et al. [2], Lin [3], and Lin and Kang [5]. The findings in the present work are offered as a partial guide for a rational design of relevant industrial processes and devices.

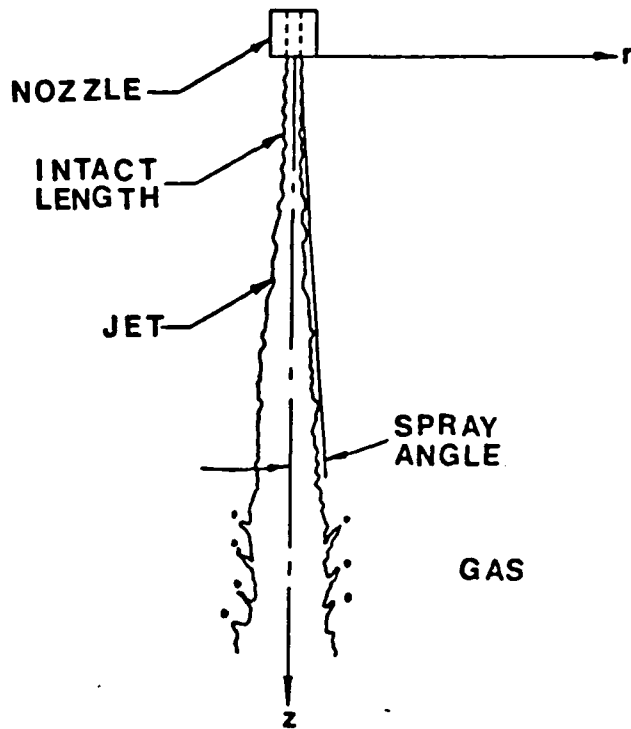


Figure 1. Definition sketch.

STABILITY ANALYSIS

Consider an inviscid liquid jet issued into an unbounded inviscid gas, as shown in Figure 1. The governing equations of motion of the fluids are:

$$\rho_i(\partial_t \underline{V}_i + \underline{V}_i \cdot \nabla \underline{V}_i) = -\nabla P_i \quad (1)$$

$$\nabla \cdot \underline{V}_i = 0 \quad (i = 1, 2)$$

where $i = 1$ denotes the liquid and $i = 2$ denotes the gas
 \underline{V} = velocity
 ∇ = gradient operator
 ρ = density
 t = time
 P = pressure

The boundary conditions at the interface $r = \eta$ [6] are the kinematic condition:

$$\underline{V}_i = \partial_r \eta + \underline{V}_i \cdot \nabla \eta \quad (2)$$

and the dynamic boundary condition:

$$P_1 \underline{n} - P_2 \underline{n} = \sigma (1/R_1 + 1/R_2) \quad (3)$$

where \underline{n} = a unit normal vector pointing into the liquid
 subscripts r and z = r - and z -components of the velocity in the
 cylindrical coordinate system
 σ = constant surface tension
 R_1 and R_2 = principal radii of the interface

R_1 and R_2 are positive if measured from the center of curvature in the direction of \underline{n} .

There exists a basic state:

$$\begin{aligned} \underline{\underline{V}}_i &= \underline{i}_z W_o + \underline{i}_\theta (\Gamma/r), \quad \underline{\underline{V}}_2 = 0, \quad \eta = a \\ \overline{P}_1 - \overline{P}_2 &= (\rho_1 \Gamma^2/2)(a^{-2} - r^{-2}) + \sigma/a \end{aligned} \quad (4)$$

where \underline{i} = a unit vector
 subscripts θ and z = the directions in the cylindrical coordinates (r, θ, z)
 Γ = constant circulation
 a = radius of the jet
 \overline{P}_2 = constant pressure in the ambient gas

It is easily verified that Equation 4 satisfies Equation 1 and its boundary conditions (Equations 2 and 3) with $R_1 = a$ and $R_2 \rightarrow \infty$. Hence the basic state Equation 4 represents an axisymmetric cylindrical jet of radius a swirling with the tangential velocity Γ/r and injecting at a constant speed W_o into an unbounded quiescent gas of constant pressure \overline{P}_2 .

To investigate the manner in which this basic state becomes unstable, we perturb the flow with disturbances:

$$\underline{V}_i = \underline{\underline{V}}_i + \underline{V}'_i, \quad P_i = \overline{P}_i + P'_i, \quad \eta = a + \xi \quad (5)$$

Substituting Equation 5 into Equation 1, canceling out the basic state part, neglecting the nonlinear terms, and expressing the resulting equations in terms of the dimensionless variables:

$$(x, \theta, y, d) = (r, \theta a, z, \xi)/a, \tau = t/(a/W_0)$$

$$\underline{v}_i^* = (u_i^*, v_i^*, w_i^*) = (V_{ix}', V_{iy}', V_{iz}')/W_0$$

$$p_i^* = P_i'/\rho_1 W_0^2$$

we have:

$$\partial_r \underline{v}_i^* + \delta_{ii} [\partial_\theta \underline{v}_i^* + (\gamma/x^2) \partial_z \underline{v}_i^*] = -(\rho_1/\rho_0) \nabla p^* \quad (6)$$

$$\nabla \cdot \underline{v}_i^* = 0 \quad (7)$$

where δ_{ii} = Kronecker delta function

$\gamma = (\Gamma/aW_0)$ = swirl number

In order to obtain the corresponding linearized boundary conditions, we need explicit expressions of \underline{n} and the mean curvature $K = (1/R_1) + (1/R_2)$. These can be obtained from the equation of free surface:

$$f = r - \eta(\theta, z, t) = 0$$

and,

$$\underline{n} = -\nabla f / |\nabla f|$$

$$K = -\nabla \cdot \underline{n}$$

It follows that:

$$-\underline{n} = (1, -\eta_\theta/a, -\eta_z)$$

$$K = a^{-1} - a^{-2}\eta - a^{-2}\eta_{\theta\theta} - \eta_{zz} \quad (8)$$

In arriving at Equation 8, we expanded r about a in the Taylor series and neglected all nonlinear terms of η and its derivatives. Substituting Equation 8 into Equations 2 and 3, subtracting out the basic state, and expressing the resulting linearized boundary conditions in terms of the dimensionless variables, we have, at $x = 1$:

$$u_i^* = \partial_r d + \delta_{ii}(\partial_\theta d + \gamma \partial_z d) \quad (9)$$

$$\bar{p}_{1x}d + p_1^* - p_2^* = -(\sigma/\rho_1 W_0^2 a)(1 + \partial_{\theta\theta} + \partial_{zz})d \quad (10)$$

where $\bar{p}_1 = \bar{P}_1/\rho_1 W_0^2$, and thus $\bar{p}_{11} = \gamma^2$. The first term in Equation 10 arises from the Taylor series expansion about $x = 1$ of the liquid pressure in the basic state.

The normal mode solution of Equations 6 and 7 with the boundary conditions of Equations 9 and 10 can be written as:

$$\begin{bmatrix} u_i^* \\ v_i^* \\ w_i^* \\ p_i^* \\ d \end{bmatrix} = \begin{bmatrix} u_i(x) \\ v_i(x) \\ w_i(x) \\ p_i(x) \\ \delta \end{bmatrix} \cdot \exp[i(ky + n\theta - \omega\tau)] \quad (11)$$

where k = wave number in the y -direction

n = wave number in the θ -direction

ω = wave frequency

For temporally growing disturbances, k is real but ω is complex. If the imaginary part of ω is positive, then the disturbance will grow exponentially with time everywhere in space at the same rate. Therefore, treating the disturbances in a liquid jet emanating from a nozzle as temporally growing is not totally realistic, since the disturbance at the nozzle exit never grows due to the no-slip condition. Hence, we model the disturbance as a spatially growing disturbance for which $k = k_r + ik_i$ is complex but ω is real. It is seen from Equation 11 that if the imaginary part of k is negative, the disturbance will grow in the positive y -direction, i.e., in the direction of the jet flow. Substituting Equation 11 into Equation 6, and eliminating the pressure terms between the x - and θ -components and between the θ - and y -components of the resulting equations, we have, respectively:

$$v_i = n w_i / kx \text{ and } u_i = -i(xv_i)' / n \quad (12)$$

where primes denote differentiation with x .

Substituting Equation 11 with the expressions of u_i and v_i in terms of w_i , given by Equation 12, into Equation 7, we have:

$$w_i'' + w_i'/x - (k^2 + n^2/x^2)w_i = 0 \quad (13)$$

which is the modified Bessel equation of order n . The solution of Equation 13 is:

$$w_i = A_i I_n(kx) + B_i K_n(kx) \quad (14)$$

where I_n and K_n are the modified Bessel functions of order n of the first and second kind, respectively, and A_i and B_i are constants to be determined from the boundary conditions. It follows from Equation 12 that:

$$\begin{aligned} v_i &= (n/kx)[A_i I_n(kx) + B_i K_n(kx)] \\ u_i &= -(i/k)[A_i I_n'(kx) + B_i K_n'(kx)] \end{aligned} \quad (15)$$

The corresponding pressure disturbance amplitudes can be found from the y -component of Equation 6 with the aid of Equation 11 as:

$$p_i = (\rho_1/\rho_2)(\omega - \delta_{ii}n\gamma/x^2 - \delta_{ii}k)[A_i I_n(kx) + B_i K_n(kx)]/k \quad (16)$$

The interfacial displacement amplitude δ can be obtained from Equations 9, 11, and 15:

$$\delta = [A_i I_n'(k) + B_i K_n'(k)]/[\omega - \delta_{ii}(k + n\gamma)] \quad (17)$$

For the boundness of the obtained solutions, we must demand:

$$A_2 = B_1 = 0$$

It follows from Equation 17 that:

$$A_i I_n'(k)/(\omega - k - n\gamma) - B_i K_n'(k)/\omega = 0 \quad (18)$$

The remaining boundary condition to be satisfied is the dynamic one, i.e., Equation 10, which demands:

$$\begin{aligned} &\{k(1 - n^2 - k^2 + \beta\gamma^2)I_n'(k)/(\omega - k - n\gamma) \\ &+ \beta(\omega - k - n\gamma)I_n(k)\}A_1 - \rho \beta\omega K_n(k)B_2 = 0 \end{aligned} \quad (19)$$

where $\rho = \rho_2/\rho_1$
 $\beta = \rho_1 W_o^2 a/\sigma$

Equations 18 and 19 constitute a system of homogeneous equations in two unknowns A_1 and B_2 . This system has a nontrivial solution only if the

determinant of its coefficient matrix vanishes. This requirement yields the characteristic equation:

$$(\omega - n\gamma - k)^2 + \beta\rho\omega^2 a_1 + k[(n^2 - 1 + k^2)/\beta - \gamma^2]a_2 = 0 \quad (20)$$

where $a_1 = -I_n'(k)K_n(k)/I_n(k)K_n'(k)$
 $a_2 = -I_n'(k)/I_n(k)$

For the case of a jet without swirl emanated into vacuum, we have $\rho = \gamma = 0$, and Equation 20 reduces to:

$$(\omega - k)^2 = (k/\beta)(n^2 + k^2 - 1)I_n'(k)/I_n(k)$$

which is the result of Rayleigh modified by Keller et al. [2]. Equation 20 corresponds to (2.31) of Ponstein [9] when his basic state gas velocity is neglected. Here we consider the spatially growing disturbances, rather than the temporally growing disturbances considered by Ponstein.

Before solving Equation 20 numerically for the complex k for various given values of ρ , β , γ , n , and ω , we obtain the asymptotic values of k , in the limits of $k_r \rightarrow 0$ and $k_r \rightarrow \infty$. By use of the series representations of $I_n(k)$ and $K_n(k)$ near $k = 0$, it can be shown that in this limit, Equation 20 reduces to:

$$ak^2 + bk + c = 0 \quad (21)$$

where $a = n(1 - 2n - 3n^2) + n\beta(2n + 2 + \gamma^2) + \beta\rho\omega^2$
 $b = -4n(n + 1)(\omega - n\gamma)\beta$
 $c = 2n(n + 1)[\beta(\omega - n\gamma)^2 - n(n^2 - 1 - \beta\gamma^2) + \rho\beta\omega^2]$

Hence:

$$k = [-b \pm \sqrt{b^2 - 4ac}]/2a$$

It follows that at $k_r = 0$, $b = 0$, which requires:

$$\omega = n\gamma$$

Moreover, at $k_r = 0$, k_i is given by, if it exists:

$$k_i = \pm (c/a)^{1/2}$$

The negative root gives rise to spatial instability. Note that $k_r = 0$, $k_i = 0$ is a solution for all ρ , β , and γ , when $n = 0$. The eigen-frequency corresponding to $k_r = k_i = 0$ is zero. As $n \rightarrow \infty$, both the denominator and the

numerator, excluding the term $\beta\rho\omega^2$, are negative. It follows that the gas density is destabilizing for highly nonaxisymmetric disturbances as $n \rightarrow \infty$. Similarly, by use of the asymptotic expansions of $I_n(k)$ and $K_n(k)$ for large k , we reduce Equation 20 to:

$$k^3 - \beta k^2 + Ak - \beta C = 0 \quad (22)$$

where $A = 2\beta(\omega - n\gamma) + n^2 - 1 - \beta\gamma^2$
 $C = (\omega - n\gamma)^2 + \rho\omega^2$

The three roots of Equation 22 are given by:

$$\begin{aligned} k_1 &= (\beta/3) + M^{1/3} + N^{1/3} \\ k_2 &= (\beta/3) + mM^{1/3} + m^2N^{1/3} \\ k_3 &= (\beta/3) + m^2M^{1/3} + mN^{1/3} \end{aligned} \quad (23)$$

where $M = -q/2 + Q^{1/2}$
 $N = -q/2 - Q^{1/2}$
 $Q = q^2/2 + p^3/27$
 $p = A - \beta^2/3$
 $q = A\beta/3 - 2\beta^3/27 - \beta C$
 $m = (-1 + i\sqrt{3})/2$

Note that when $Q > 0$, k_1 is real, and k_2 and k_3 are complex conjugates. It is seen from Equation 23 that $k_r \rightarrow \infty$ only when $\omega \rightarrow \infty$. Moreover, when $k_r \rightarrow \infty$, so does $|k_i|$. Hence, the extremely short waves are highly unstable. However, this physically unrealistic situation is probably due to the neglect of the viscosity. The damping effect of viscosity, especially on the short nonaxisymmetric wave in a swirling jet, will be investigated in the near future. These asymptotic results are used to guide the numerical solutions of Equation 20.

The complex k has been obtained from Equation 20 for various sets of given β , γ , n , ρ , and ω . The numerical method used is Muller's method [8]. It should be pointed out that there are many roots of Equation 20. Only the negative roots of k , which give rise to instability are reported in the next section.

Before presenting the results, we mention that the amplification rate is related to the spray angle φ by $\tan \varphi = (d/dy)(\text{envelope of } d) = -\delta k_i \exp(-k_i y)$, where δ is the amplitude of the first wave at the nozzle exit. δ remains an arbitrary constant within the framework of linear theory.

Unless $-\delta k_i$ is sufficiently large, for unstable disturbances with $k_i < 0$, a discernible φ may not appear until some distance downstream in the y -direction. This is the origin of the so-called intact length over which the jet does not appear to diverge. However, within the intact length, small-amplitude periodic waves may be observable, since they are after all the unstable disturbances, although their growth rate happens to be small.

RESULTS

The amplification rates of the axisymmetric and the first three nodes of nonaxisymmetric disturbances are plotted against the wave number in Figure 2, for $\beta = 400$, $\beta\gamma^2 = 15$, and $\rho = 0$. It is seen that the jet is actually more unstable with respect to nonaxisymmetric disturbances than to the axisymmetric ones. However, the maximum amplification rates of the nonaxisymmetric modes corresponding to $n = 2$ and 3 both occur at $k_r = 0$. Thus these modes of disturbances cannot be observed at their maximum amplification rates in a short jet, since their wave lengths are infinitely long. The mode with $n = 1$ represents a circular jet flagging

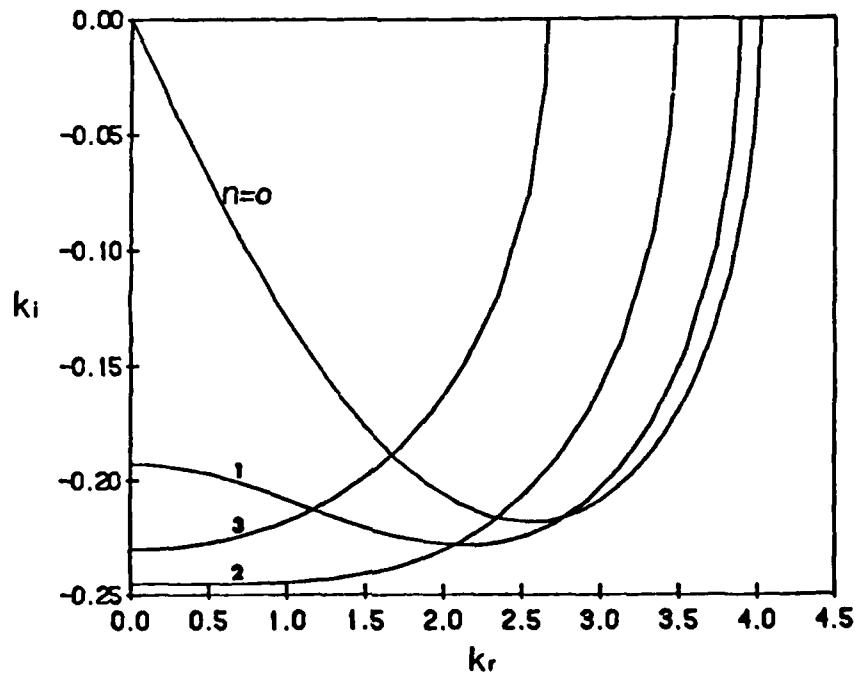


Figure 2. Amplification rates of non-axisymmetric disturbances, $\beta = 400$, $\beta\gamma^2 = 15$, $\rho = 0$.

sinuously in the axial direction. Its maximum amplification rate is slightly larger than that of the axisymmetric disturbance with $n = 0$, and the corresponding wave length of the former is slightly longer than that of the latter. Note that only the amplification rate curve corresponding to $n = 0$, but not those with $n \neq 0$, passes through the origin. This is consistent with the asymptotic analysis for $k_r \rightarrow 0$ given in the previous section. Each curve intersects with the k_i -axis at a finite critical value k_{rc} , below which each particular mode is unstable. Above this k_{rc} , k_i remains zero until a second k_i critical value, depending on the flow parameters, above which each particular mode becomes once again unstable ($k_i < 0$). In the limit of $k_r \rightarrow \infty$, $k_i \rightarrow -\infty$ as was predicted by the asymptotic analysis for $k_r \rightarrow \infty$. The portions of the curves for large values of k_i are not given in the figure, since the disturbance will be strongly damped by the neglected viscosity when k_i is very large. The observable droplet sizes will probably correspond to the wave lengths near the maximum amplification rates of various modes. The behavior of the disturbance with large k_i will be further elucidated shortly. It is seen from Figure 1 that axisymmetric and nonaxisymmetric disturbances of different wave lengths may amplify at the same rates in practice. The smallest obtainable droplets are limited by the value of k_{rc} , which decreases as n is increased. Thus, one may expect to see a wider size distribution of droplets caused by axisymmetric disturbances than the nonaxisymmetric ones. Similar dependence of k_{rc} on n was found for other values of ρ , β , and γ . For smaller values of β and/or larger values of γ , the maximum growth rates generally increase. It should be pointed out that a similar situation was found by Ponstein for the temporally growing disturbances. However, his results are independent of the value of β . Hence there are not only quantitative but also qualitative differences between the two fundamentally different types of disturbances.

Figure 3 shows the effects of the ambient gas density on the instability with respect to the axisymmetric disturbances in a liquid jet with $\beta = 400$, $\beta\gamma^2 = 15$, and $n = 0$. Both the maximum amplification rate and the range of unstable wave numbers increase as ρ increases. Thus the atomization rate can be increased by increasing the gas to liquid density ratio, but at the expense of having to accept a wider size distribution. The same trend was also found for jets without swirl, as shown in Table 1. Figure 4 shows that the swirl has the same effect as the gas to liquid density ratio, except that its effect is more pronounced.

Figure 5 gives amplification curves for various values of β for a jet with $\beta\gamma^2 = 15$, $n = \rho = 0$. For β less than a value of approximately 16, the curves do not possess the critical wave number above which $k_i = 0$ for a finite range of k_r . For $\beta > 16$, the amplification curve possesses k_{rc} ,

(text continued on page 58)

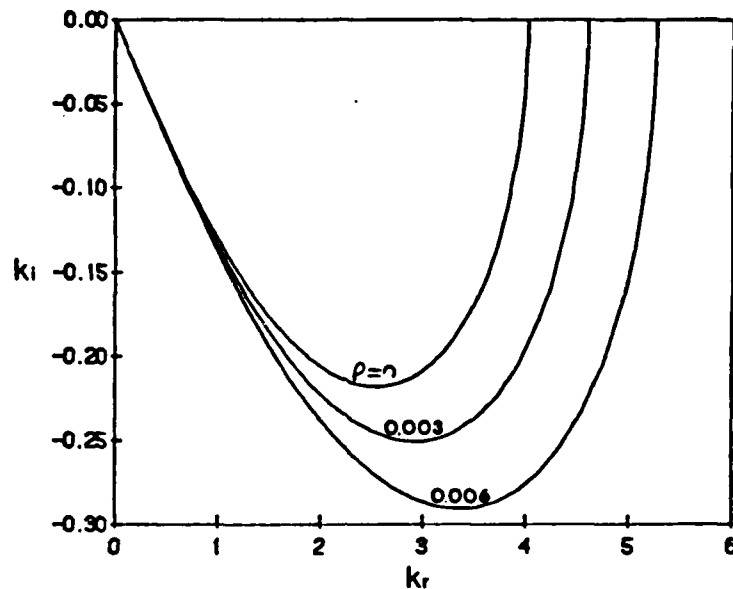
Figure 3. Effects of densities on amplification rates; $\beta = 400$, $\beta\gamma^2 = 15$, $n = 0$.

Table 1
Amplification Rate ($\beta = 400$, $\gamma = n = 0$)

ω	$\rho = 0.0012$		$\rho = 0$	
	k_r	k_t	k_r	k_t
0.10	0.100	-0.0035	0.100	-0.0035
0.20	0.200	-0.0070	0.200	-0.0069
0.30	0.300	-0.0104	0.300	-0.0100
0.40	0.400	-0.0136	0.400	-0.0128
0.50	0.500	-0.0164	0.500	-0.0151
0.60	0.600	-0.0187	0.600	-0.0166
0.70	0.700	-0.0204	0.700	-0.0170
0.75	0.750	-0.0210	0.750	-0.0169
0.80	0.800	-0.0213	0.800	-0.0164
0.85	0.850	-0.0214	0.850	-0.0152
0.90	0.900	-0.0212	0.900	-0.0133
1.00	1.000	-0.0194	1.000	0.0000
1.18	1.181	-0.0053	1.180	0.0000
1.19	1.191	0.0000	1.190	0.0000

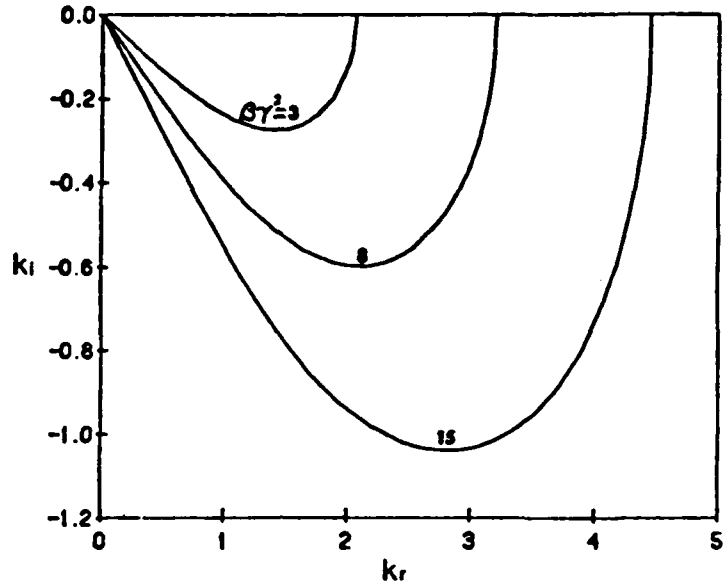


Figure 4. Effects of swirl on amplification rates; $\beta = 25$, $\rho = 0$, $n = 0$.

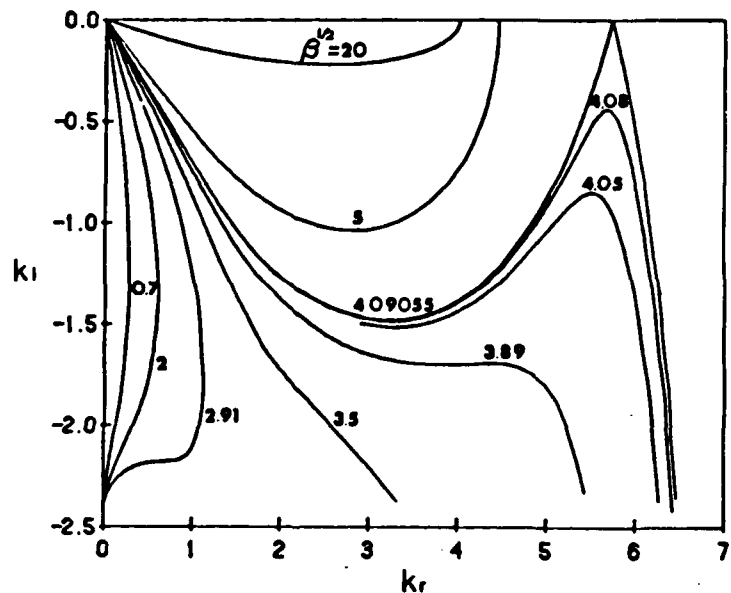


Figure 5. Effects of β on amplification rates; $\beta\gamma^2 = 15$, $n = \rho = 0$.

(text continued from page 55)

which increases with decreasing β . The second critical wave numbers above which the disturbances are all unstable also exist for $\beta > 16$. They fall outside of Figure 5, however. Qualitatively similar curves were also found for nonswirling jets and other parameter ranges. According to the asymptotic analysis for $k_r \rightarrow \infty$ given in the previous section, $k_i \rightarrow -\infty$ as $k_r \rightarrow \infty$ for all flow parameters. The curves in Figure 5 do indicate this asymptotic behavior. It is seen that the most populous drop size corresponding to the most amplified waves in an inviscid jet of finite diameters can be reduced by decreasing the value of β , i.e., by using a smaller jet velocity, a smaller jet diameter, or a smaller liquid density for a given surface tension.

Physically, β represents the ratio of inertia force to the surface tension force. The values of β encountered in the intact jet applications (ink jets, jet cutting, etc.) are of orders ten to hundreds [1], and those encountered in the present-day atomization applications are of order greater than or equal to thousands [10]. Some asymptotic results for large values of β are given in Table 2. As can be seen, the qualitative behaviors of the jet breakup described above remain the same over the range of β mentioned. Thus the present findings are useful for a wide range of applications.

Table 2
Amplification Rate ($\rho = 0.0012$, $\gamma = n = 0$)

$\beta = 30,276$			$\beta = 10,000$		
ω	k_r	k_i	ω	k_r	k_i
4.5	4.5010	-0.1464	4.0	4.0024	-0.1149
6.5	6.5021	-0.2046	6.0	6.0054	-0.1490
9.5	9.5045	-0.2835	8.0	8.0096	-0.1624
15.5	15.5119	-0.4073	8.5	8.2602	-0.1622
20.5	20.5208	-0.4695	9.0	9.0121	-0.1585
24.0	24.0286	-0.4849	11.0	11.0182	-0.1136
25.5	25.5323	-0.4827	12.0	12.0216	-0.0271
27.5	27.5376	-0.4698	12.050	12.0718	-0.0023
30.0	30.0447	-0.4333	12.0503	12.0721	-0.0008
35.0	35.0609	-0.2269	12.05035	12.0724	0.0000
36.261	36.3261	0.0000			

CONCLUSION

It is shown that an inviscid liquid jet with a swirl is more unstable with respect to nonaxisymmetric disturbances than to axisymmetric distur-

bances. This is contrary to the results for a jet without a swirl obtained by Keller et al. [2]. The jets are unstable with respect to disturbances of wave lengths longer than certain values which depend on the relevant flow parameters. For a given set of flow parameters, a maximum growth rate may exist at a finite wave number. The maximum growth rate may be enhanced by increasing the density of the ambient gas into which the liquid jet emanates. This enhancement is accompanied by sometimes undesirable broadening of the size distribution. The enhancement can be achieved more effectively by introducing a larger swirl without entailing an undesirable side effect greater than that introduced by the dense gas. On the other hand, if a larger intact length without a jet breakup is desired, the swirl inside the nozzle and the unnecessarily large ambient gas density must be avoided. A smaller disturbance amplitude at the nozzle exit is also shown to promote a smaller spray angle. It may even make a finite intact length attainable.

Acknowledgments

This work was supported in part by Grant No. DAAL03-86-K-0072 of the Army Research Office. We also acknowledge the use of Cornell National Supercomputer Facility, which is funded in part by National Science Foundation, New York State, and IBM Corporation.

REFERENCES

1. Bogy, D. B., "Drop Formation in a Circular Liquid Jet," *Ann. Rev. Fluid Mech.*, **11**, 207 (1979).
2. Keller, J. B., Rubinow, S. I., and Tu, Y. O., "Spatial Instability of a Jet," *Phys. Fluids*, **16**, 2052 (1973).
3. Lin, S. P., "Stability of a Viscous Liquid Curtain," *J. Fluid Mech.*, **104**, 111 (1981).
4. Lin, S. P., "Waves in a Viscous Liquid Curtain," *J. Fluid Mech.*, **112**, 443 (1981).
5. Lin, S. P., and Kang, D. J., "Atomization of a Liquid Jet," *Phys. Fluids*, **30**, 2000 (1987).
6. Lin, S. P., and Wang, C. Y., "Modeling of Wavy Film Flows," Ch. 28 in *Encyclopedia of Fluid Mechanics* Vol. 1 (N. P. Cheremisinoff, Ed.), Gulf Publishing Company, Houston, Texas, p. 931 (1986).
7. McCarthy, M. J., and Molloy, N. A., "Review of Stability of Liquid Jets and the Influence of Nozzle Design," *Chem. Eng. J.*, **7**, 1 (1974).

62 International Journal of Engineering Fluid Mechanics

8. Muller, D. E., "A Method for Solving Algebraic Equations Using an Automatic Computer," *Math. Tables and Aids to Computation*, 10, 208 (1956).
9. Ponstein, J., "Instability of Rotating Cylindrical Jets," *Appl. Sci. Res.*, 8, 425 (1960).
10. Reitz, R. D., and Bracco, F. V., "Mechanism of Atomization of a Liquid Jet," *Phys. Fluids*, 25, 1730 (1982).
11. Taylor, G. I., "Generation of Ripples by Wind Blowing Over a Viscous Fluid," *The Scientific Papers of G. I. Taylor*, Vol. 3, No. 25, Cambridge U. Press, Cambridge, p. 244 (1963).

APPENDIX D

Mechanisms of the Breakup of Liquid Jets

S.P. Lin* and Z.W. Lian

*Department of Mechanical and Industrial Engineering
Clarkson University, Potsdam, New York 13676*

A general theory of the onset of breakup of liquid jets in an ambient gas is given. The theory is based on the linear stability analysis of a viscous liquid jet with respect to spatially growing disturbances. The three independent parameters in the theory are the Reynolds number R, the Weber number We, and the gas to liquid density ratio Q. The numerical results obtained from a single characteristic equation over a wide range of the parameter space reveal that there are two fundamentally different mechanisms of the jet breakup. The first is the capillary pinching which breaks up the jet into segments. The second is the capillary wave resonance with the gas pressure fluctuation which generates droplets much smaller than the jet diameter. An argument based on the boundary-layer instability theory is used to demonstrate that the shear waves at the liquid-gas interface plays a secondary role in the jet breakup.

*Professor
Graduate Student

I. Introduction

Atomization is a process of breaking up a jet into droplets of diameter much smaller than the jet diameter. This process is widely used in industrial applications including fuel injections in internal combustion engines. A good knowledge of the fundamental mechanism of atomization is essential for raising the combustion efficiency and reducing the environmental pollution. Unfortunately our understanding of the fundamental mechanism is far from complete. This work delineates the parameter range of operation in which atomization can be achieved. Distinctive mechanisms of jet breakup in the atomization regime as well as other regimes are elucidated.

Plateau¹ observed that the surface energy of a uniform circular cylindrical jet is not the minimum attainable for a given jet volume. He argued that the jet tends to break up into equal segments of length, which is 9 times the jet radius, because the spherical droplets formed from these segments give the minimum surface energy for the same jet volume. Neglecting the effects of gravity and ambient gas, Rayleigh² showed that the mechanism of the jet breakup is the hydrodynamic instability caused by the surface tension. He introduced into the jet infinitesimal disturbances which may grow or decay everywhere in the jet at the same rate. He found that the fastest growing disturbance has a wavelength equaling 9 times the jet radius. Weber³ and Chandrasekhar⁴ found that the viscosity has only a stabilizing effect which reduces the breakup rate and increases the drop size. Keller et al.⁵ observed that these theories were based on the assumption that the disturbances are temporally growing, while the observed disturbances actually grow in space in the flow direction. In particular the disturbance at the nozzle exit cannot grow in time. They extended Rayleigh's analysis for spatially growing disturbances and found that Rayleigh's results are relevant only to the case of small values of the Weber number which is the ratio of the surface tension force to the liquid inertia force. For the Weber number of order one or greater, they found a new mode of faster growing disturbances of much larger wave lengths than those of the Rayleigh mode. An association of this mode with the absolute instability was made by Leib and Goldstein^{6,7}. Note that in the above mentioned theories, the effect of the ambient gas is neglected, and that the predicted drop sizes are of the same order as the jet diameter. Thus, these theories cannot be applied to the atomization phenomenon which is the breakup of a liquid jet into droplets much smaller than the jet diameter. To explain the atomization process, Taylor⁸ took the gas density into account. He considered the limiting case of an infinitely thick jet and extremely small gas to liquid density ratio. Taylor's analysis for the case of temporally growing disturbances with small density ratios was extended by Lin and Kang⁹ to the case of spatially growing disturbances with finite density ratios. Lin and Kang showed that the spray angle is proportional to the imaginary part of the complex wave number corresponding to the fastest growing disturbances. They compared the predicted drop sizes caused by the pressure fluctuation and by the shear waves at the liquid-gas interface with the experiments of Reitz and Bracco¹⁰ and concluded that the basic mechanism of atomization is the interfacial instability caused by the pressure fluctuation. Lin and Kang also discussed the relationship between temporally and spatially growing disturbances. Their results showed that the maximum growth rates of disturbances all occur at wave numbers of order one in the parameter range relevant to atomization. The drop size being proportional to the wave length and the wave length being normalized by the capillary length, a , which is the ratio of surface tension to the inertia force per unit volume of the ambient gas; i.e. $\sigma/\rho_2 U^2$ where σ is the surface tension, ρ_2 is the gas density, and U is the jet speed. Since the atomized droplets are much smaller than the jet radius r_0 , we must have

$$a/r_0 = \sigma/(\rho_1 U^2 r_0) (\rho_1/\rho_2) = We(\rho_1/\rho_2) \ll 1, \quad (1)$$

where ρ_1 is the liquid density. It follows from Eq. (1) that the necessary condition for atomization is $We \ll Q$ where $Q = \rho_2/\rho_1$. The work of Lin and Kang⁹ covered only this atomization regime. Consequently, they were unable to delineate both Taylor's atomization regime and Rayleigh's capillary pinching regime in the same parameter space. This delineation is done here for the first time with the aid of numerical results obtained from the same characteristic equation. This enables us to gain a more unified understanding of the mechanism of jet breakup. It follows from the definition of a that we must have for the Rayleigh regime $a/r_0 = We/Q > 1$, since Rayleigh's capillary pinching results in droplets of diameters larger than the jet diameter. The effect of the Reynolds number on this regime is expounded in this work.

Efforts to gain a unified understanding of the mechanism of jet breakup are well documented^{11,12}. While the previous works were based on various asymptotic analysis of temporally growing disturbances, the present unified theory is based on extensive numerical solutions of the single characteristic equation for spatially growing disturbances in a jet of finite radius. One of the main conclusions in this work is that atomization is not due to capillary pinching but rather due to the interfacial pressure fluctuation. This conclusion is arrived at not by resorting to a comparison of the theory with experiments as was done in our previous work⁹. Careful analyses by Reitz and Bracco¹⁰ of existing experimental works on atomization seemed to eliminate the turbulence fluctuation, cavitation, pressure fluctuation and boundary-layer instability in the nozzle as the fundamental mechanism of atomization, and thus identify the pressure fluctuation at the interface as the fundamental cause by implication. However, the present theoretical work is the first to demonstrate this point explicitly.

II. Unified Theory

Consider a circular cylindrical jet of an incompressible viscous Newtonian liquid issued from a nozzle into an unbounded inviscid gas. The governing dynamic equations of motion in the liquid and the gas phases are respectively the Navier-Stokes and the Euler's equations. The boundary conditions are the vanishing of the net force per unit area of the interface, and the equality of radial fluid velocity in each phase with the total time rate of change of the interfacial position. A uniform velocity distribution in a circular jet of constant cross-section in a quiescent gas is an exact solution to this set of differential equations in the absence of gravity. This exact mathematical solution representing a possible basic state is physically unstable. The stability analysis of this basic state with respect to disturbances which grow in the axial direction from the nozzle exit has already been given⁹ and will not be repeated here. The characteristic equation of any Fourier component of the disturbances of the form $C_0 \exp[i\omega t + iky]$, is given by Eq. (2) when viewed in a reference frame with its origin fixed at the nozzle exit

$$\begin{aligned}
 (\omega - ik)^2 + & \frac{2k^2}{R} \left(\frac{I_1'(k)}{I_0(k)} \right) - \frac{2k\lambda}{\lambda^2 + k^2} \left(\frac{I_1(k)I_1'(\lambda)}{I_0(k)I_1(\lambda)} \right) \\
 & x(\omega - ik) + \omega^2 Q \left(\frac{\lambda^2 - k^2}{\lambda^2 + k^2} \right) \left(\frac{K_0(k)I_1(k)}{K_1(k)I_0(k)} \right) \\
 & - We k(1 - k^2) \left(\frac{\lambda^2 - k^2}{\lambda^2 + k^2} \right) \left(\frac{I_1(k)}{I_0(k)} \right) = 0, \tag{2}
 \end{aligned}$$

where C_0 is the wave amplitude, ω is the complex wave frequency the real part of which gives the exponential temporal growth rate and imaginary part of which gives the wave frequency of disturbances, k is the complex wave number the real part of which is equal to $2\pi r_0$ /(wave length) and the imaginary part of which gives the spatial amplification rate, τ is time and y is the axial distance respectively nondimensionalized with the jet radius divided by the maximum axial velocity and the jet radius, and I and K are respectively the modified Bessel functions of the first and second kind, their subscripts denote the order of the functions, and λ is defined by

$$\lambda^2 = k^2 + R(\omega - ik).$$

It is seen from Eq. (2) that the instability of the liquid jet is characterized by the three independent parameters R , We and Q . In a reference frame moving with the jet velocity U , Eq. (2) can be formally reduced to that obtained by Sterling and Sleicher¹³ for temporally growing disturbances, if the wave number is treated as real and the wave frequency is treated as complex. However such a Galilean transformation is physically inadmissible for spatially growing disturbances in a jet which possesses no translational invariance, and hence there is a fundamental difference between these two theories.

In the limiting case of $R \rightarrow \infty$ and $Q \rightarrow 0$, Eq. (2) with $\omega = i\omega_i$ reduces to

$$(\omega_i - k)^2 = We k(k^2 - 1) I_1(k)/I_0(k). \quad (3)$$

This is the result obtained by Keller et al.⁴ for the case of spatially growing axisymmetric disturbances. They showed that Eq. (3) is related to Rayleigh's result

$$\omega_R^2 = We k(k^2 - 1) I_1(k)/I_0(k) \quad (4)$$

by the Galilean transformation of the reference frame moving with the basic state jet velocity, where ω_R is Rayleigh's temporal complex wave frequency appearing in his solution of the form constant $x \exp[i(kz - \omega_R t)]$. They also show that the asymptotic solution of Eq. (3) for $We \rightarrow 0$ near the maximum of the spatial growth rate, k_i is related to the Rayleigh temporal growth rate ω_{Ri} by

$$k_r = \omega_i + O(We^2), \quad (5)$$

$$k_i = \pm \omega_{Ri} + O(We^2), \quad (6)$$

where the subscripts r and i denote respectively the real and imaginary parts. Thus the spatial growth rate k_i can be obtained accurately from the temporal growth rate ω_{Ri} of the Rayleigh mode by use of Eq. (6) only when $We \rightarrow 0$. When We is of order one Keller et al.⁴ found from the solution of Eq. (3) a new mode of disturbances the growth rate of which is two order of magnitude larger than the above Rayleigh mode. Leib and Goldstein^{6,7} and Lin and Lian¹⁴ recently showed that this new Keller's mode actually exists in the parameter range in which absolute instability occurs. The consequence of the absolute instability and the physical meaning of Keller's mode can be made clear only by use of a nonlinear theory, and will not be pursued here. This is a simple example demonstrating the qualitative difference between the temporal and spatial disturbances. Another example demonstrating this point is given by Lin^{15,16} in his studies of the stability of a viscous sheet. It should be pointed out that Eq. (6) is consistent with the Gaster¹⁷ theorem which states that, to the first order approximation, the temporal growth rate is given by the product of the corresponding spatial growth rate and the group velocity of the disturbances i.e. $\omega_{Ri} = k_i (d\omega_i/dk_r)$, which is Eq. (6) by virtue of Eq. (5). The growth rate of the Rayleigh mode obtained from Eq. (3) with $We = 2.5 \times 10^{-3}$ is given as curve R in Fig. 1.

In the limiting case of $Q \rightarrow 0$, after using the equation preceding Eq. (3), Eq. (2) is reduced to

$$2k^2(k^2 + \lambda^2) \frac{I_1'(k)}{I_0(k)} [1 - \frac{2k\lambda}{k^2 + \lambda^2} \frac{I_1(k)I_1'(\lambda)}{I_1(\lambda)I_1'(k)}] - (k^4 - \lambda^4) \cdot (1 - k^2) J k \frac{I_1(k)}{I_0(k)} = 0, \quad (7)$$

where $J = R^2 We$. This is the characteristic equation given by Chandrasekhar⁵ for the breakup of viscous liquid threads in vacuum.

In the Taylor limit $r_0 \rightarrow \infty$, k in Eq. (1) can be rescaled with the capillary length a as

$$k = Ka(r_0/a) \equiv k(r_0/a); K = 2\pi/(wave length)$$

where K is the dimensional wave number. Note that $k \rightarrow \infty$ needs not imply that $k \rightarrow \infty$. In fact Taylor's results show that $k=0(1)$. By use of asymptotic expansions of the Bessel functions for $k \rightarrow \infty$ as $(r_0/a) \rightarrow \infty$, we reduce Eq. (2) to

$$[R(\omega - ik)^2 + R^2 We k^3 + QR^2 \omega^2 - 4k^2 \lambda = 0. \quad (8)$$

This is the equation obtained by Taylor.^{8,9} Note that $(r_0/a) \rightarrow \infty$ implies $R \rightarrow \infty$, and by virtue of Eq. (1) $We/Q \rightarrow 0$. The growth rate curve obtained from Eq. (8) with $\omega = i\omega_i$ for the values of $R = 2 \times 10^4$ $We = 1.964 \times 10^{-5}$, $Q = 0.0013$ is plotted as curve T in Fig. 1. The curve right below curve T is obtained from Eq. (2) for the same parameters. Lin and Kang showed that when $Q \ll 0.01$, Taylor's temporal growth rate is related to the spatial growth rate of Lin and Kang by the Gaster¹⁶ theorem. However when the density ratio is of order 10^{-2} or greater, the spatial and temporal theories differ significantly.

The rest of the paper will be devoted to the elucidation of the breakup of viscous liquid jets of finite radius in the gas by use of hitherto unavailable results. The results are obtained from the solution of Eq. (2) over a wide range of the relevant parameter We , R and Q . The method of solution used is the Muller method¹⁸. Since the observed disturbances grow spatially and oscillate temporally in atomization, we treat ω as purely imaginary but k as complex, i.e. $\omega = i\omega_i$ and $k = k_r + ik_i$. Here we do not consider the case of absolute instability for which the disturbance grows both spatially and temporally¹⁴.

The solution of the equation obtained by Keller et al. for the case of $R = \infty$, $Q = 0$, and $We = 0.0025$ is reproduced as curve R in Fig. 2. For the same values of $We = 0.0025$ and $R = 2 \times 10^4$ two additional curves in the same figure are obtained from Eq. (2) respectively with $Q = 10^{-4}$ and $Q = 0.0013$. The value of $Q = 0.0013$ corresponds to the air to water density ratio in one atmosphere at room temperature. It is seen that the presence of the atmosphere tends to increase the maximum amplification rate by more than 20 percent over that predicted by the Rayleigh equation (3). This deviation is even greater either when Q becomes greater or R becomes smaller. Hence Rayleigh's results are good approximations if $Q < 0.0013$ and $R > 10^4$. The experimental results of Goedde & Yuen¹⁹ and Donnelly & Glaberson²⁰ are included in the same figure for comparisons. Their experiments were conducted at one atmospheric pressure and room temperature. They did not record the values of R and We for each of the experimental points, since their experiments were intended for comparisons with Rayleigh's theory which is independent of the jet velocity. However, the ranges of R and We can be calculated from their experimental data to be respectively $(3 \sim 10) \times 10^3$ and $(1.44 \sim 8) \times 10^{-3}$. Note that the values of We used for the theoretical curve in Fig. 2 are of the same orders as those in the experiments. However the values of R used for the plots including Rayleigh's curve are larger than the experimental values. Note that the temporal growth rate $\omega / (\sigma / r_0^3 \rho_1)^{1/2} \equiv \omega'$ reported by Goedde & Yuen is related to k_i through Eq. (6) by $k_i = \omega R_i = We^{1/2} \omega'$, because of different nondimensionalizations used. It appears that the results of experiments in the atmosphere agree better with the theory of the inviscid jet breakup in a vacuum rather than with the corresponding theory of breakup of a viscous jet in atmosphere. The better agreement is probably fortuitous. The growth rates at the swell and the neck in the experiments were found to be different constants. The growth rate was taken to be the logarithm of the difference between those at the neck and the swell in the jet. This is neither consistent with the temporal growth rate which is theoretically the same constant everywhere in the jet nor is it consistent with the definition of spatial growth rate. Thus, the comparisons were made between two physically different quantities. New measurements of spatial growth rates as functions of R , We and Q are very desirable. Two amplification curves for two different values of We are plotted near curve R in Fig. 3 for $Q = 0.0013$ and $R = 2 \times 10^4$. The curve R is the same curve R given in Fig. 1. The amplification rate increases as We is increased, clearly indicating that surface tension is the destabilizing factor. The jet axial velocity relaxation was shown by Leib and Goldstein⁶ to make the Rayleigh mode more unstable. However, the mechanism remains the capillary pinching.

On the contrary, surface tension is a stabilizing factor for the Taylor mode. This is seen from the three curves plotted near curves T of Fig. 4 for three different values of We . The curve T is the same curve T appeared in Fig. 1. As We is increased with $R = 2 \times 10^4$ and $Q = 0.0013$ held constant, we see that the amplification is decreased. Thus, the major difference between the jet breakup by the Rayleigh mode and by the Taylor mode is that while the former is due to capillary pinching⁵, the latter is due to a mean other than surface tension, because surface tension is stabilizing. This other mean is either due to the pressure fluctuation or shear stress at the interface. The interfacial shear will be eliminated as the cause of atomization on physical ground. The factors involved in the nozzle are excluded, because the site of atomization is at the interface. These factors can affect the atomization only indirectly⁹. Note that $We = 2.5 \times 10^{-3} \sim 10^{-2}$ for the Rayleigh mode, and $We = 2 \times 10^{-4} \sim 2 \times 10^{-6}$ for the Taylor mode at $Q = 0.0013$.

and $R = 2 \times 10^4$. Hence, there is a value of We between 10^{-3} and 10^{-4} below which the breakup is due to pressure fluctuation but above which it is due to the capillary pinching. The specific turn around value of We depends on the values of R and Q given, and will be further explained later.

The curves A in Fig. 5 is the amplification curve for $R = 34.5$, $Q = 0.0013$ and $We = 0.0025$. The curve S is obtained from Eq. (7) with the same values of We and R but for $Q = 0$. The ambient gas is again destabilizing. The corresponding experimental results of Goedde and Yuen¹⁸ are also presented for comparison. The measured growth rate ω for this case was normalized by $(v/r_0)^2$. Thus their growth rate is related to our k_i through Eq. (6), and is given by

$$k_i = \omega_{Ri} = \omega/(v/r_0)^2 R.$$

The two additional curves in Fig. 5 for two different values of We and $Q = 0$ show that, when compared with the Rayleigh modes depicted in Fig. 1, the surface tension remains a destabilizing factor even if the liquid viscosity is increased to reduce R to 34.5. Note that in the case of $Q = 0$, the only relevant parameter is $J = R^2 We$. Thus the curve S in Fig. 5 can be used for any R and We as long as the corresponding J remains 2.976. This fact will be used to show that the non-vanishing of Q is essential for the Taylor mode. Consider the curve with $Q = 0.0013$, $We = 0.744 \times 10^{-8}$ and $R = 2 \times 10^4$ belonging to the Taylor atomization regime in Fig. 1. Retaining the same values of We and R but putting $Q = 0$, we obtain an amplification curve which is exactly the curve S given in Fig. 5 since the value of J remains 2.976. Thus the curve in the Taylor regime is brought down to the Rayleigh regime simply by reducing the values of Q from 0.0013 to 0. Hence in order to remain in the atomization regime, the presence of ambient gas is essential. Without the ambient gas, atomization cannot occur even if the surface tension is so small that $We = 0.744 \times 10^{-8}$.

Fig. 6 shows that even when R is reduced to 0.1 the breakup mechanism remains the capillary pinching when $We > Q$, since the amplification rate increases with We .

The amplification curves for $We = 1.964 \times 10^{-5}$, $R = 3.371 \times 10^4$, and two different values of Q given in Fig. 7 together with the curve for the same values of We and R but with $Q = 0.0013$ given in Fig. 1 show how the amplification rate and the range of unstable wave lengths of the Taylor mode are increased as Q is increased from 0.0013 to 0.13. This range of Q corresponds to the air to water density ratio under pressure ranging from 1 to 100 atmospheric pressure. The same destabilizing effect of Q for the Rayleigh mode is depicted in the lower left corner of Fig. 1. Figs. 8 and 9 show the damping effect of viscosity on the Rayleigh and Taylor modes.

The present theory can be used to explain the spray angle θ of an atomizing jet. The displacement of the interface from its unperturbed position is $d = C_0 \exp[i(\omega_i t + kz)]$, where C_0 is the initial amplitude at the nozzle exit, which remains arbitrary in the linear theory. Thus,

$$\tan(\theta/2) = - \frac{d}{dy} (\text{envelope of } d) = C_0 k_i \exp(-k_i y). \quad (9)$$

Expanding Eq. (9) in Taylor's series, we have

$$\tan(\theta/2) = C_0 k_i (1 - k_i y + \dots). \quad (10)$$

Hence, unless $C_0 k_i$ is sufficiently large, a measurable θ may not appear until some distance downstream in the $-y$ direction. This may be the origin of the so called intact length over which the jet does not appear to diverge. Table 1 compares the spray angles θ measured by Reitz and Bracco¹⁰ in their test series 64 to 67 with that predicted with the present theory. Tangent of half of the measured spray angles i.e. $\tan(\theta/2)$ are given in the fourth column of Table 1. The predicted values of k_i , which is related to spray angle by Eq. (10), are given in the seventh column of the same table. When the measured values of $\tan(\theta/2)$ are substituted into the left side of Eq. (10), and the predicted values of k_i are substituted into the

right side of Eq. (10), it is found that at the nozzle exit where $y=0$ this equation is satisfied only if the values of the coefficients C_0 are given by that given in the sixth column of Table 1. C_0 represents the initial disturbance amplitude at the nozzle exit. It appears that the spray angles depend not only on the spatial growth rate k_i but also on the initial disturbance amplitude C_0 at the nozzle exit. Note that these values of C_0 are all of the same order of magnitude, probably reflecting the fact that the level of disturbances at the nozzle exit in the different series of test are about the same. A full nonlinear theory is required to make a quantitative statement, however.

III. DISCUSSION

The results for some limiting cases of the unified theory and their comparisons with some limited experimental results have been used to demonstrate the validity and the limitations of the theories of Rayleigh, Weber, Chandrasekhar, Taylor and Keller et al. on the onset of the liquid jet breakup. However, it was assumed that the viscosity of gas is of secondary importance in the process. This assumption must be examined. If the viscosity is present in the ambient gas, the high speed of the liquid jet will cause the formation of a thin boundary-layer near the liquid-gas interface. The boundary-layer may become unstable and generates the Tollmein-Schlichting²¹ waves (shear waves). The shear waves may extract kinetic energy from the mean flow and amplify. Thus the shear waves may participate with the pressure fluctuation and capillary force in bringing about the breakup of liquid jets. The order of magnitude of the size of droplets generated by the shear waves may be estimated with the critical shear wave length at the onset of the boundary layer instability. The velocity profile in the boundary-layer near the free surface of a jet is not known, the boundary-layer flows over continuously moving solid surfaces in an otherwise quiescent fluid²²⁻²⁴ are probably the closest known flows to the free surface boundary-layer flows. Unfortunately the stability results of these flows are not available. For this reason, we will use the stability results for the Blasius²¹ flow over a stationary solid surface to estimate the size of droplets generated by shear waves. It should be pointed out that the shear stress and the velocity distributions in both types of solid surface boundary-layers are of the same order of magnitude. Therefore we do not expect to obtain a different order of magnitude of drop size from a "solid jet" boundary-layer flow even if the stability results of this flow are available. The critical Reynolds number and the critical wave length of the Blasius profile are given respectively by²⁵

$$R_c = U\delta/v_2 = 400, \quad \lambda_c = (2\pi/0.3)(\delta/0.32), \quad (11)$$

It follows from Eq. (11) that

$$\lambda_c = 26180 v_2/U. \quad (12)$$

Thus, in general, there are three length scales λ_c , r_o and a characterizing the size of droplets caused respectively by shear waves, capillary pinching and the pressure fluctuation. Depending on the range of parameters, one or two characteristic lengths may be predominant.

For example consider a jet of 0.034 cm diameter with a maximum velocity of 1.11×10^4 cm/sec. This is the water jet atomized under 1 atmosphere in test 23 of Reitz and Bracco.¹⁰ Using $v_2 = 0.15$ cm²/sec at room temperature, we find from Eq. (11) $\lambda_c = 0.35$ cm. Using $v_1 = 0.01$ cm²/s, $\sigma = 72$ dynes/cm, $\rho_1 = 1$ gm/cm³, $\rho_2 = 0.0013$ gm/cm³, we find $R = 18870$, $We = 3.438 \times 10^{-5}$, $Q = 1.3 \times 10^{-3}$. Thus the present jet is operating in the Taylor regime since $We \ll Q$, and the characteristic wavelength is $2\pi a = 2.8 \times 10^{-3}$ cm. This is several orders of magnitude smaller than λ_c and $2\pi r_o = 0.11$ cm. Therefore, in the process of atomizing this jet, the shear waves play little role, since the measured atomized droplets scale with a .

If both the diameter and the velocity of the jet in the last example is reduced by a factor of 10, we have $R = 188.7$, $We = 3.438 \times 10^{-2}$, and $Q = 1.3 \times 10^{-3}$. Thus $We \gg Q$ and the jet is now operated well within the Rayleigh regime although the damping effect of the liquid viscosity neglected by Rayleigh is now significant at $R = 188.7$. The characteristic length is of order $2\pi r_o = 0.011$ cm which is two order of

magnitude smaller than the critical shear wave length $\lambda_c = 3.5$ cm and one order of magnitude smaller than $2\pi a = 0.28$ cm. Hence the shear wave and the pressure fluctuation are not responsible for the breakup. The breakup in the Rayleigh regime is by the capillary pinching.

We conclude by reiterating that there are three characteristic lengths in the jet breakup. They are relevant to three distinctive mechanisms which operate in different parameter ranges. These are summarized in Table 2. However, it can be seen from this table that a jet may actually breakup by more than one mechanisms in the overlap regions of the characteristic parameter space. For example, it may break up under the simultaneous actions of the capillary pinching and the pressure fluctuation. This occurs when $We/Q = O(1)$. Consider a water jet of 0.034 cm diameter issued at 1.11×10^3 cm/sec into the atmosphere at room temperature. The relevant parameters are $R = 1887$, $We = 3.438 \times 10^{-3}$, $Q = 0.0013$. Then $We \sim Q$, and the jet is broken up at the outer edge of the Rayleigh regime discussed in the previous section. The characteristic wave length is now of the order of $2\pi r_0 = 0.11$ cm which is of the same order as the atomization length $2\pi a = 0.28$ cm, but much smaller than the possible shear wave length $\lambda_c = 3.5$ cm. Therefore the shear wave is again a bystander of the event of the breakup. However, the breakup is now under the simultaneous actions of the capillary pinching and the pressure fluctuation which may, in general, produce a bimodal distribution of the drop sizes. In order to enable the shear waves to assist significantly the capillary pinching in the breakup process, we must have $r_0 - \lambda_c$, and $We > Q$. It follows from Eq. (12) that this requires

$$\sigma > (26180 v_2)^2 \rho_2 / r_0.$$

For the sake of demonstration, let $v_2 = 0.15$ cm² and $\sigma = 72$ dyn/cm. Then the above inequality becomes

$$(\rho_2 / r_0) < 4.67 \times 10^{-6} \text{ gm/cm}^4.$$

This condition is difficult to satisfy in common practice for gases in one atmosphere. However, for a water jet of 0.35 cm radius and $U = 3 \times 10^3$ cm/sec in a rarefied gas of $\rho_2 = 10^{-6}$ gm/cm³, we have $We = 2.29 \times 10^{-5} > Q = 10^{-6}$, $R = 105000$, $\lambda_c = 1.31$ cm, $2\pi r_0 = 2.1$ cm and the above inequality is satisfied. Only when the density of the gas is reduced to such a low level can the capillary pinching and the interfacial shear work hand in hand without the interference from the pressure fluctuation. Finally, in order to induce the shear waves to assist the atomization, we require $\lambda_c \sim a$ and $We < Q$, i.e.

$$\sigma \sim 26180 \rho_2 v_2 U \quad \text{and} \quad \sigma < (\rho_2 U^2 r_0).$$

Using $v_2 = 0.15$ cm²/sec, we can combine the above two relations to give

$$4.668 \times 10^{-6} \text{ gm/cm}^4 > \rho_2 / r_0.$$

Again, this condition can be satisfied only in a very low density gas and by a relatively thick jet. Thus, for example, if $\rho_2 = 10^{-5}$ gm/cm³, $\rho_1 = 1$ gm/cm³, $\sigma = 72$ dyn/cm, $v_2 = 0.15$ cm²/sec, $r_0 = 10$ cm, and $U = 3000$ cm/sec we have $R = 3 \times 10^6$, $We = 0.8 \times 10^{-6} < 10^{-5}$, $\lambda_c = 1.31$ cm, $a = 1.8$ cm and the required condition is satisfied. This example demonstrates how hard it is to induce the shear wave to assist in the onset of atomization. It should be emphasized that we are referring here to the role of the shear waves on the onset of atomization. Obviously, in a fully turbulent gas the atomization process may be assisted by the small part of turbulence spectrum whose wave lengths are of the same order of magnitude as the capillary length a . It should also be pointed out that the gas viscosity is treated as a parameter in this analysis. A more precise delineation of the breakup regimes can be achieved by a more complete stability analysis which considers the coupled effects of the gas viscosity with all other relevant physical properties.²⁶ A nonlinear theory of atomization of a viscous liquid jet in a viscous gas is not yet available.²⁶

ACKNOWLEDGMENT

This work was supported in part by Grant No. DAAL03-86-K-0072 of the Army Research Office, Grant No. MSM-8817372 of NSF and a New York State Science and Technology Grant. The numerical computation was carried out with the Cornell National Supercomputer Facility at Cornell University, which is funded in part by NSF, New York State and IBM.

REFERENCES

- 1 Plateau, J., *Statique Experimentale Et Theorique Des Liquids Soumis Aux Seules Forces Moleculaires*. Canthier Vallars, Paris, 1873.
- 2 Rayleigh, Lord, "On the Instability of Jets," *London Math Soc.*, Vol. 10, 1879, pp. 3 61-371.
- 3 Weber, C.Z., "Zum Zerfall eines Flüssigkeitsstrahles," *Math. Mech.*, Vol. 11, 1931, pp. 136-154.
- 4 Keller, J.B., Rubinow, S.I. and Tu, Y.O., "Spatial Instability of a Jet," *Phys. of Fluids*, Vol. 16, 1972, pp. 2052-2055.
- 5 Chandrasekhar, S., *Hydrodynamic and Hydromagnetic Stability*, Oxford U. Press, Oxford England, 1961, p. 537.
- 6 Leib, S.J. and Goldstein, M.E., "The Generation of Capillary Instabilities on a Liquid Jet" *J. Fluid Mech.*, Vol. 168, 1986, pp. 479 - 500.
- 7 Leib, S.J. and Goldstein, M.E., "Convective and Absolute Instability of a Viscous Liquid Jet," *Physics Fluids*, Vol. 29, 1986, pp. 952-954.
- 8 Taylor, G.I., "Generation of Ripples by Wind Blowing over a Viscous Fluids," *The Scientific Papers of G.I. Taylor*, Cambridge U.P. Cambridge, 1963, Vol. 3, pp. 244-254.
- 9 Lin, S.P. and Kang, D.J., "Atomization of a Liquid Jet," Vol. 30, *Physics of Fluids*, 1987, pp. 2000-2006.
- 10 Reitz, R.D. and Bracco, F.V. "Mechanism of Atomization of a Liquid Jet," *Physics Fluids*, Vol. 25, 1982, pp. 1730-1742.
- 11 Reitz, R.D. and Bracco, F.V., "Mechanisms of Breakup of Round Liquid Jets," in *Encyclopedia of Fluid Mechanics*, Vol. 3, edited by Cheremisinoff, N.P., Gulf P. Houston, 1986, p. 233-249.
- 12 Reitz, R.D., "Modeling Atomization Processes in High-Pressure Sprays," *Atomization and Spray Technology*, Vol. 4, 1988, pp. (to appear).
- 13 Sterling, A.M. and Sleicher, C.A., "Stability of Capillary Jets," *J. Fluids Mech.*, Vol. 68, 1975, pp. 477-495.
- 14 Lin, S.P. and Lian, Z.W., "Absolute Instability of a Liquid Jet in a Gas," *Phys. of Fluids A*, Vol. 1, 1989, pp. 490-493.
- 15 Lin, S.P., "Stability of a Viscous Liquid Curtain," *J. Fluid Mech.*, Vol. 104, 1981, p. 111-118.
- 16 Lin, S.P., "Waves in a Viscous Liquid Curtain," *J. Fluid Mech.*, vol. 112, 1981, pp. 443-458.
- 17 Gaster, M., "A Note on the Relation Between Temporally-Increasing and Spatially-increasing Disturbances in Hydrodynamic Stability," *J. Fluid Mech.*, Vol. 14, 1962, pp. 222-224.
- 18 Muller, D.E., "A Method for Solving Algebraic Equations Using an Automatic Computer," *Math. Tables and Aids to Computation*, Vol. 10, 1956, pp. 208-230.

- ¹⁹Goedde, E.F. and Yuen, M.C., "Experiments on Liquid Jet Instability," *J. Fluid Mech.*, Vol. 40, 1970, pp. 495-512.
- ²⁰Donnelly, R.J. and Glaberson, W., "Experiments on the Capillary Instability of a Liquid Jet," *Proc. Roy. Soc. A.*, Vol. 209, pp. 547-556.
- ²¹Schlichting, H., *Boundary-Layer Theory*, McGraw-Hill, New York, 1968, p. 447.
- ²²Sakiadis, B.C., "Boundary-Layer Behavior on Continuous Solid Surfaces: III. The Boundary Layer on a Continuous Cylindrical Surface," *AIChE J.*, Vol. 7, 1961, pp 467-472.
- ²³Koldenhof, E.A., "Laminar Boundary Layers on Continuous Flat and Cylindrical Surface," *AIChE J.*, Vol. 9, 1963, pp 411-418.
- ²⁴Tsou, F.K., Sparrow, E.M. and Goldstein, R.J., "Flow and Heat Transfer in the Boundary Layer on a Continuous Moving Surface," *Int. J. Heat Mass Transfer*, Vol. 10, 1967, pp. 219-235.
- ²⁵Drazin, P.G. and Reid, W.H., *Hydrodynamic Stability*, Cambridge U.P., Cambridge, 1981, p. 224.
- ²⁶Bogy, D.B., "Drop Formation in a Circular Liquid Jet," *Ann. Rev. Fluid Mech.*, Vol. 11, 1979, pp. 207-228.

TABLE 1 Spray angles of atomizing jets

Series	$Q \times 10^3$	$W \times 10^5$	r_0/a	$10^2 x \tan(\theta/2)$	C_0	$10^2 x k_i$	$a \times 10^5$ cm
64	1.3	2.754	944	1.66	0.6	2.77	36.02
65	7.7	2.754	559	8.31	1.43	5.81	6.08
66	25.8	2.504	2061	16.46	2.13	7.73	1.65
67	51.5	2.527	4096	14.95	2.60	5.75	0.83

Table 2. Onset of jet breakup

Mechanism	Characteristic	Parameter
	Length	range (mode)
$R > 10^4$ (Rayleigh)		
Capillary Pinching	r_0	$Q \ll We$
$R < 10^4$ (Weber-Chandrasekhar)		
Pressure Fluctuation	$a = (W_c/Q)r_0$	$We \ll Q < 1, \quad 1 \leq R$ (Taylor)
$Q \ll We$		
Shear Waves	$\lambda_c = 26180r_0(v_2/v_1)/R$	$R - 26180(v_2/v_1)Q/We$
$Q \gg We$		

Fig. 1. The Rayleigh and Taylor modes.

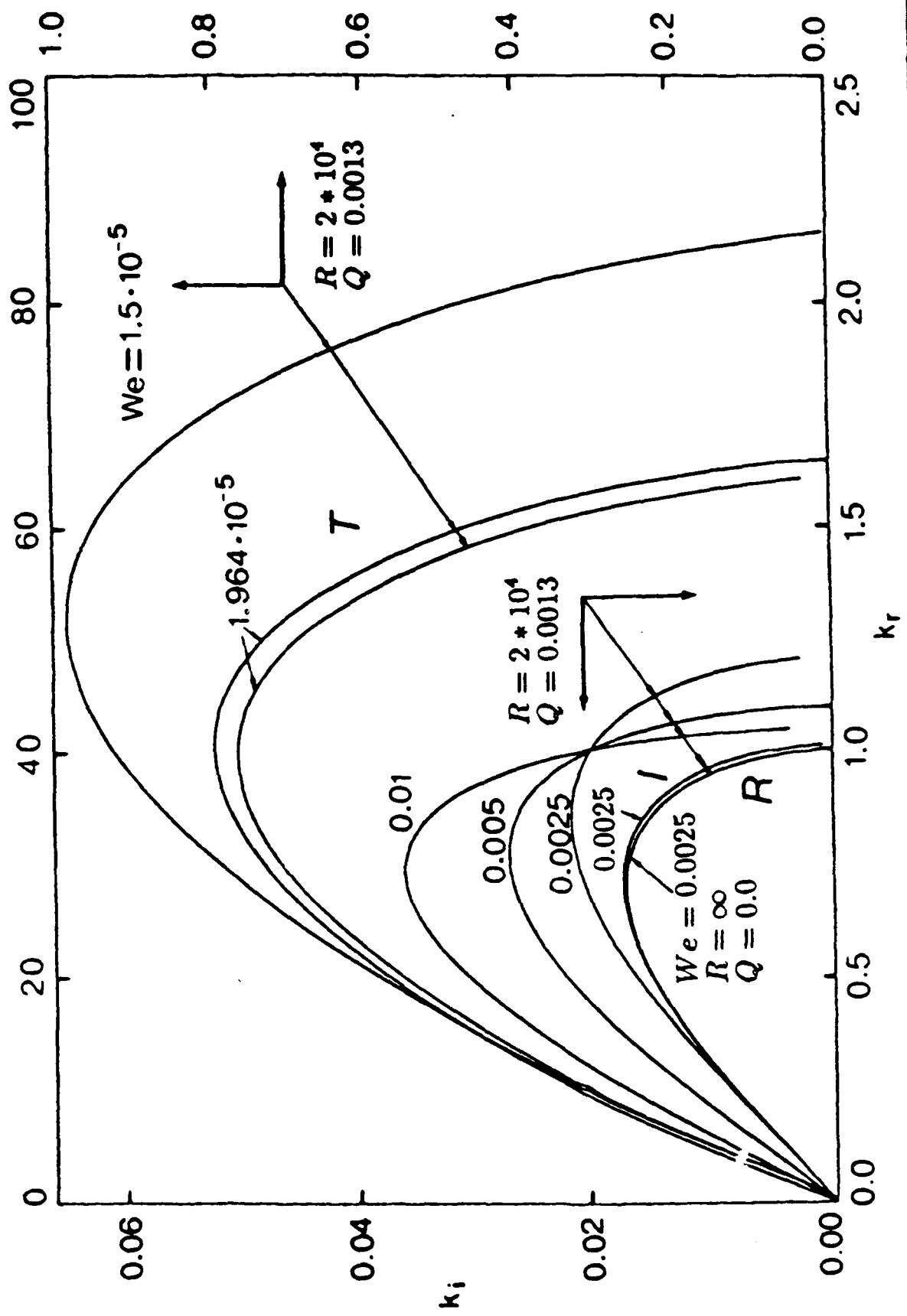


Fig. 2. Ambient gas is destabilizing in the Rayleigh mode; $We = 0.0025$; experiments of Geodde & Yuem. \diamond , experiments of Domnclly & Glaberson.

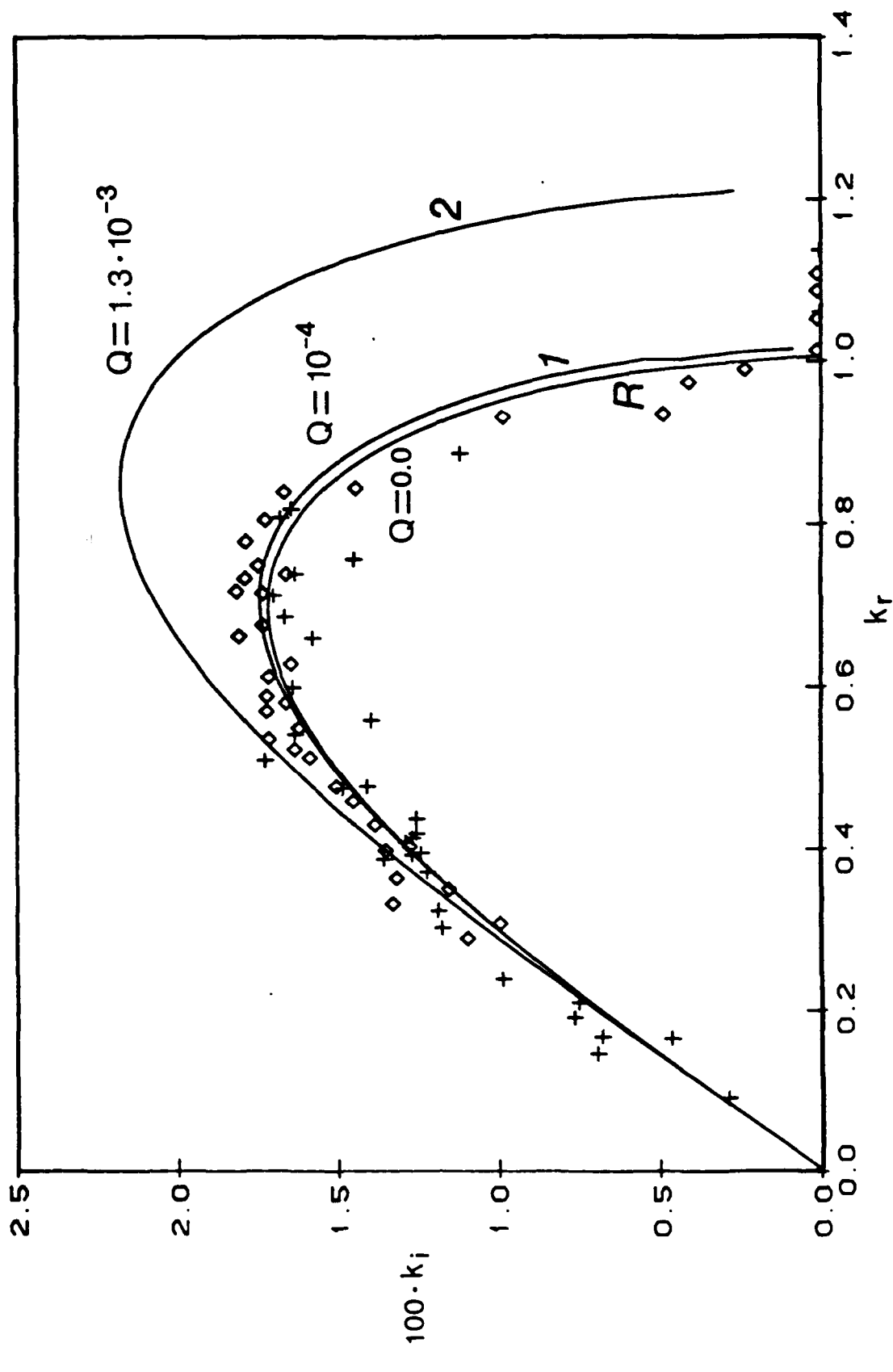


Fig. 3. Capillary pinching in the Rayleigh mode. $Q = 0.0013$.

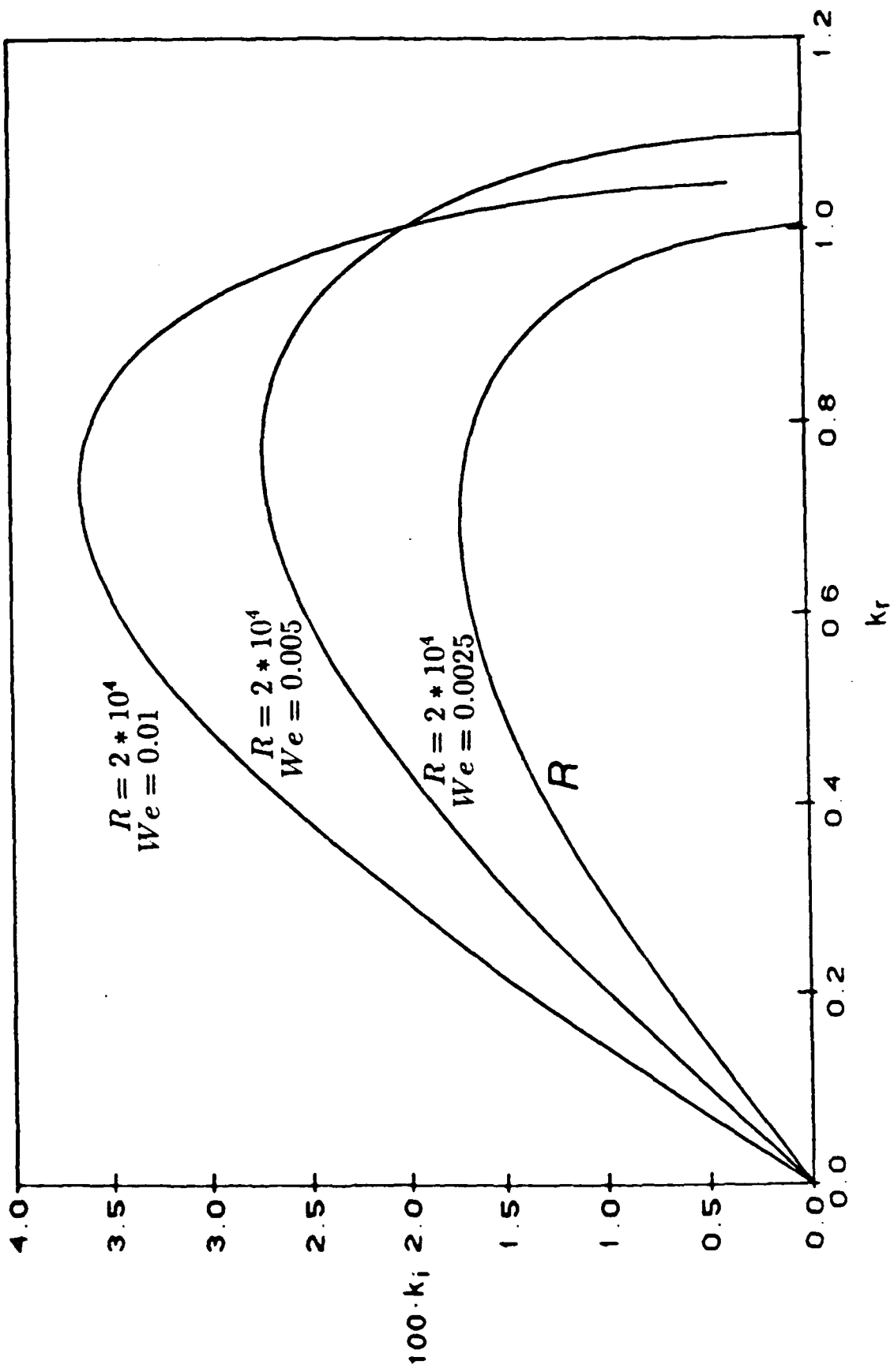


Fig. 4. Surface Tension is stabilizing in the Taylor mode. $R = 2 \times 10^4$, $Q = 0.0013$.

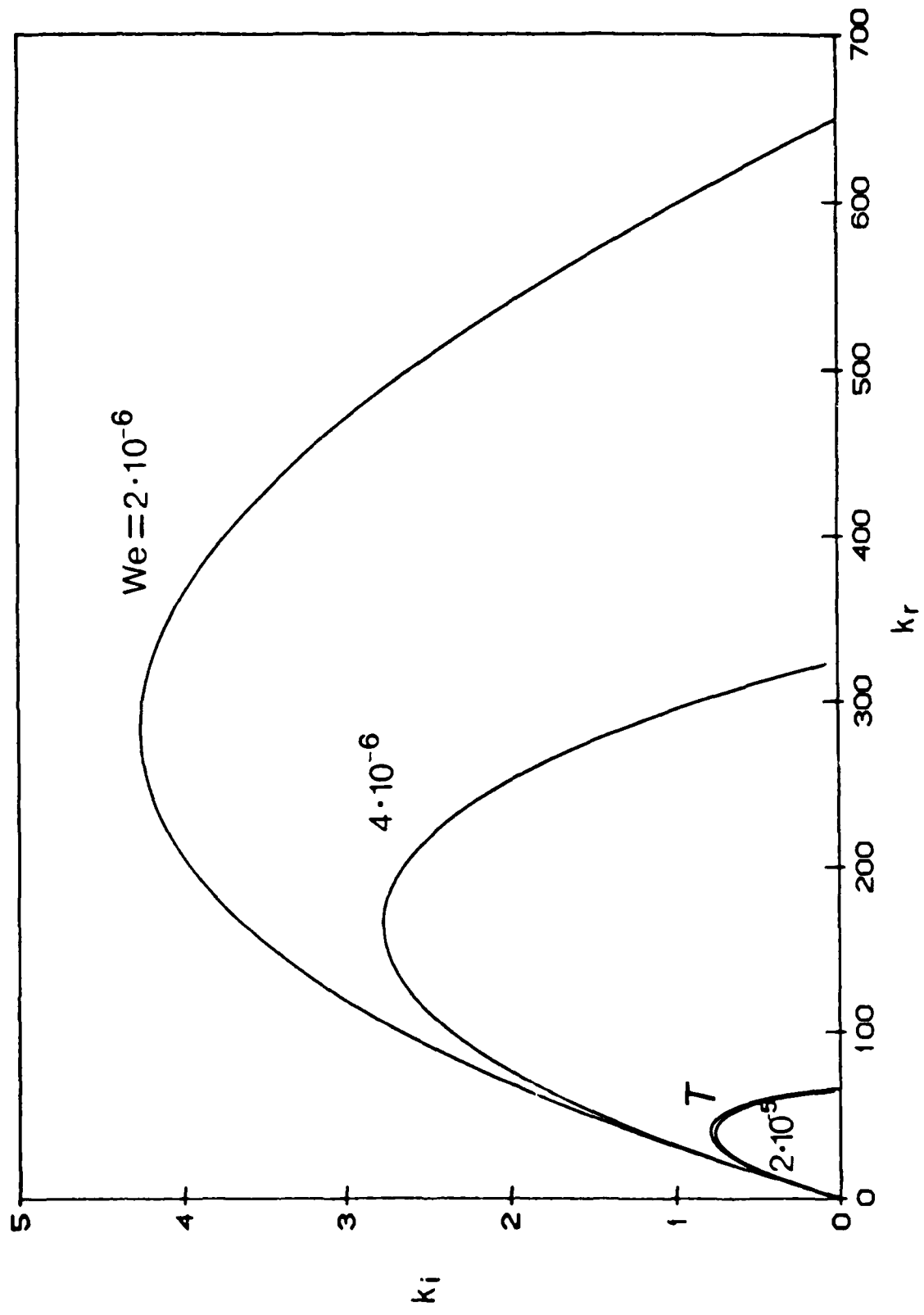


Fig. 5. Ambient gas and surface tension are destabilizing in the viscous Rayleigh jet, $R = 34.5$. 0,
experiments of Goedde & Yuen.

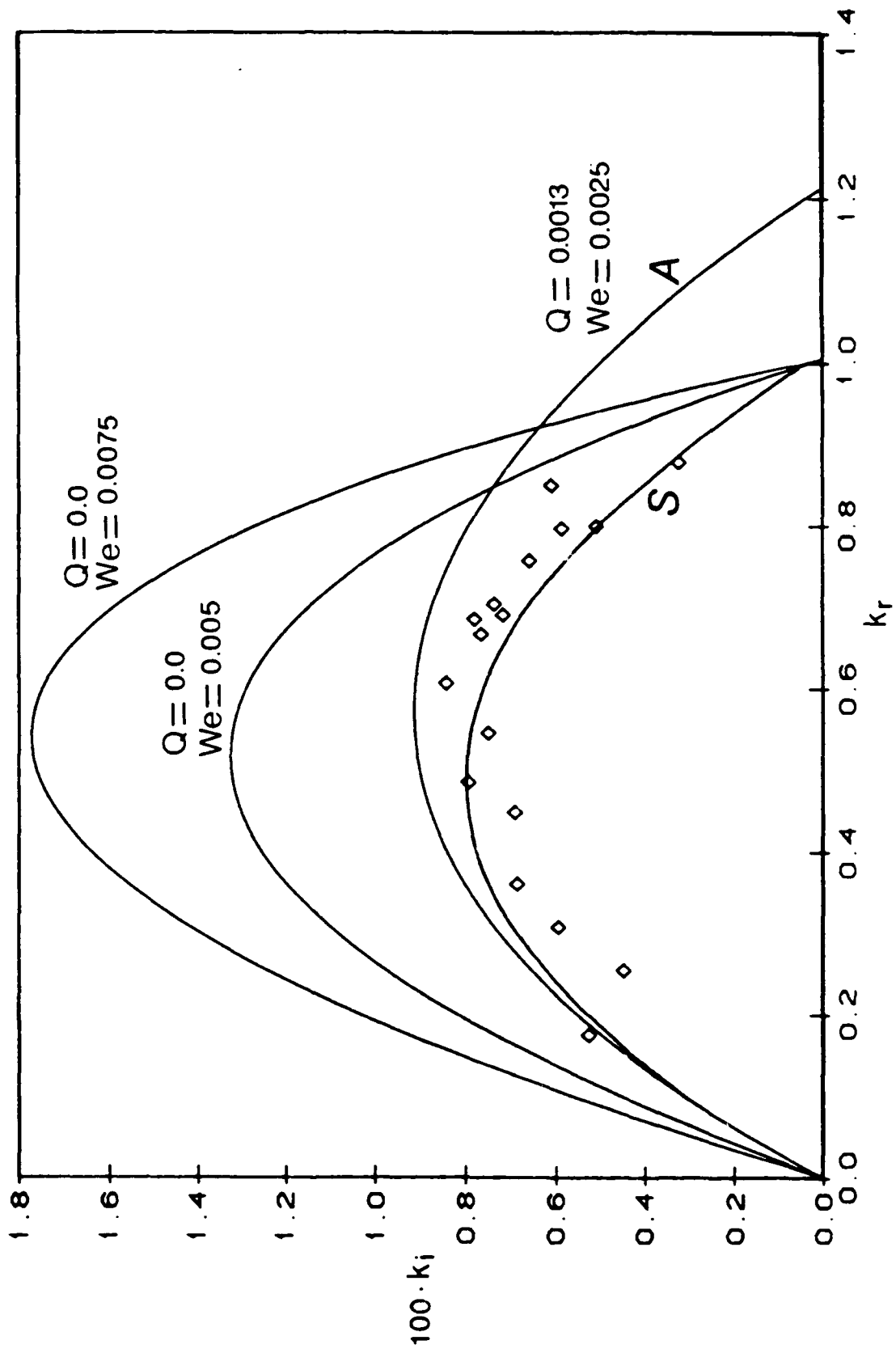


Fig. 6. Surface tension is destabilizing in a very viscous thread; $R = 0.1$, $Q = 0.001$.

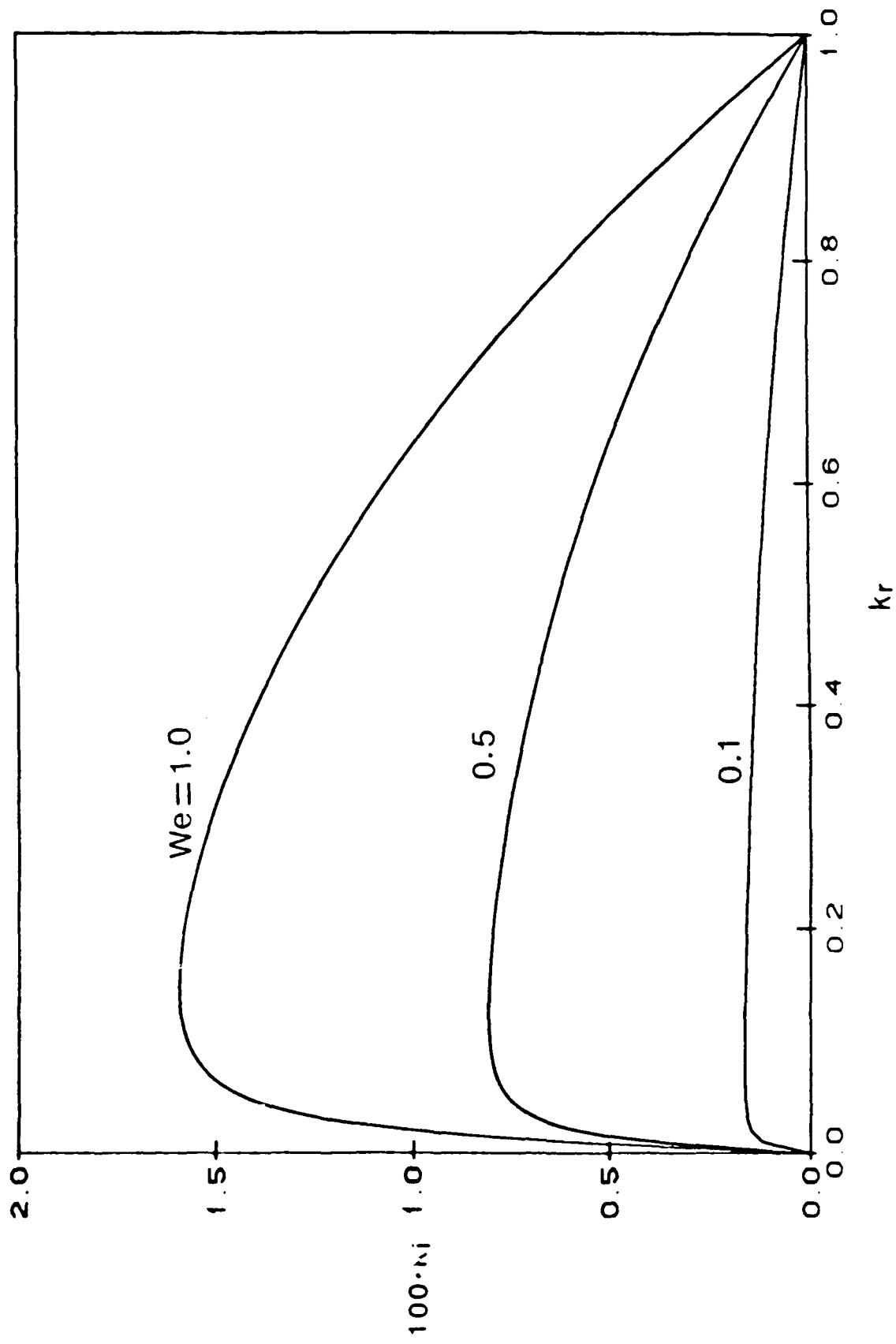


Fig. 7. Destabilizing effects of the ambient gas in the Taylor mode, $We = 1.964 \times 10^{-5}$, $R = 33705$.

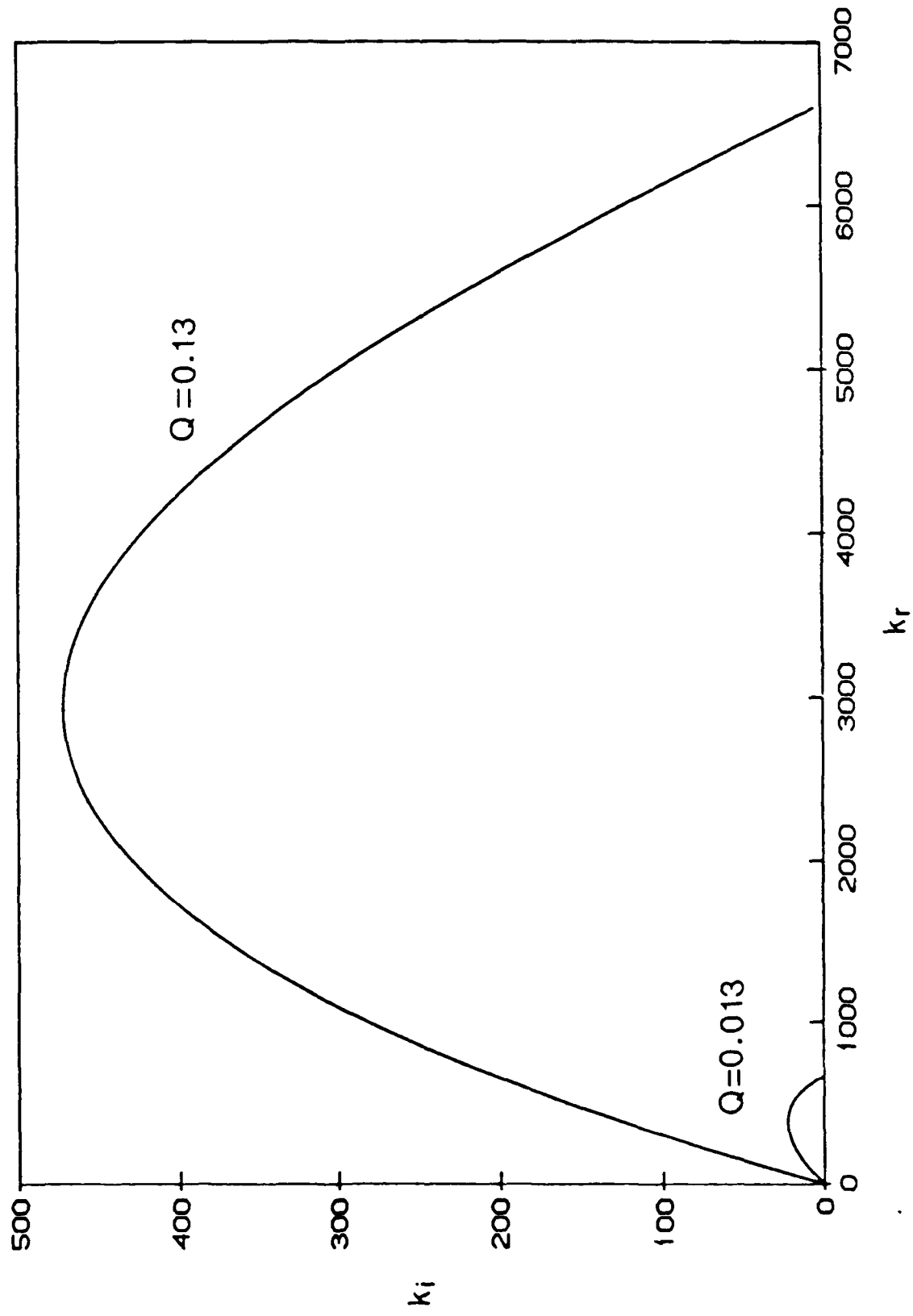


Fig. 8. Viscous damping of the Rayleigh mode in the presence of ambient gas; $We = 0.0025$, $Q = 0.0013$.

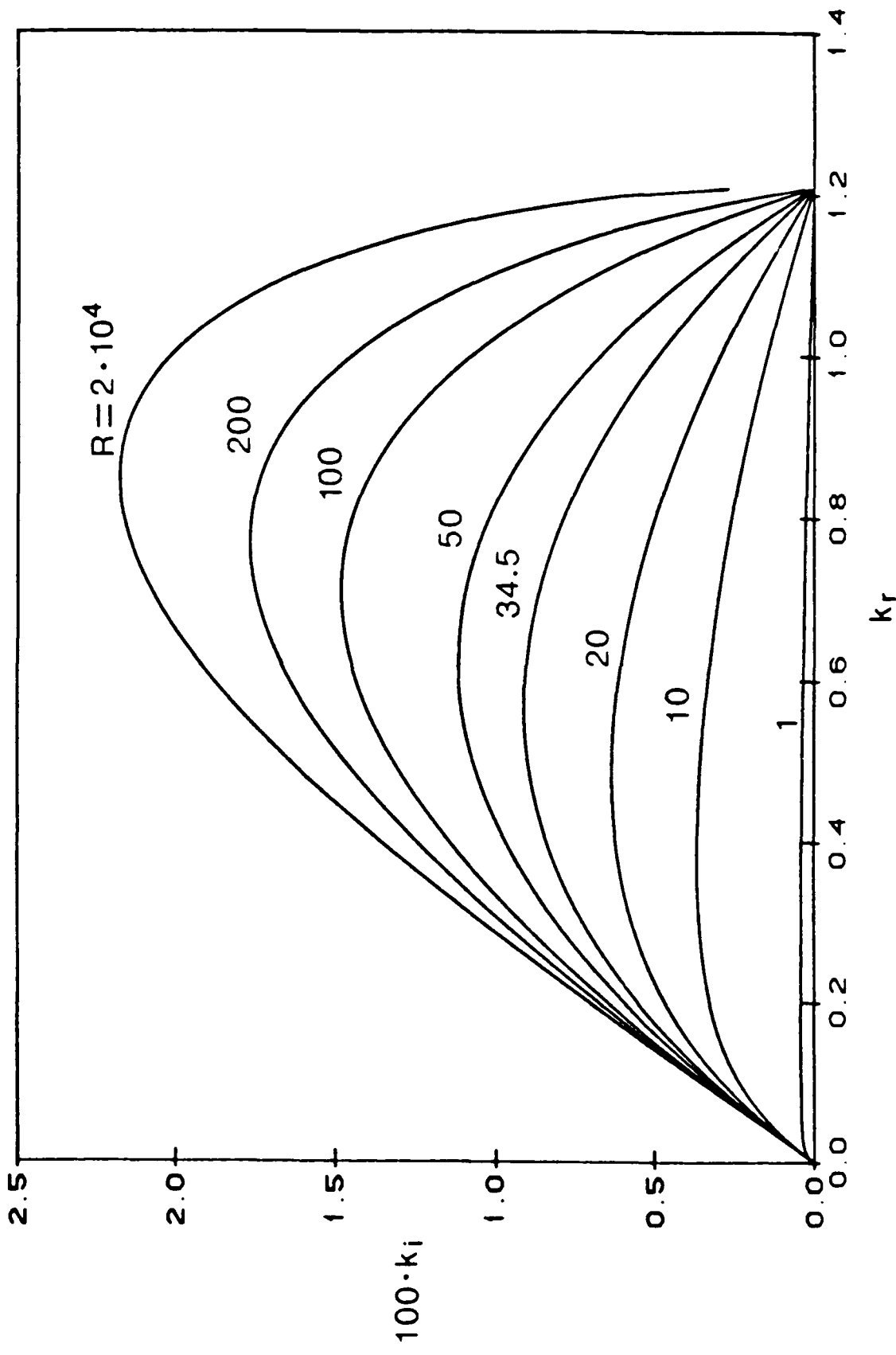
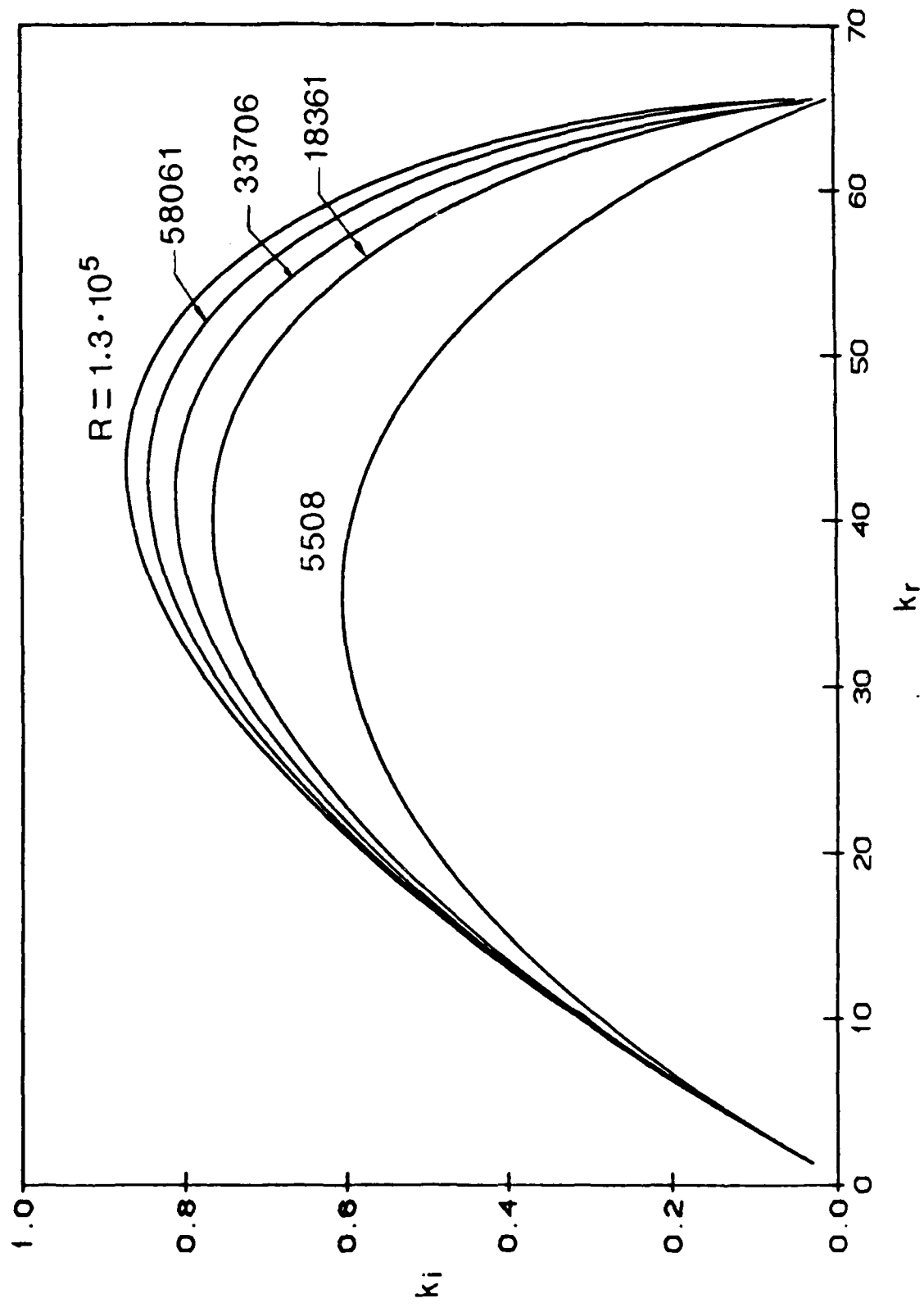


Fig. 9. Viscous damping of the Taylor mode; $We = 1.964 \times 10^{-5}$, $Q = 0.0013$.



Energy Budget in Atomization

S.P. Lin* and B. Creighton
Mechanical and Industrial Engineering Department
Clarkson University, Potsdam, NY 13676

An equation of mechanical energy balance in a liquid jet atomizing in an ambient gas is derived. The time rate of change of kinetic energy of the fluctuating disturbance in a given volume of the jet is shown to be equal to the sum of four types of works done per unit time on the jet and the energy dissipation rate through the agent of viscosity. The four types of works involved are the work by the surface tension, the work by the pressure fluctuation in the ambient gas, the work done by the fluctuating pressure in the jet, and the work by the viscous stress. Numerical results obtained for a wide range of relevant parameters are used to show that the surface tension work is negative in jet atomization. This is contrary to the situation in the breakup of an ink jet for which the surface tension work is positive, and thus the breakup is due to capillary pinching. It is shown that the work by the fluctuating gas pressure is responsible for the atomization process, since the pressure work term is the dominant positive term in the energy budget of the jet atomization.

* Author to whom correspondence should be directed.

INTRODUCTION

Rayleigh (1878) showed that a circular inviscid jet issued straight into vacuum is dynamically unstable. The instability is associated with the resonant capillary wave which tends to breakup the jet into droplets of diameters larger than the jet diameter. This Rayleigh mode of breakup also occurs in a slow viscous jet which has a small inertial force compared with the surface tension force. However, a viscous jet issued at a sufficiently high speed into an ambient gas may breakup into droplets of diameter much smaller than the jet diameter (Taylor, 1963). This mode of jet breakup is called atomization. From an energy consideration, Chandrasekhar (1961) showed that the basic mechanism of the jet breakup in the Rayleigh mode is capillary pinching. However the basic mechanism of atomization, despite its wide industrial applications, remains relatively unclear. Experimental and theoretical works on atomization are reviewed in recent articles by Reitz and Bracco (1986), Dietrich (1987), and Reitz (1988). Most of the known aerodynamic theories of jet breakup attribute the breakup to the temporal growth of the disturbance inherent in the jet. However more recent works (Keller et al. 1972; Leib and Goldstein, 1986; Lin and Kang, 1987) took notice that the observed disturbances actually grow spatially from zero amplitude at the nozzle exit along the jet axis. Lin and Kang (1987) discussed the relation between the temporal and spatial disturbances. They compared their theoretical results with the experiments of Reitz and Bracco (1982) and conjectured that the basic mechanism of atomization is the interfacial pressure fluctuation. They demonstrated with a physically plausible estimate that the shear waves generated at the liquid air interface are incapable of generating droplets as small as the capillary length to which the atomized droplets scale. Here we isolate the work done by the fluctuating gas pressure from other effects. We show that the pressure work term is indeed the dominant term in the energy budget of an atomizing jet. The itemized budget includes the energy dissipation through the agent of viscosity, the surface tension work, the pressure works and the work by the viscous stress. An equation which equates the sum of these items for a given volume of the jet with the time rate of change of the kinetic energy of the disturbance is derived in the next section. The numerical values of each item in the energy budget is evaluated over a wide range of relevant parameters in the third section. The numerical results demonstrate that the pressure work by the fluctuating pressure of the ambient gas dominates all other terms, and causes the kinetic energy of the disturbance in a given volume of jet to grow as the given volume of jet fluid travels downstream.

ENERGY EQUATION

Consider a liquid jet injected into an unbounded gas. The governing equations of motion are the Navier-Stokes equations

$$\rho_i [\partial_t V_i + (V_i \cdot \nabla) V_i] = -\nabla P_i + \nabla \cdot \sigma_i + g, \quad (1)$$

$$\nabla \cdot V_i + D \rho_i / Dt = 0, \quad (i = 1, 2) \quad (2)$$

where the subscript $i=1$ denotes the liquid and $i=2$ denotes the ambient gas, ρ is the density, V is the velocity, t denotes time, ∇ is the gradient operator, P is the pressure, σ is the stress tensor excluding the pressure, g is the gravitational acceleration, and D/Dt is the substantial derivative

$$D/Dt = \partial_t + V_i \cdot \nabla .$$

Let us consider the fluids to be incompressible, then

$$\frac{D \rho_i}{Dt} = 0 . \quad (3)$$

Let the fields of velocity, pressure and stress in the fluids be written as the superpositions of the steady basic state in equilibrium and the perturbations,

$$\bar{V}_i = \bar{V}_i + v_i' , \quad \bar{P}_i = \bar{P}_i + P_i' , \quad \bar{\sigma}_i = \bar{\sigma}_i + \sigma_i' , \quad (4)$$

where the upper bar denotes the basic state, and the primes denote perturbation. Substituting Eqs. (3) and (4) into (1) and (2), and subtracting the basic state which satisfies Eqs. (1) and (2), we have

$$\rho_i (\partial_t v_i' + \bar{V}_i \cdot \nabla v_i' + v_i' \cdot \nabla \bar{V}_i + v_i' \cdot \nabla v_i') = -\nabla P_i' + \nabla \cdot \sigma_i' , \quad (5)$$

$$\nabla \cdot v_i' = 0 .$$

For the Newtonian fluids considered

$$\sigma_i' = \mu_i (\nabla v_i' + \nabla v_i'^T) ,$$

where μ is the dynamic viscosity, and the superscript T stands for transposition. Here we are interested in the origin of the onset of atomization. At the onset of atomization the nonlinear term $v' \cdot \nabla v'$ in Eq. (5) is small compared with the linear terms. In the subsequent analysis, this nonlinear term will be neglected.

Forming a dot product of Eq. (5) with v' , using the incompressibility condition $\nabla \cdot v' = 0$ to simplify the pressure term, then integrating over the control volume shown in Figure 1, and upon applying the divergence theorem we have

$$\begin{aligned} & \int (\partial_t + V \cdot \nabla) e' dV + \int \rho v' \cdot [(\nabla \cdot V) V] dV \\ &= - \int P_1' v' \cdot n dS + \int (v' \cdot \sigma') \cdot n dS - (1/2\mu) \int \sigma' \cdot \sigma' dV , \end{aligned} \quad (6)$$

where the subscript 1 has been and will be omitted except for P , $e' = \rho v' \cdot v'/2$ is the disturbance kinetic energy per unit volume of the liquid jet, n is the unit normal vector pointing away from the liquid, and dS is the element of the control surface. The first integral on the right side of Eq. (6) is the time rate of reversible work done on the surrounding gas by the pressure fluctuation in the liquid. The integral following the reversible work term is the rate of irreversible work done by the viscous stress on the control surface. The last integral in Eq. (6) is always positive, representing the mechanical energy dissipation through the agent of viscosity.

In the atomization application, the inertial force and the surface tension force are much larger than the gravitational force and the viscous force in the gas. The effect of gas viscosity is discussed in the last section. With $g = \mu_2 = 0$, Eqs. (1) and (2) possess an exact solution representing a basic flow of a uniform liquid jet velocity, U , in a quiescent gas (Lin and Kang, 1987). The pressure difference at the interface between the liquid and the gas balances exactly the surface tension force on the cylindrical jet of a constant radius. For this basic state the pressure work integral in Eq. (6) can be further refined by use of the interfacial boundary condition. The interface is modeled as a mathematical surface without thickness. Thus the total force per unit area of the interface must vanish. The linearized normal component of the force balance gives (c.f. Lin and Kang 1987)

$$P_1' = P_2' + 2\mu U_R' - T(\eta/r_o^2 + \eta_{ZZ}), \text{ at } R = r_o, \quad (7)$$

where the subscripts R and Z denote respectively the partial differentiations in the radial and axial directions, U' is the radial component of the liquid velocity perturbation, T is the surface tension, r_o is the radius of the circular jet, and η is the displacement of the interface from $R=r_o$. The tangential component of the interfacial force balance yields

$$W_R' + U_Z' = 0, \quad (8)$$

$$V_R' - V'/R + U'\theta/R = 0, \text{ at } R = r_o,$$

where V' is the tangential component of the liquid velocity perturbation, the subscript θ denotes partial differentiation in the azimuthal direction. Here we consider only the axisymmetric disturbances, and hence the second equation in Eq. (8) is automatically satisfied. Substituting Eq. (7) into the first integral on the right side of Eq. (6), and expressing the results in terms of the dimensionless variables defined by

$$v = (u_i, w_i) = (u_i', w_i')/U, \quad (r, z) = (R, Z)/r_o, \quad p_i = P_i'/\rho_1 U^2, \quad \tau = t/(r_o/U), \quad d = \eta/r_o,$$

we have

$$-\int p_1 v \cdot n dS = -2\pi \int_{-\lambda}^{\lambda} u[(p_2 + 2u_r/R_e) - W_e(d + d_{zz})]dz - 2\pi \int_0^1 r[w p_1]_{-\lambda}^{\lambda} dr, \quad (9)$$

where again, the subscript 1 on u , v and w are omitted, λ is the axial length of the control volume, $[\cdot]_{-\lambda}$ denotes $[\cdot]_{z=0} - [\cdot]_{z=-\lambda}$, and

$$R_e = \rho_1 U r_o / \mu \equiv \text{Reynolds Number},$$

$$W_e = T/\rho_1 U^2 r_o \equiv \text{Weber Number}.$$

The first integral on the right side of Eq. (9) is the rate of work done on the control volume by the normal force at the liquid-gas interface, and the last integral is the rate of work done by the liquid pressure fluctuation at the two ends of the control volume. Note that the control surface is taken to be cylindrical, since the interfacial deformation will contribute to the surface integral only terms cubic in perturbations. The cubic terms are consistently neglected at the boundary as well as in the bulk of the jet in this linear theory.

Similarly, we express the viscous stress in terms of the velocity components and write the rate of irreversible work integral and the rate of viscous dissipation integral in Eq. (6) in dimensionless variables respectively as

$$\int v \cdot \sigma \cdot n dS = \int_{-\lambda}^{\lambda} (2u u_r/R_e) 2\pi dz$$

$$+ \int_0^1 [u(w_r + u_z) + 2w w_z]_{-\lambda}^{\lambda} 2\pi r dr,$$

and

$$D = -(2R_e)^{-1} \int \sigma : \sigma dV$$

$$= -R_e^{-1} \int_{-\lambda}^{\lambda} \int_0^1 [2(u_r^2 + w_z^2) + (w_r + u_z)^2] 2\pi r dr dz. \quad (10)$$

Note that the first integral in the expression of the rate of irreversible work integral is due to the viscous normal stress in the liquid. This term cancels exactly the same term in the reversible work rate integral, as it should. Note also that the viscous dissipation is always negative.

With the above dimensionless expressions of power integrals, Eq. (6) can be written as

$$E = P_g + P_l + S + V + D, \quad (11)$$

where

$$E = (\partial_T - \partial_z) \int_{-\lambda}^0 \int_0^l 0.5(u^2 + w^2) 2\pi r dr dz$$

= total time rate of change of disturbance kinetic energy in the control volume,

$$P_g = -2\pi \int_{-\lambda}^0 [u p_2]_{r=1} dz$$

= rate of work done by the gas pressure fluctuation at the interface

$$P_l = -2\pi \int_0^l r[w p_1]_{-\lambda} dr$$

= rate of work done by the liquid pressure fluctuation at the inlet and outlet of the control volume

$$S = 2\pi W_e \int_{-\lambda}^0 [u(d + d_{zz})]_{r=1} dz$$

= rate of work done by the surface tension.

$$V = R_e^{-1} \int_0^l [u(w_r + u_z) + 2w w_z]_{-\lambda} 2\pi r dr$$

= rate of work done by the viscous stress.

The integral on the left side of Eq. (6) was reduced to that of Eq. (11) by use of the fact that $V/U = -i_z$, where i_z is the unit vector in the positive axial direction. This integral represents the rate of increase or decrease of the disturbance kinetic energy in the control volume as it travels downstream, depending on if the sum of the five terms on the right side of Eq. (11) is positive or negative. Hence any dominant positive term among these five terms can be identified as the main source of the jet instability which leads to the breakup. Note that if the sign of a power integral is positive, then the particular work involved is on the control volume. Otherwise the work is done by the jet on the surrounding. In order to determine the numerical values including the sign of each term in Eq. (11), we must know the velocity and pressure fields as functions of time and space explicitly. These fields within the context of linear theory can be obtained from the bounded solution of Eq. (5) without the nonlinear term subjected to the boundary conditions Eqs. (7), (8), and the kinematic conditions at the interface

$$u_i = d_T - \delta_{1i} d_z, \quad (i = 1, 2) \quad (12)$$

where $\delta_{1i} = 1$ when $i = 1$, and $\delta_{1i} = 0$ when $i \neq 1$.

The velocity, pressure, and the interface fluctuations can be written respectively as

$$(ru, rw) = (\psi_z, -\psi_r) + C.C.,$$

$$p_i = p_i' + C.C.,$$

$$\text{and } d = H + C.C.,$$

where C.C. stands for the complex conjugate, the subscripts r and z stand for partial differentiations of the stream function ψ , p_2' stands for a complex pressure field, and H is the complex displacement of the interface. The method of determining ψ , p_2' and H can be found elsewhere (Lin and Kang, 1987). Only the final results which are not reported elsewhere but are required for the evaluation of the power and energy integral are given here,

$$\begin{aligned} \psi &= r[A I_1(\lambda r) + B I_1(kr)] \exp(i\theta - k_r z) \\ p_2' &= Q D K_0(kr) \exp(i\theta - k_z z), \\ p_1' &= B(\omega - k) I_0(kr) \exp(i\theta - k_z z), \\ H &= C \exp(i\theta - k_z z), \\ \lambda^2 &= k^2 + i(\omega - k) R_e, \\ \theta &= k_r z + \omega \tau, \end{aligned} \tag{13}$$

where A , B , C , and D are integration constants, $k = k_r + ik_z$ is the complex disturbance wave number, ω is the wave frequency, θ is the phase angle of the disturbance, I and K are the modified Bessel functions of the first and second kinds respectively, the subscripts of the Bessel functions denote their order, and Q is the density ratio, i.e.,

$$Q = p_2/p_1.$$

The real part of the wave number k_r is related to the wave length λ of the disturbance by $k_r = 2\pi/\lambda$, and the imaginary part k_z gives the exponential spatial amplification rate of the disturbance. The integration constants in Eq. (13) can be determined from the dimensionless versions of the boundary conditions Eqs. (7), (8) and the two kinematic boundary conditions in Eq. (12). A non-trivial solution of this set of four homogeneous equations for the eigenvector (A , B , C , D) exists only if the determinant of the coefficient matrix vanishes. This condition yields the characteristic equation mentioned earlier. For the sets of characteristic values (k, ω) which satisfies this condition, the system of four homogeneous equations can be solved for the corresponding eigenvector uniquely up to an arbitrary multiplicative constant. The eigenvector thus obtained is

$$\begin{aligned} A &= -2Bk^2 I_1(k)/(\lambda^2 + k^2) I_1(\lambda), \\ C &= B(\lambda^2 - k^2) I_1(k)/(\lambda^2 + k^2)(\omega - k), \\ D &= -iB(\lambda^2 - k^2)\omega I_1(k)/(\lambda^2 + k^2)(\omega - k) K_1(k). \end{aligned} \tag{14}$$

Without loss of information within the framework of linear theory, the arbitrary multiplicative constant B in the above expressions can be put to 1.

The complex wave number and the real frequency were obtained by Lin and Kang (1987) only in a limited parameter range for the limiting case of $r_o/a \rightarrow \infty$, where $a = T/\rho_2 U^2$ is the

capillary length. In order to obtain a more unified understanding of the jet breakup, we have obtained the eigenvalues in a wide parameter range including the atomization regime for finite r_0/a . The corresponding eigenvector is then obtained from Eq. (14). Hence the integrand in each item of the energy budget Eq. (11) is now a known function of time and space. Note that the integration in the axial direction is from $z = -\lambda$ to $z = 0$. This integration at any given time is equivalent to integration from $\theta = -2\pi$ to $\theta = 0$. The numerical integration was carried out with double precision by use of the method of numerical quadrature (Ralston and Wilf, 1967). Both sides of Eq. (11) were evaluated independently. The equality condition of both sides provides a check for the numerical accuracy. Numerical results over a wide range of W_e , R_e and Q have been obtained. Some representative results are summarized in Table 1.

RESULTS

Since in the linear theory the disturbance amplitudes are determined only up to an arbitrary multiplicative constant, the relative values of the power integrals rather than the absolute value of them are physically significant. We chose to normalize each power integral by use of the sum of all power integrals which is equal to E , and define

$$(p_g, p_l, s, v, d) = 100 (P_g, P_l, S, V, D)/E .$$

Calculated percentage values of the relative power integral defined above are given in the last five columns of Table 1. The entries in each row are the results corresponding to the parameter range specified by the first four columns. Note $q = Q/W_e = r_0/a$. Hence q is the ratio of the jet radius to the capillary length. The values of k_r , k_i and ω in each row correspond to the disturbance with the maximum spatial growth rates for each case. The radius of droplet resulting from the instability may be estimated by equating the volume of the circular cylindrical jet of length λ corresponding to the maximum growth rate with the volume of a spherical drop of radius R_o ,

$$\pi r_0^2 \lambda = 4 \pi R_o^3 / 3 , \text{ which gives } R_o = (3\pi/2k_r)^{1/3} r_0 . \quad (15)$$

The values k_r in the first four rows of Table 1 are all smaller than one. It follows from Eq. (15) that the radius of drops formed from the jet breakup in the ranges of the flow parameters specified in these rows are all larger than the jet radius. On the other hand the values of k_r in the last four rows are all much larger than one. Thus the droplets radius for these cases are all much smaller than the jet radius. If we define atomization as the process of breaking up a liquid jet into droplets of radius much smaller than the jet radius, then the latter cases correspond to the atomization regime. The former cases of jet breakup into drops of radius larger than the jet diameter is caused by a mechanism different from that of atomization as will be explained presently. We shall call the former mode of jet breakup the Rayleigh mode. Table 1 shows that while the surface tension power terms in the Rayleigh mode are all positive, they are all negative in the atomization mode. Thus the capillary force cannot contribute to the positive growth of the disturbance kinetic energy which is essential for the onset of atomization. However, the capillary pinching is the cause of the jet breakup in the Rayleigh mode, since the positive surface tension power integral dominates all other terms in the energy budget as can be seen from Table 1. Hence the surface tension has a dual role of destabilizing the Rayleigh mode and stabilizing the atomization mode. This feature has not been pointed out previously. The cause of atomization can be identified as the gas pressure fluctuation since its power integral is positive and dominates all other items in the energy budget. Notice that gas pressure power integrals are all positive in the Rayleigh mode as well as in the atomization mode. Thus the gas pressure fluctuation may assist the capillary pinching in the

Rayleigh mode. However it is not essential, since even in the absence of the ambient gas the gas pressure fluctuation vanishes, but the destabilizing capillary force remains dominant. On the other hand the gas pressure fluctuation is essential for the atomization process, since as Q becomes smaller than W_e the pressure power integral loses its dominance to the surface tension power integral. Then, the breakup is by capillary pinching. Observe that $q < 1$ for the Rayleigh mode, and $q > 1$ for the atomization mode. It appears that q is the most convenient parameter to use to determine whether an operation is in the atomization regime or in the Rayleigh regime. Note that q involves only the physical properties T , ρ_2 and the jet velocity U .

DISCUSSION AND CONCLUSIONS

In this study the effect of gas viscosity is neglected. A justification is required. It is seen in Table 1 that as the Reynolds number is increased dramatically with W_e and Q held constant, the ratio of drop radius to jet radius for the fastest growing mode is relatively constant. This signifies that the size of the atomized droplets scales with the capillary length $a = r_0 W_e / Q$, and is insensitive to the viscous force variation. This is consistent with known experiments, because the observed droplet size scales with a but not with the shear wave length. Shear waves are the product of the interfacial boundary-layer instability caused by the viscous force in gas. The shear wave length was estimated by Lin and Kang (1987) to be two order of magnitude larger than the capillary length. This result justifies the neglect of gas viscosity in the analysis. However, the precise effect of gas viscosity remains to be investigated by keeping the gas viscosity in the complete stability analysis. Cavitation and other effects inside the nozzle flow are not considered explicitly in this study. They are treated as sources of disturbances which create interfacial instability. This is justifiable because the actual sites of atomization are at the liquid-gas interface, although some of the seeds of atomization may have already been sowed inside the nozzle. With these understandings, we arrive at the following conclusions.

The main energy source of atomization of a viscous Newtonian liquid in an inviscid gas is the power imparted by the fluctuating pressure of the gas on the liquid jet. When the ambient gas is so thin that the capillary length is larger than the jet diameter, i.e. $q < 1$, the jet breakup is no longer by atomization but by an entirely different mechanism of capillary pinching.

This work was supported in part by Grant No. DAAL0-386-K-0072 of the Army Research Office, Grant No. MSM-8817372 of National Science Foundation, and a New York State Science and Technology Grant. The computation was carried out with the Cornell National Supercomputer Facility which is funded in part by NSF, New York State, and the IBM Corporation.

REFERENCES

- Dietrich, D.E. (1987). *Encyclopedia of Fluid Mechanics*, (N.P. Cheremisinof, ed.) Syntax International, Singapore, Vol. 3. p. 365.
- Kang, D.J. and Lin, S.P. (1988), Int. J. of Eng. Fluid Mech. (to appear).
- Keller, J.B., Rubinow, S.I. and Tu, Y.O. (1972), Physics Fluids 16:2052-2055.
- Lin, S.P. (1970), J. Fluid Mech. 40:307-314.
- Lin, S.P. and Kang, D.J. (1987), Phys. Fluids, 30:2000-2006.
- Leib, S.J. and Goldstein, M.E. (1986), J. Fluid Mech. 168:479-500.
- Leib, S.J. and Goldstein, M.E. (1986), Physics Fluids, 29:952-954.
- Rayleigh, Lord (1878), London Math Soc. 10:4-13.
- Reitz, R.D. and Bracco, F.V. (1986), *Encyclopedia of Fluid Mechanics*, (N.P. Cheremisinoff, ed.) Gulf P. Houston, Vol. 3, p. 233.
- Reitz, R.D. and Bracco, F.V. (1982), Physics Fluids, 25:1730-172.
- Reitz, R.D. (1988) Atomization and Spray Technology, 4:(to appear).
- Ralston, A. and Wilf, H.S. (1967), *Mathematical Methods for Digital Computers*, Vol. 2, Wiley, New York, p. 1.
- Taylor, G.I. (1963), *The Scientific paper of G.I. Taylor*, Cambridge U.P. Vol. 3, No. 25, pp. 244-254.

TABLE I. Energy Budget in Atomization. $q = r_0/a$; $(s, p_g, p_l, v, d) = 100$ (S, P_g, P_l, V, D) $/E$, see Eq. (11) for the right side of the last equation.

q	Re	$We \times 10^3$	$Q \times 10^3$	k_r	k_i	ω_i	s	p_g	p_l	v	d
0.52	10^6	2.5	1.3	0.1669	4.15(-4)	0.167	117.5	3.5	-0.2	0.2	-21.0
0.52	5×10	2.5	1.3	0.5725	9.13(-3)	0.580	97.7	26.2	-4.9	1.6	-20.6
0.26	2×10^2	5.0	1.3	0.7701	0.0177	0.770	65.5	41.8	0.0	0.1	-7.4
0.04	2×10^4	2.5	0.1	0.7088	0.0175	0.708	96.2	3.5	0.4	0.0	-0.1
66.2	5508.2	1.964(-2)	1.3	35.417	0.6058	35.30	-296.0	547.7	-2.1	-0.1	-149.5
66.2	18360	1.964(-2)	1.3	40.051	0.7662	4.008	-215.1	351.7	-2.0	0.1	-34.7
66.2	33705.5	1.964(-2)	1.3	41.580	0.8125	41.532	-210.4	331.6	-1.9	0.0	-19.3
66.2	58061.24	1.964(-2)	1.3	42.368	0.8460	42.30	-214.7	332.1	-1.0	-0.2	-16.2

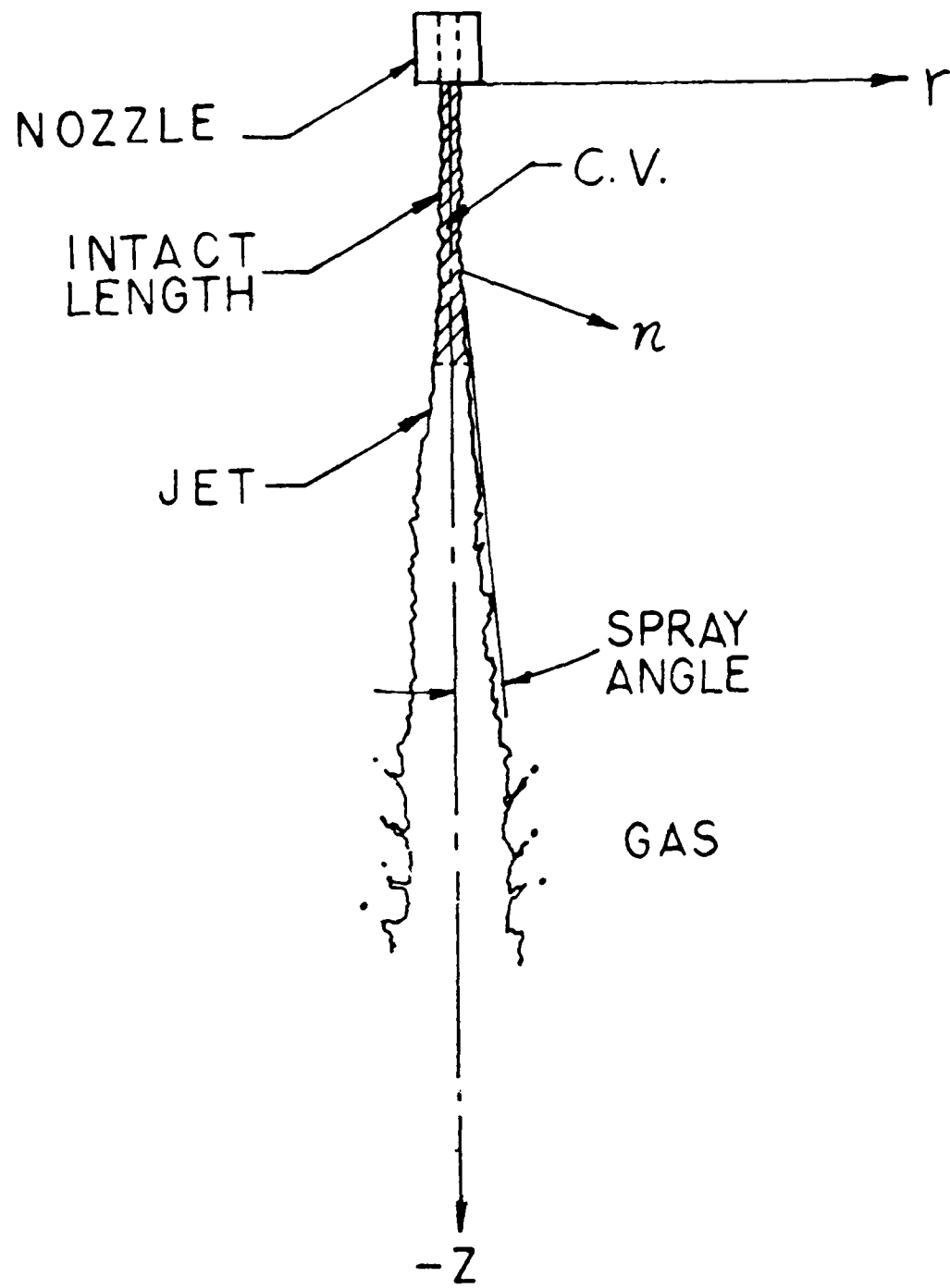


FIGURE 1. Control volume. C.V.

Navier-Stokes Flow for the Initial Stage of Atomization

D.J. Kang and S.P. Lin

*Department of Mechanical and Industrial Engineering
and Institute of Colloid and Surface Sciences
Clarkson University, Potsdam, New York 13676*

A nonlinear theory of atomization is given. The governing equations are the Navier-Stokes equations. The boundary conditions involve the unknown boundary of an atomizing jet. The relevant system of partial differential equations are reduced to a system of nonlinear ordinary differential equations by use of the Galerkin projection and a finite difference discretization respectively in the radial and the axial direction of the jet. The reduced system is solved numerically with given initial conditions for various flow parameters. The theoretical results reveal that origin of atomization is the pressure fluctuation at the core of the liquid jet. This pressure fluctuation resonates subharmonically the interfacial capillary waves which lead to the formation of ligaments which are the precursors of the atomized droplets.

INTRODUCTION

The process of breaking up a liquid jet, which emanates from a nozzle into an ambient gas, into droplets of diameters much smaller than the jet diameter is called atomization. The process has various applications including aerosol generation, liquid fuel injection in internal combustion engines, formation of pharmaceutical mist, and spray coatings. Despite its practical importance, our understanding of the fundamental mechanism of atomization is far from complete, as can be seen from the recent review articles (1,2). Careful analyses by Reitz and Bracco (3) of existing experimental works on atomization seemed to eliminate the turbulence fluctuation, cavitation, pressure fluctuation and boundary-layer instability in the nozzle as the fundamental mechanisms of atomization. While the above mentioned factors certainly influence the outcome of atomization, the site of atomization is actually at the liquid-gas interface. It has been shown recently (4-7) that in contrast to the breakup of ink jets, which is due to capillary pinching, the cause of atomization is the pressure fluctuation at the liquid-gas interface. However, these findings are based on the large time asymptotic linear stability theory. Moreover, the source of energy which generates the interfacial pressure fluctuation was not identified. A nonlinear nonstationary theory of atomization is not yet available. The purpose of this work is to fill this gap. The results of the nonlinear theory show that the energy of atomization is supplied from the core of the jet to the interface, instead of from the gas to the jet through the action of interfacial shear as is commonly believed (8).

STABILITY ANALYSIS

The detail of stability analysis is available (9). Only the outline of the analysis will be given. Previous studies (10,11) show that a jet without swirl is most unstable with respect to axisymmetric infinitesimal disturbances. We consider here only the axisymmetric disturbances in Newtonian incompressible liquid and gas. Moreover, the gravity effect on atomization is neglected. The governing differential equations are the Navier-Stokes equations which in terms of Stokes stream function can be reduced to

$$E^2 \psi_{i\tau} - \frac{1}{x} \frac{\partial(\psi_i, E^2 \psi_i)}{\partial(x,y)} - \frac{2}{x^2} \psi_{iy} E^2 \psi_i - \frac{1}{R_e} \frac{v_i}{v_l} E^4 \psi_i = 0, \quad [1]$$

where x, y are respectively the radial and axial distances nondimensionalized with the nozzle radius r_0 , τ is the time normalized with r_0/W_0 , W_0 being the maximum jet velocity, ψ is the stream function nondimensionalized with $W_0 r_0^2$, $\partial(,)/\partial(x,y)$ is the Jacobian operator, and R_e is the Reynolds number related to the liquid density ρ_l and the liquid dynamic viscosity μ , by

$$R_e = \rho_l W_0 r_0 / \mu_l \quad , \quad E^2 = \partial_{xx} - \frac{1}{x} \partial_x + \partial_{yy}$$

The subscripts τ, x and y in [1] denote partial differentiations and the subscript i denotes the liquid phase or the gas phase depending on if $i = 1$ or 2.

The boundary conditions of [1] are:

the boundness of the flow along the jet axis at $x = 0$, i.e.,

$$\psi_{1y} = \psi_{1x} = 0; \quad [2]$$

the normal force balance at the interface $x = h(y,\tau)$,

$$\begin{aligned}
R_e W_e \{ h_{yy} (1 + h_y^2)^{-3/2} - h^{-1} (1 + y^2)^{-1/2} \}_y = \\
[(\mu_i/\mu_1) \{ \psi_x/x^3 - \psi_{xx}/x^2 + \psi_{xxx}/x + \psi_{xyy}/x + h_{yy}(\psi_x/x)_x + 2(\psi_{yy}/x)_x \\
+ h_y^2 (\psi_x/x)_{xx} + 2h_y(\psi_y/x)_{xx} - 2h_y \psi_{yyy}/x - h_{yy} \psi_{yy}/x \\
- h_y^2 (\psi_{xyy}/x - \psi_{yy}/x^2) \} - (\psi_{tx}/x + (\psi_y/x)(\psi_x/x)_x - \psi_x \psi_{yx}/x^2 \\
- h_y (\psi_{ty}/x + \psi_y(\psi_{xy}/x - \psi_y/x^2)/x - \psi_x \psi_{yy}/x^2)] R_e (\rho_i/\rho_1)]^{1/2}, \quad [3]
\end{aligned}$$

where $[f(\psi)]^{1/2} \equiv \{ f(\psi_1) - f(\psi_2) \}$;

the tangential interfacial force balance including the surface tension σ ,

$$[(\mu_i/\mu_1) \{ (1 - h_y^2) (\psi_{yy}/x - \psi_{xx}/x + \psi_x/x^2) + 2h_y (2\psi_{xy}/x - \psi_y/x^2) \}]^{1/2} = 0, \quad [4]$$

$W_e \equiv$ Weber number = $\sigma/\rho_1 r_0 W_o^2$;

the kinematic interfacial boundary condition

$$h h_t - \psi_{ix} h_y - \psi_{iy} = 0; \quad (i = 1 \text{ or } 2); \quad [5]$$

the continuity of velocity at interface $x = h(t, y)$

$$\psi_{1y} - \psi_{2y} = 0, \quad [6]$$

$$\psi_{1x} - \psi_{2x} = 0; \quad [7]$$

and the no-slip condition at the cylindrical gas chamber wall at $r = l$, i.e.,

$$\psi_{2x} = \psi_{2y} = 0 \quad [8]$$

The initial condition is chosen to be a flow which satisfies the governing equation [1] and its boundary conditions [2] to [8] exactly. The initial flow is

$$\begin{aligned}
 \psi_1(x,y,0) &= 0.5 x^2(0.5x^2/c - 1) = \psi_{10} \\
 \psi_2(x,y,0) &= 0.5 x^2/\mu c(0.5 x^2 - l^2) = \psi_{20} \\
 h(y,0) &= 1 \\
 c &= 1 - (1 - l^2)/\mu, \mu = \mu_2/\mu_1. \tag{9}
 \end{aligned}$$

The flow inside the nozzle will be assumed to remain unperturbed and remains the same as the initial flow given by [9], i.e.,

$$\psi_1(x,y,\tau) = \psi_{10}, h(y,\tau) = 1, y \leq 0. \tag{10}$$

Similarly the flow in the region $y \leq 0$ of the gas chamber will be assumed to be

$$\psi_2(x,y,\tau) = \psi_{20}, y \leq 0. \tag{11}$$

The solution of [1] will be expanded as

$$\begin{aligned}
 \psi_1(x,y,\tau) &= \psi_0(x,\tau) + \sum_{m=1}^M A_{1m}(\tau,y)x^{m+1} \\
 \psi_2(x,y,\tau) &= \sum_{m=1}^M A_{2m}(\tau,y)(x-l)^{m+1} \\
 \psi_0(x,\tau) &= (e/16)(x^4 - 2cx^2), \quad e = [4(1+\delta\cos(\omega\tau))]/c(1+\delta), \tag{12}
 \end{aligned}$$

where δ and ω are respectively the amplitude and frequency of the external forcing. Note that [9] satisfies the boundness condition [2] and the no-slip condition [8]. In order to satisfy the initial condition of ψ_1 , we must choose

$$A_{1m}(0,y) = 0, \quad 1 \leq m \leq M.$$

By use of the relation

$$x^2 = (x - l)^2 + 2(x - l)l + l^2,$$

$$x^4 = (x - l)^4 + 4l(x - l)^3 + 6l^2(x - l)^2 + 4l^3(x - l) + l^4,$$

it is easily shown that in order to satisfy the initial condition for ψ_2 , we must have

$$A_{21}(0,y) = l^2/\mu c, A_{22}(0,y) = l/\mu c,$$

$$A_{23}(0,y) = l/4\mu c, A_{2m}(0,y) = 0, (m \geq 4).$$

[13]

Substituting [12] into [1] and multiplying the resulting equation with $2\pi x B_{im}$, B_{im} being the coefficients of A_{im} in [12] and integrating from $x=0$ to h for $i=1$

$$\int_0^h 2\pi x x^{\bar{m}+1} \{eq. [1]\} dx, \quad (\bar{m} = 1, 2, \dots, \bar{M})$$

and between $x=h$ to l for $i=2$,

$$\int_h^l 2\pi x(x-l)^{\bar{m}+1} \{eq. [1]\} dx, \quad (\bar{m} = 1, 2, \dots, \bar{M})$$

we obtain 2 sets of \bar{M} differential equations in dependent variable $A_{im}(\tau, y)$ and $h(\tau, y)$. Then we discretize $A_{im}(\tau, y)$ and $h(\tau, y)$ in y , i.e.,

$$A_{imn}(\tau) \approx A_{im}(\tau, n\Delta y), h_n(\tau) \approx h(\tau, n\Delta y), (n = 1, 2, \dots, N). \quad (14)$$

The system of $2\bar{M}$ differential equations must be satisfied at each spatial nodal point at $n=1$ to N . Hence we have a system of $2\bar{M}N$ equations in $2M N + N$ unknowns, $A_{imm}(\tau)$, ($i = 1, 2$) and $h_n(\tau)$. The interfacial boundary conditions [3] and [4] provide $2N$ differential equations and the rest of interfacial conditions [5], [6] and [7] provide additional $3N$ algebraic equations in time. The total number of equations is therefore

$$2\bar{M}N + 5N.$$

It is easily seen that in order to make the number of equations equal to that of the unknowns, we must choose \bar{M} such that $M = \bar{M} + 2$. This is a Galerkin method which minimizes the residual (11) associated with eq. [1] and its boundary conditions in the radial direction.

The spatial discretization in the y -direction was achieved by use of the fourth order central difference scheme. In order to solve the resulting system of $(2M+1)N$ equations for A_{1mn} and A_{2mn} and h_n , we must specify the inlet conditions [10] and [11] in terms of them. It is easily verified from [12]-[14] that these conditions for the fourth order scheme require

$$A_{1m(-n)}(\tau) = 0, (1 \leq m \leq M);$$

$$A_{21(-n)}(\tau) = A_{21}(0,y), A_{22(-n)}(\tau) = A_{22}(0,y)$$

$$A_{23(-n)}(\tau) = A_{23}(0,y), h_{(-n)}(\tau) = 1, (n=0,1,2,3).$$

As the discretization in the y -direction is truncated at a finite axial distance, we must also specify the downstream conditions. The following periodic conditions are used as the downstream condition for the fourth order finite difference scheme,

$$A_{im(N+n)} = A_{im(n)},$$

$$h_{N+n} = h_n, \quad (i=1,2; n=1,2,3,4).$$

The above constructed nonlinear system of ordinary differential equations in time was solved by use of ODEPACK (13). The results are presented in the next section.

RESULTS

The streamline patterns of the disturbance in the liquid phase velocity at $\tau = 0.01$ and $\tau = 0.1$ are given respectively in Fig. 1(a) and Fig. 1(b) for the flow parameters, $\rho = \rho_2/\rho_1 = 1.3 \times 10^{-3}$, $\mu = 0.018$, $\delta = 0.05$, $\omega = 0.02$, $W_e = 1.963 \times 10^{-5}$, $R_e = 18360.5$. The given values of ρ and μ correspond to a water jet in atmosphere. $W_e = 1.963 \times 10^{-5}$ and $R_e = 18360.5$ are typical values encountered in the liquid jet atomization process. It is observed that a series of counterrotating vortex rings are quickly formed around the core of the liquid jet. This series of vortex rings creates a meandering axisymmetric jet stream in the axial direction. The meandering is obviously created by the pressure fluctuation along the jet axis. This jet stream in turn drives a series of vortex rings near the liquid-gas interface. The average distance between these interfacial vortices is approximately 0.02 which scale with the capillary length $\sigma/\rho_2 W_0^2$, since

$$(\sigma/\rho_2 W_0^2)/\tau_o = (\rho_1/\rho_2)W_e = 0.015.$$

Note that the average distance between the counterrotating core vortex rings is approximately one half of the distance between interfacial vortex rings. To see if these disturbance length scales are affected by the extent of the chosen computational domain and its step size Δy , we increased the domain and its step size in the axial direction by fifty percent. The length scales changed by approximately ten percent. This is not surprising, in view of the fact that our results were obtained with $M=4$ and $N=20$. However the qualitative features of the vortex generation remains the same. The effects of larger values of M and N will be discussed later. The dotted lines in Fig. 1 are streamlines obtained by extrapolation.

Fig. 2 gives the corresponding streamline pattern of the disturbance in the gas chamber. The disturbance velocity gradients near the interface are two orders of magnitude larger than

their counterparts in the liquid phase as they should be, since the dynamic viscosity of the gas is two orders of magnitude smaller than that of the liquid and the tangential dynamic boundary condition can be satisfied only by a velocity gradient which is two orders of magnitude larger. The distance between two neighboring vortex rings again scales with the capillary length rather than the shear wave length. The shear wave length, λ can be estimated (4) with the critical wave length of the unstable Blasius boundary-layer profile which gives

$$\lambda/r_0 = 800(v_2/v_1)/0.096R_e = 6.8$$

with $R_e = 18360$ and $v_2/v_1=15$ which is the kinematic viscosity ratio. Thus, the shear wave is approximately two orders of magnitude longer than the capillary length at such a small Weber number 1.964×10^{-5} and $\rho_2/\rho_1 \gg W_e$. Owing to the same sense of rotation for the vortex rings on both sides of the interface, the vortices in the air cannot be driven by their counterpart in the liquid across the interface. The larger eddies in the middle of gas chamber seem to extract energy from the basic flow and feed into the eddies near the interface. Similar flow patterns are found for other parameter ranges in the atomization regime in which $W_e \ll \rho$. Thus the origin of the atomization appears to be the pressure fluctuation at the core of the basic flow because the interfacial wavelength does not scale with the shear waves. The interfacial capillary waves seem to resonate subharmonically with the pressure fluctuation around the jet axis. The pressure fluctuation at the interface gives rise to the radial component of the interfacial velocity, and causes the formation of ligaments. The formation of ligaments is the precursor of atomization. It should be pointed out that the interfacial displacements in these figures are not drawn to the same scale as the radial position for clarity.

The parameter values for Figs. 3 and 4 are identical to those for Figs. 1 and 2 except the dynamic viscosity ratio is now decreased by a factor of 10. It is seen that the jet core vortex

rings are now retarded by the strong viscous effect. The transmission of the pressure fluctuation becomes less efficient, in spite of the fact that the eddies in the gas phase are now much more vigorous. This is consistent with the experimental observation that viscosity of the liquid tends to hinder atomization (1,3).

The transient growth of the disturbance depicted in Figs. 1-4 are only up to $\tau=0.1$. When computation is advanced beyond $\tau=0.1$, no qualitative changes have been observed. However as τ increases, the time steps of integration required for the convergent iterative solution become increasingly smaller. When τ exceeds approximately 0.3, the iterative solutions become explosively large. This is most likely due to the exaggerated instability associated with the fact that the differential system obtained with $M=4$ and $N=20$ is no longer adequate to capture the everdecreasing small length and time scales which are actually present in the physical phenomenon. When M was increased to 5, we are able to advance the computation beyond $\tau=0.3$ only when the time and spatial resolution are increased to 10^{-6} and 10^{-3} respectively. However, the iterative solution requires several hours of supercomputer time to converge. Even then only a few time steps can be advanced, and the solutions including the interfacial wave amplitude become again explosively large. It is most likely that neither the truncated system nor the method of solution are adequately to resolve the fine scales involved in the physical phenomenon for large times. For this reason, the results are presented only up to $\tau=0.1$. However, the obtained results seem to capture the essential mechanism of atomization which is already discernable in the initial stage. It should be pointed out that the vortex structure predicted in the work has not yet been experimentally demonstrated. Quantitative measurements which are accurate enough to resolve a length scale smaller than the capillary length in the flow field are required to substantiate the present finding.

Fig. 5 shows the effect of the frequency of external forcing on the capillary wave formation. The variations of the wave amplitude along the jet axis are plotted for the atomization parameters indicated in the figure caption and for three frequencies of external forcing at $\tau = 0.1$. The capillary wave frequency corresponding to the zero external forcing frequency is 40. As the external forcing frequency ω is increased from zero to 0.02, the disturbance amplitude increases dramatically and modulates to form a wave packet. The wave length of the wave packet is decreased slightly as ω is increased further from 0.02 to 0.05 without altering appreciably the capillary wave length. The practical implication is that an external forcing with a frequency much smaller than the capillary wave frequency cannot alter the most popular droplet size but tends to increase the number of larger drops which scale with the wave packet length. Fig. 6 shows that the capillary wave amplitude can be increased dramatically by increasing the amplitude of the external forcing. However, the wavelength cannot be changed at $\omega = 0.02$ which is much smaller than the natural frequency.

ACKNOWLEDGMENTS

This work was supported in part by Grant No. DAALO-386-K-0072 of the Army Research Office, Grant No. MSM-8817372 of National Science Foundation, and a New York State Science and Technology Grant. The computation was carried out with the Cornell National Supercomputer Facility which is funded in part by NSF, New York State, and the IBM Corporation.

REFERENCES

1. Reitz, R.D. and Bracco, F.V., Encyclopedia of Fluid Mechanics (N.P. Cheremisinoff, Ed.), Vol. 3, pp. 233, Gulf P. Houston, 1986.
2. Dietrich, D.E., Encyclopedia of Fluid Mechanics (N.P. Cheremisinoff, Ed.), Vol. 3, p. 365 Gulf P., Houston, 1986.
3. Reitz, R.D. and Bracco, F.V., Phys. Fluids, 25, 1730 (1982).
4. Lin, S.P. and Kang, D.J., Phys. Fluids, 30, 2000 (1987).
5. Lin, S.P. and Lian, Z.W., Phys. Fluids, 32, (1989)
6. Lin, S.P. and Lian, Z.W., AIAA Journal, (to appear)
7. Lin, S.P. and Creighton, B., Aerosol Science and Technology, 11, (1989).
8. Elkotb, M.M., "Spray-Gas Stream Interaction in Diesel Engines", Proceeding of ICLASS-88, 1988, p. 28, The Fuel Society of Japan.
9. Kang, D.J., "Fundamental Mechanism of Liquid Jet Atomization", Ph.D. Dissertation, Clarkson University (1988).
10. Rayleigh, Lord, London Math Soc., 10, 361 (1879).
11. Kang, D.J. and Lin, S.P., Int. J. of Eng. Fluid Mech., (to appear).
12. Bender, C. and Orszag, S.A., "Advanced Mathematical Methods for Scientists and Engineers", McGraw-Hill, New York, 1978.
13. Hindmarsh, A.C., "ODEPACK, a Systematized Collection of ODE Solvers", in Scientific Computing (R.S. Stepleman et al. Ed.) Vol. 1 of IMACS Transaction on Scientific Computation, pp. 56-64, North Holland, Amsterdam, 1983.

FIGURE CAPTIONS

FIG. 1. Streamline pattern of disturbances in liquid phase.

(a) $\tau = 0.01, \Delta\psi_1' = 0.2 \times 10^{-6},$

(b) $\tau = 0.10, \Delta\psi_1' = 0.2 \times 10^{-5}.$

FIG. 2. Streamline pattern of disturbances in gas phase.

(a) $\tau = 0.01, \Delta\psi_2' = 0.47684 \times 10^{-5},$

(b) $\tau = 0.1, \Delta\psi_2' = 0.49591 \times 10^{-4},$

FIG. 3. Streamline pattern of disturbances in liquid phase at $\tau = 0.1, \Delta\psi_1' = 0.1 \times 10^{-4}, \mu = 0.0018.$

FIG. 4. Streamline pattern of disturbances in gas phase at $\tau = 0.1, \Delta\psi_2' = 0.49591 \times 10^{-4}, \mu = 0.0018.$

FIG. 5. Effects of the forcing frequency at $\tau = 0.1; R_e = 18360.5, W_e = 1.964 \times 10^{-5}, \rho = 1.3 \times 10^{-3}, \mu = 0.018, \delta = 0.05, l = 7.$

FIG. 6. Effects of the forcing amplitude at $\tau = 0.1; R_e = 18360.5, W_e = 1.964 \times 10^{-5}, \rho = 1.3 \times 10^{-3}, \mu = 0.018, \omega = 0.02, l = 7.$

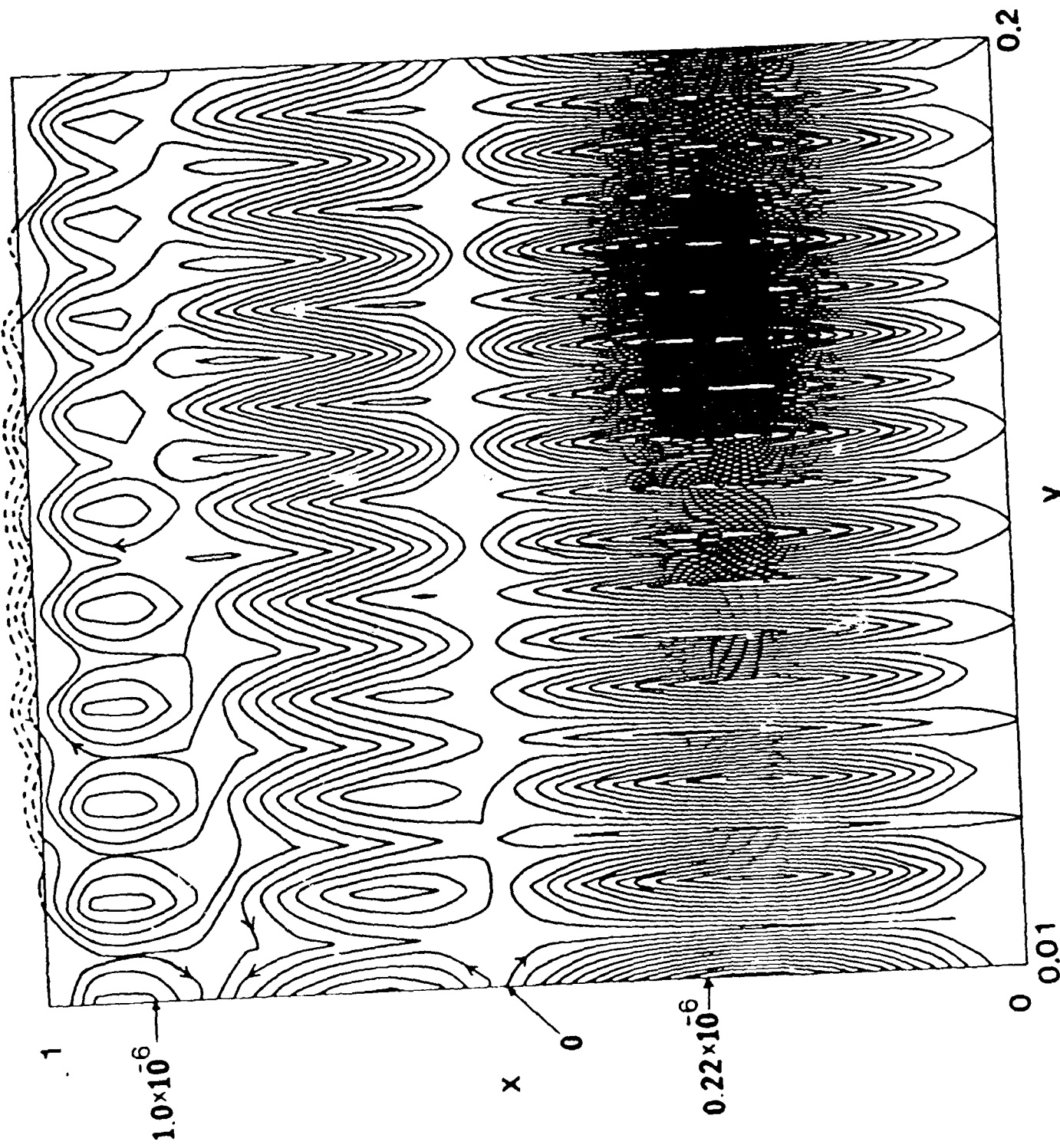


FIG. 1(a)

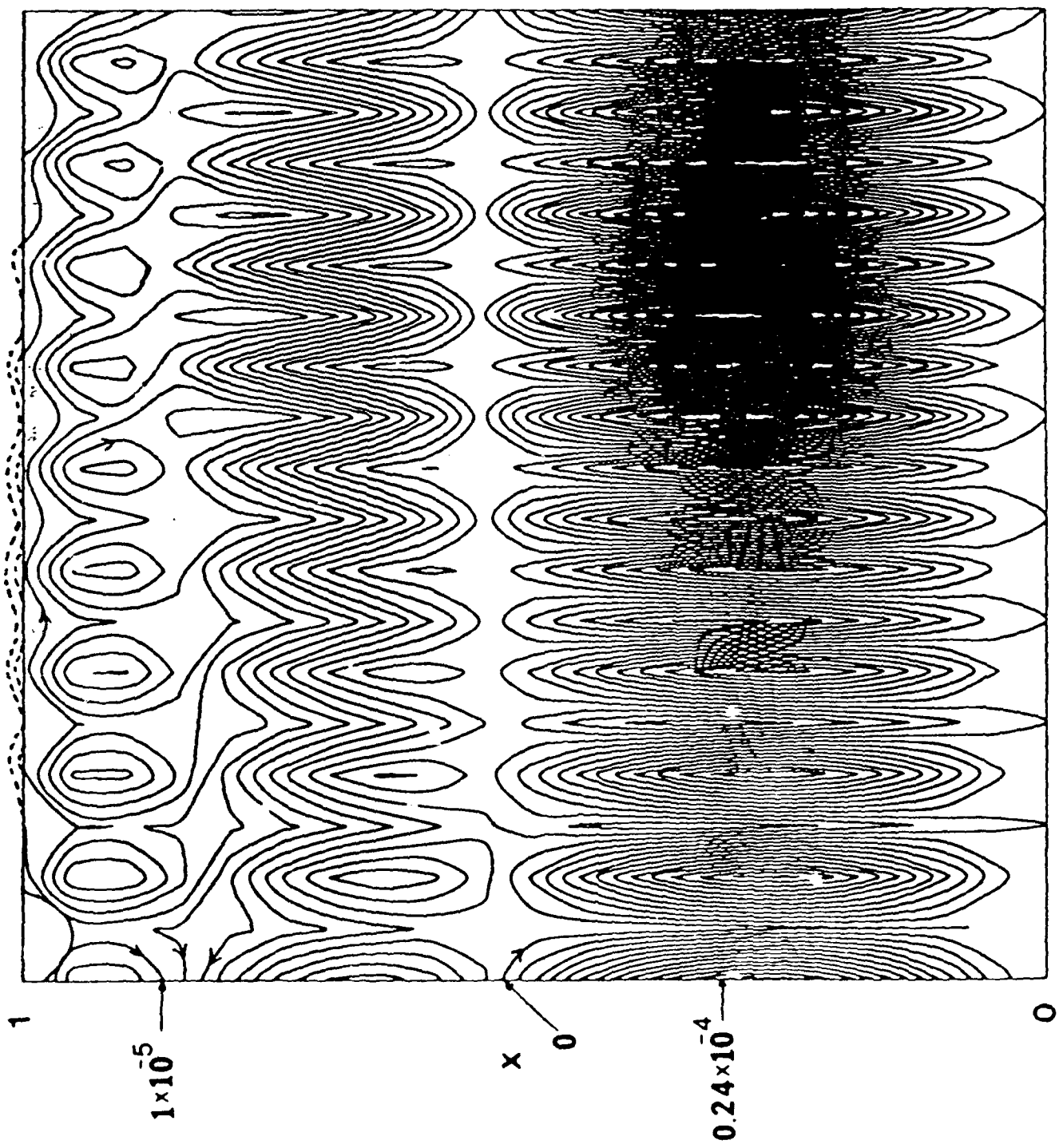


FIG. 1(b)

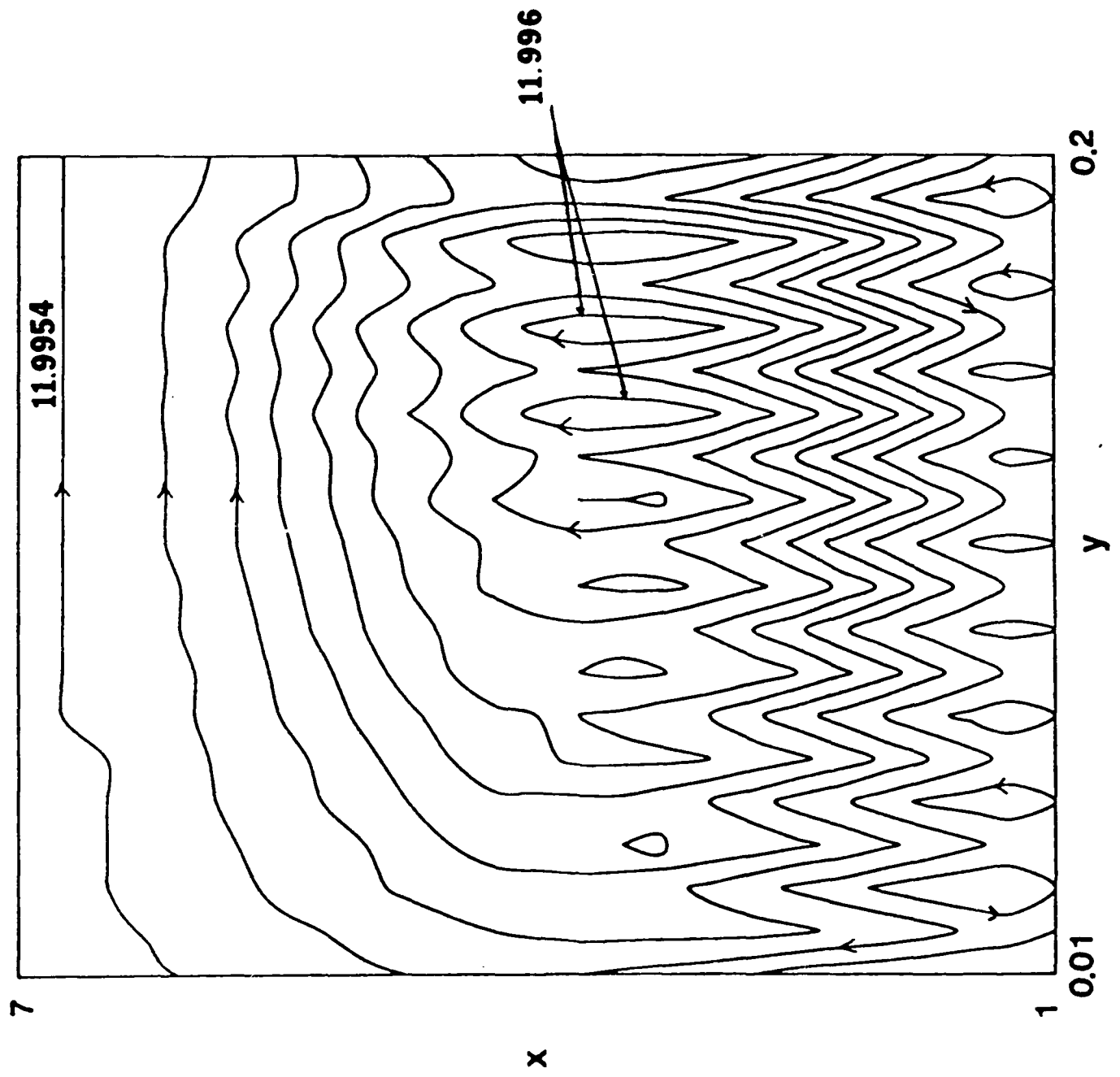


FIG. 2 (a)

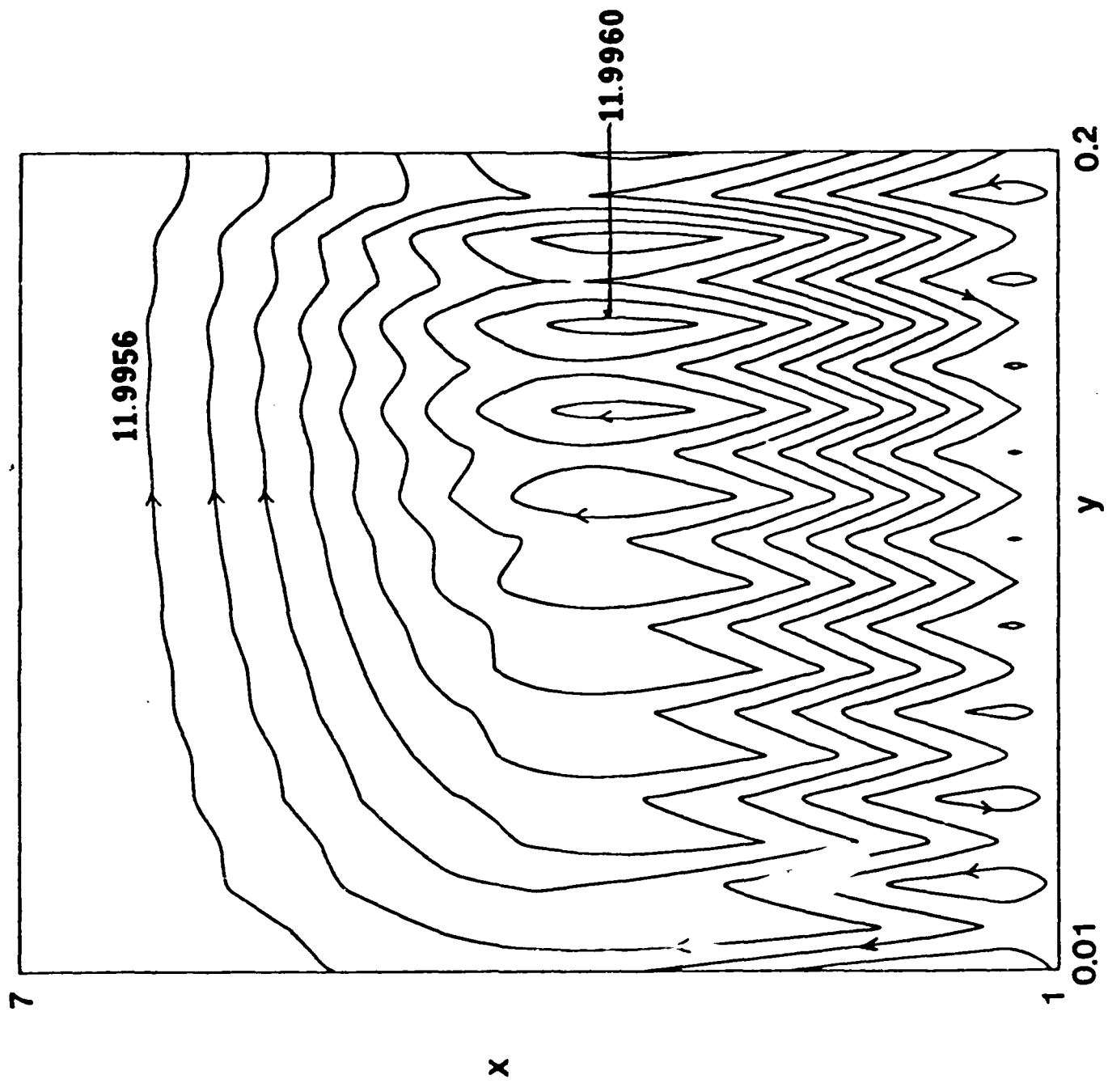
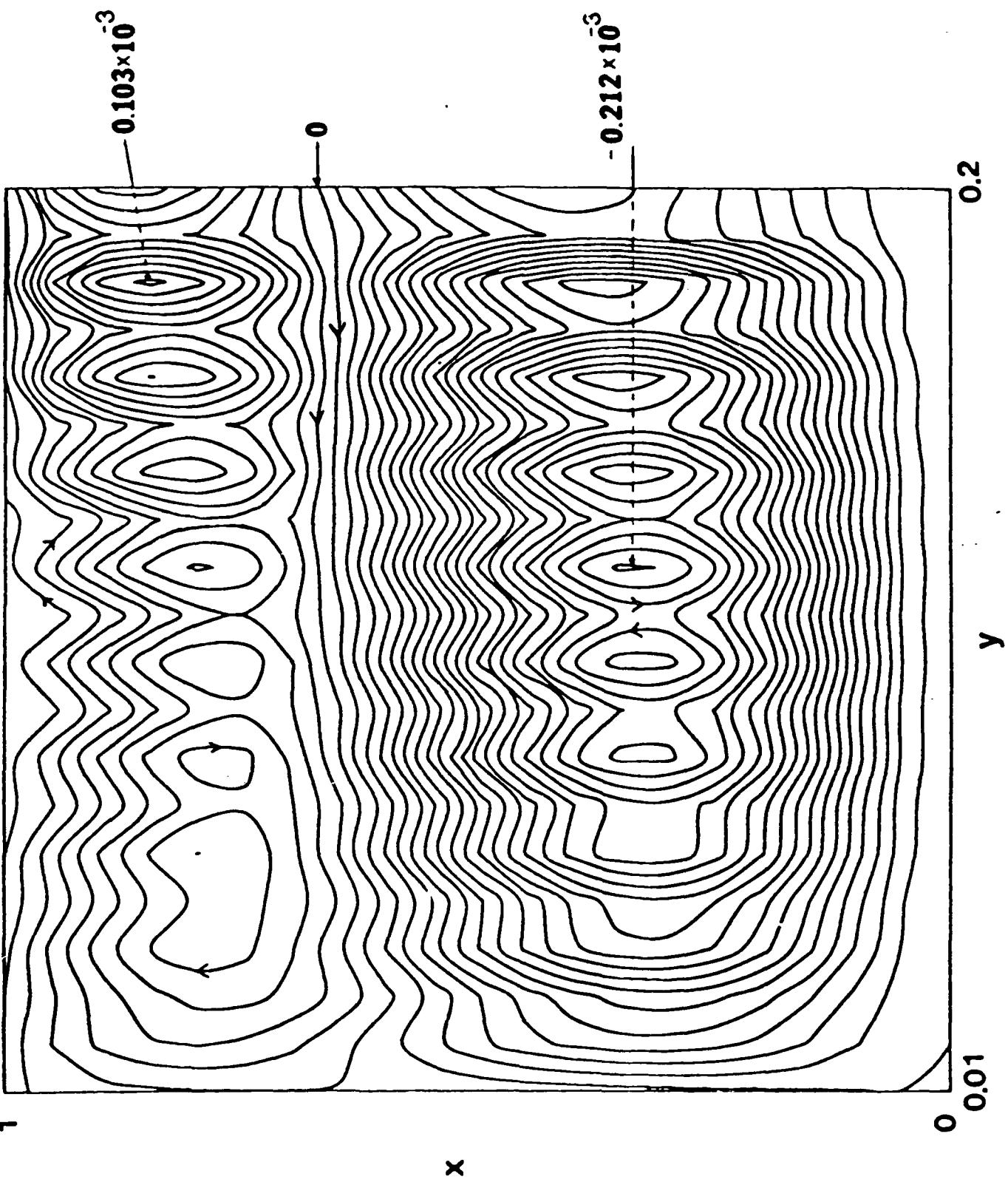


FIG. 2(a)



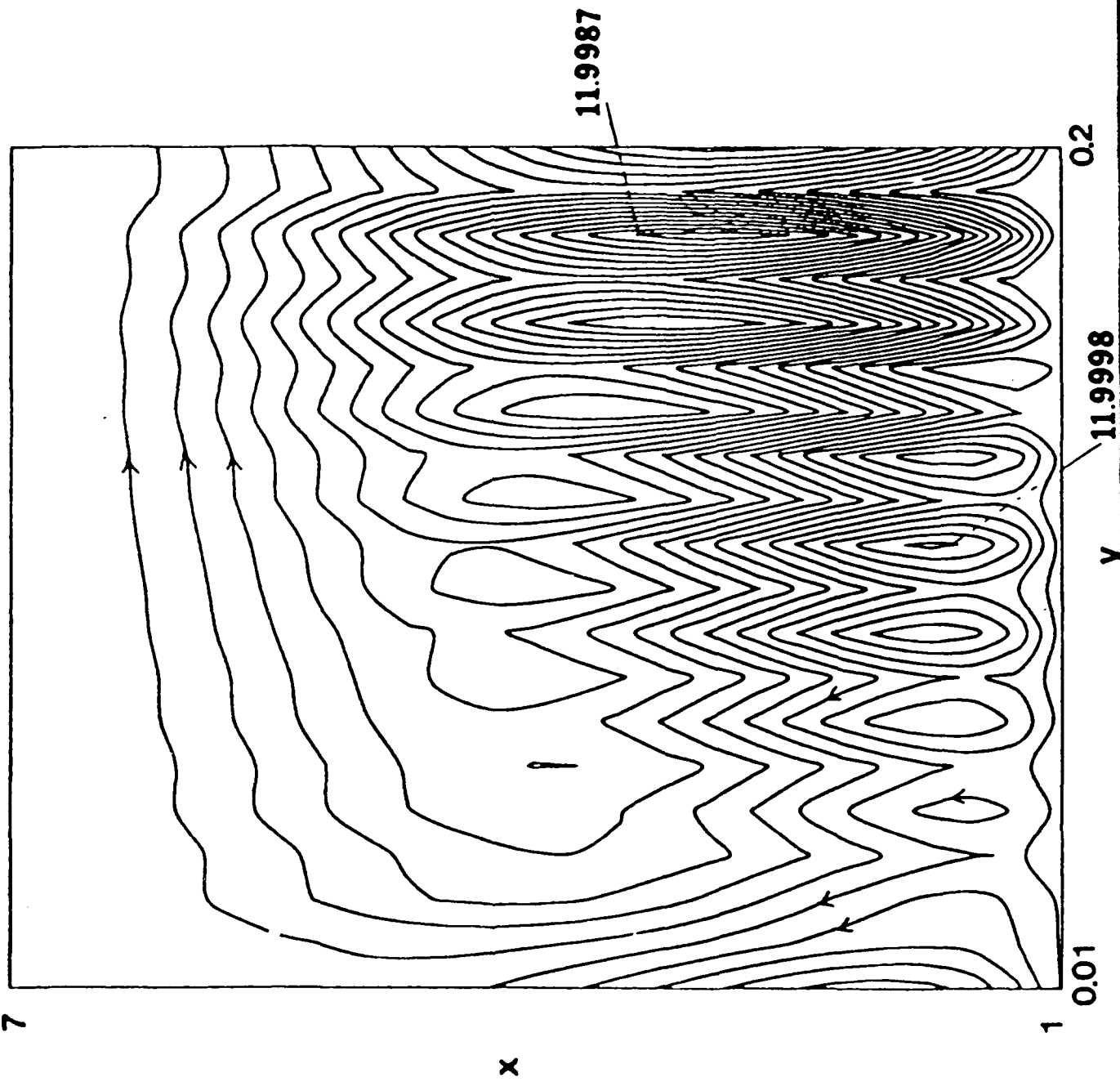
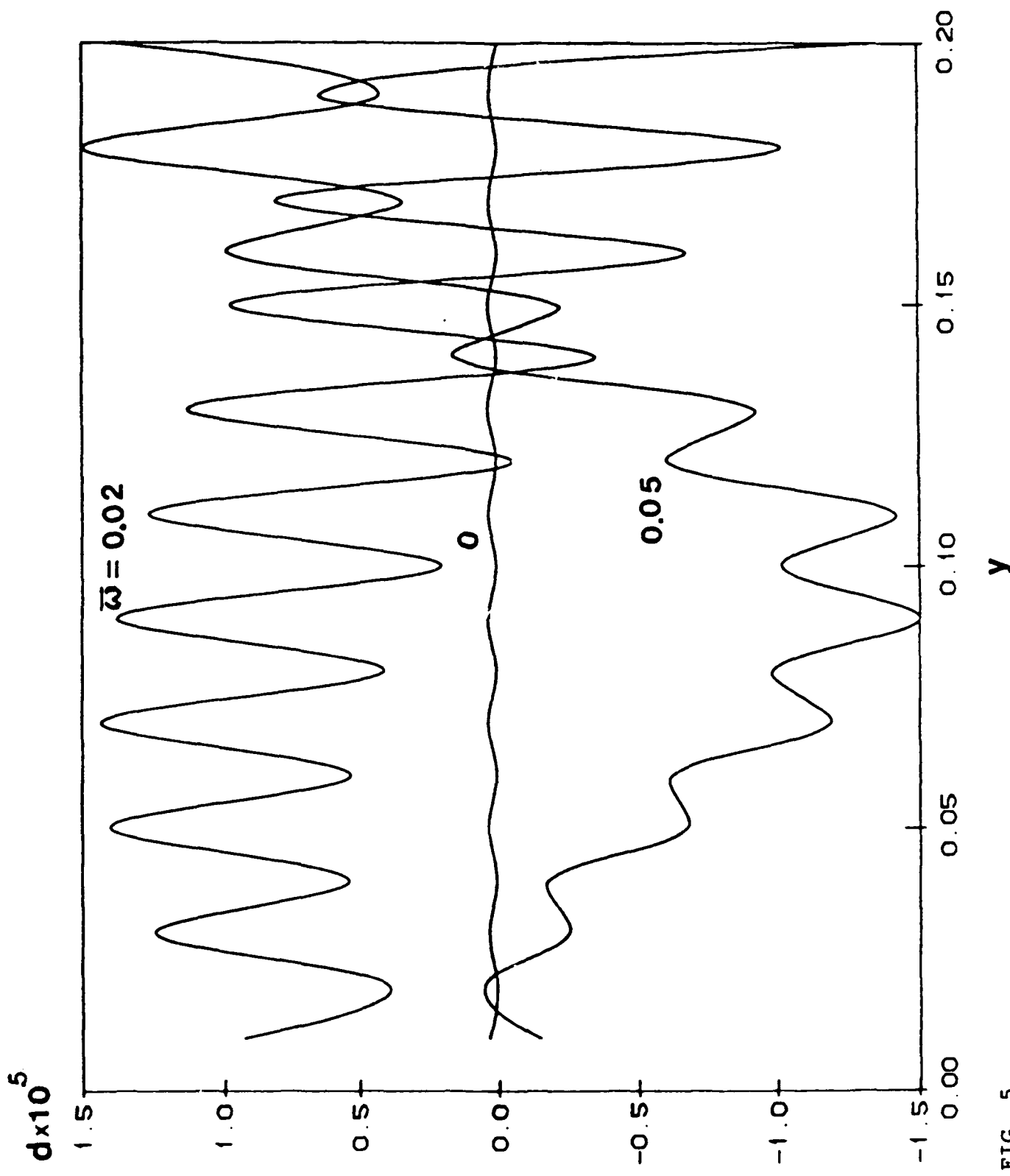


FIG. 4

FIG. 5



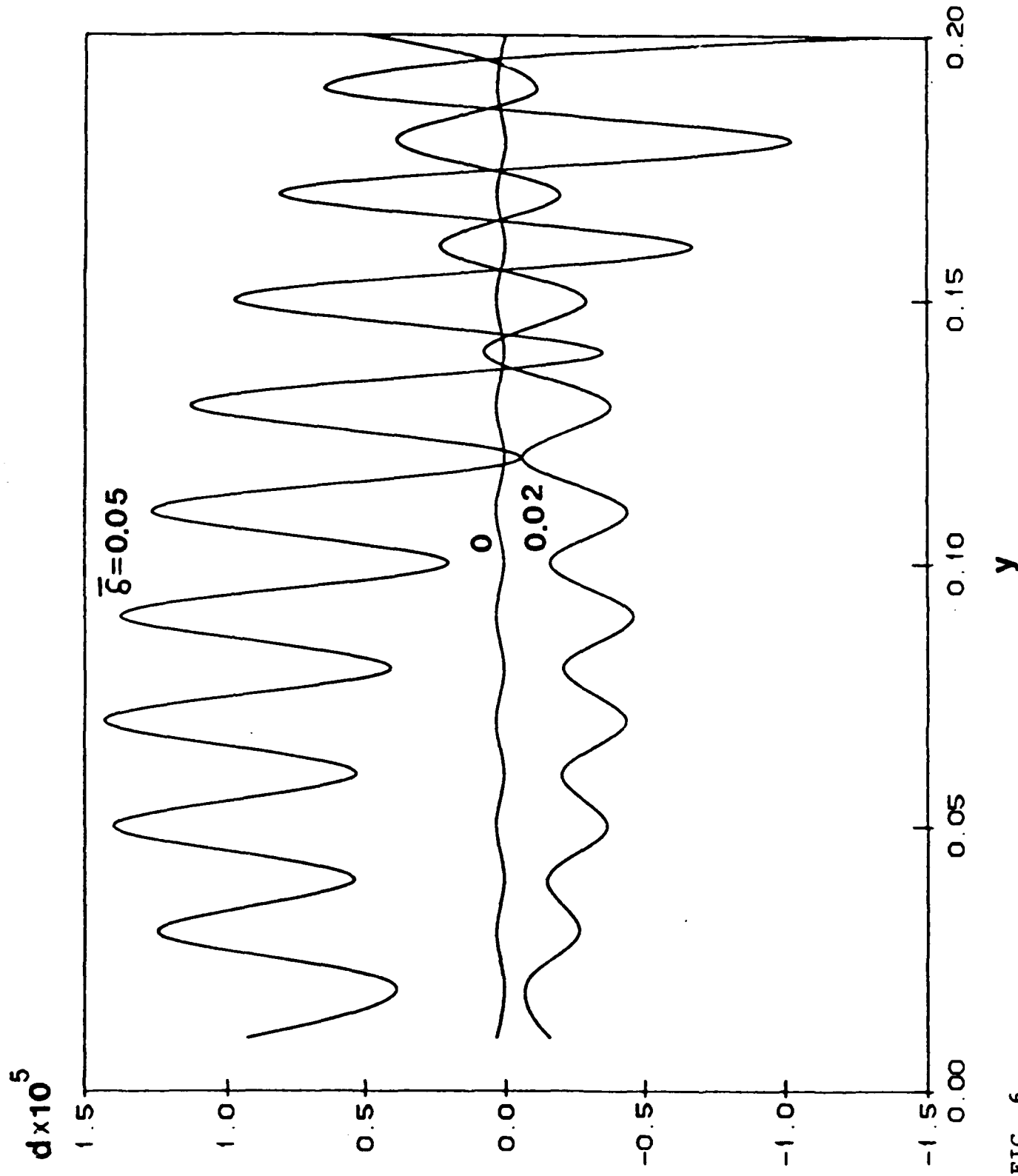


FIG. 6

APPENDIX G

Toward Monodispersed Atomization

The objective of this preliminary test is to demonstrate that the mean diameter of the droplets generated by a jet atomizer can be reduced by imparting an external vibration of sufficiently high frequency near the nozzle exit. The general layout of the experiment is given in Figure D-1.

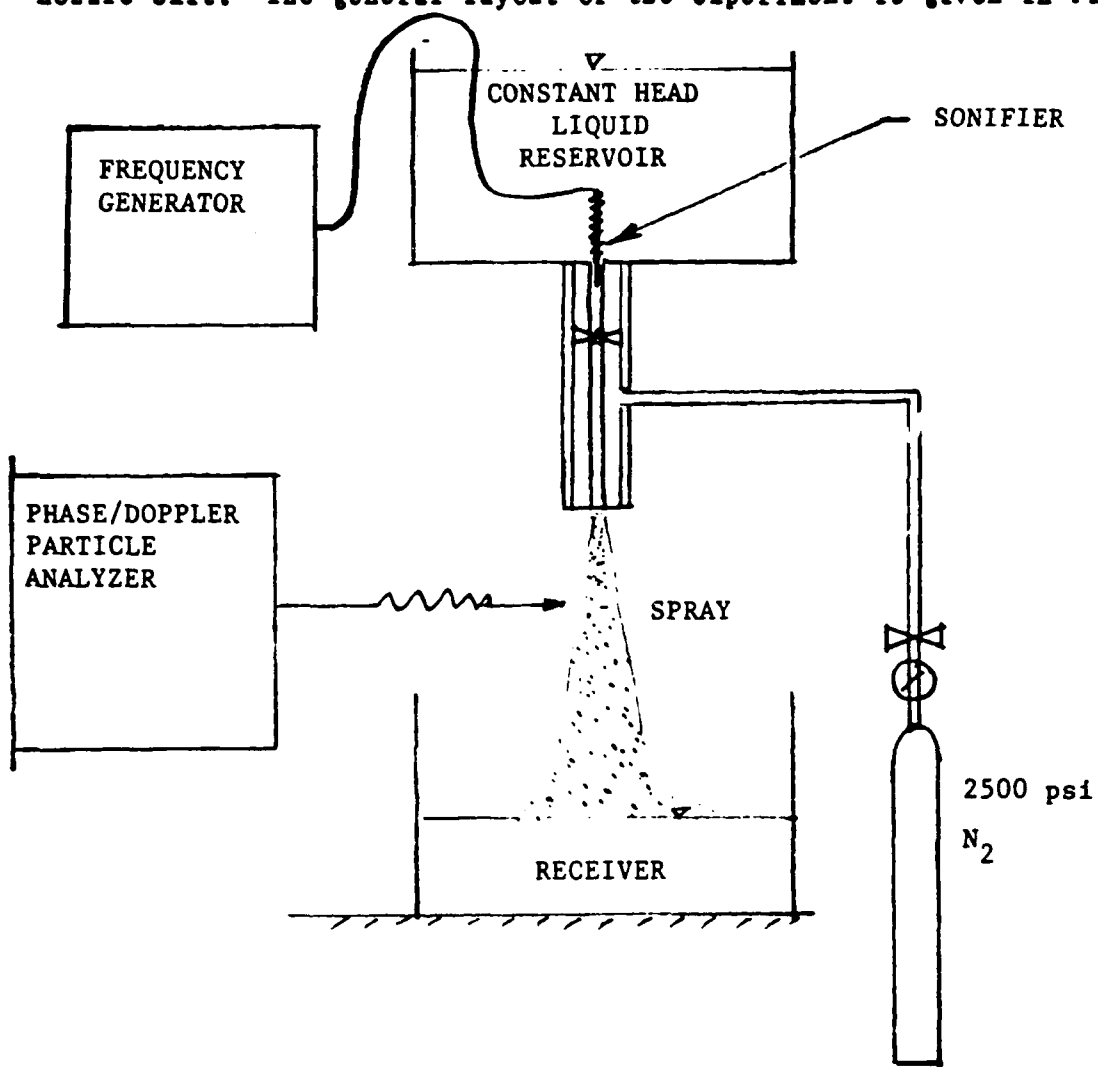


FIGURE D-1

A twin-fluid injector, whose important dimensions are given Figure D-2, is connected to a water reservoir from above. The injector has a side inlet connected to a 2500 psia N₂ canister. When the valves at the canister and the reservoir are opened a spray emanates from the nozzle. The pressure of N₂ entering into the injector is controlled by a pressure gauge. The size distribution and the velocity of the droplet in the spray are measured by use of the Aerometrics Phase/Doppler particle analyzer. The droplets are collected in a receiver on the floor of a hood. In order to demonstrate the effect of an external forcing, a sonifier (Model 185, Branson, Sonic

Power) is inserted into the reservoir and reaches as far as possible into the injector. The sonifier is connected to a variable power frequency generator at 20 kHz_z .

The results for a fixed small volume in the jet without external forcing is given in Figure D-3. The velocity of the water jet is determined by dividing the water discharge rate by the jet cross sectional area. The air velocity is measured with a hot wire at several key points. The average relative velocity of gas-to liquid is found to be approximately 40 M/s. The corresponding capillary length $\delta/\rho_2 U^2$ is calculated to be 38um. The measured arithmetic mean, area mean, volume mean and Sauter mean diameters are 38.8, 42.6, 46.7 and 56.2 um respectively. Thus the droplet sizes do indeed scale to the capillary length as predicted by the theory. The results for the case of external forcing with the sonifier is given in Figure D-4. The arithmetic, area, volume, and Sauter mean diameters are now 33.0, 36.5, 40.3 and 49.1 um respectively. Thus the mean diameter is reduced by approximately 6 um. Moreover, it is seen from the histograms that the most populous droplets diameter is reduced from approximately 30 to 20 um. Note that the external forcing is applied at the nozzle inlet instead of at the outlet which is the ideal place as explained in the main proposal. Consequently the whole reservoir system is set into motion which created unwanted noise. Moreover the introduced frequency is one order of magnitude smaller than the resonant frequency which is hundreds of kHz_z according to the theory. This high frequency will be achieved by use of the piezoelectric crystal described in the main proposal. Despite of these inadequacies, the results of this preliminary test seem to convincingly demonstrate that nearly uniform micron and submicron droplets may be formed by regulating the external forcing at the tip of the atomization nozzle, precisely at the resonant frequency.

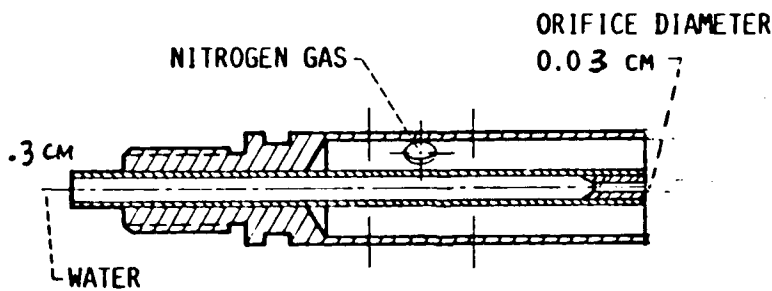


FIGURE D2. - DIAGRAM OF PNEUMATIC TWO-FLUID ATOMIZER.

* CHANNEL 1 SETUP ***** Date: 4 MAY 1988 ** Time: 2:40:06
 ***** USER VARIABLES ***** ***** INSTRUMENT SETUP *****
 A1 Pressure (psi) = 5.000 L1 Collimating Lens Select = 300 mm
 B1 Axial distance (cm) = 2.000 M1 Transmit Lens = 495 mm
 C1 Radial distance (cm) = 0.000 N1 Receiver Aperture = 100 m
 D1 Water(distilled) = 0.000 O1 Collection Angle = +/- 30
 ***** Velocity Settings ***** P1 High Voltage = 310 V
 ***** Velocity Settings ***** ***** Experiment Status *****
 E1 Velocity Offset = 5.00 m/s Q1 Diameter Collection - On
 F1 Velocity Range = 0.39 - 60.81 m/s
 G1 Velocity Minimum = -3.00 m/s
 H1 Velocity Maximum = 70.00 m/s
 Measurement Range = 0.39 - 60.81 m/s
 ***** Diameter Settings ***** Data Drive - C:
 I1 Refractive Index = 1.330 Experiment - LDK
 J1 Diameter Range = 0.8 - 116.7 m U1 Time Out = 0 Seconds
 K1 Diameter Maximum = 120 m U1 Stop Mode = Samples
 Measurement Range = 3.3 - 116.7 m V1 Stop After = 60000 Samples
 ***** ***** ***** ***** ***** ***** ***** *****
 ***** ***** ***** ***** ***** ***** ***** *****

C - DATA ACQUISITION (Run Number: 006, Date: 4 MAY 1988, Time: 2:40:06)

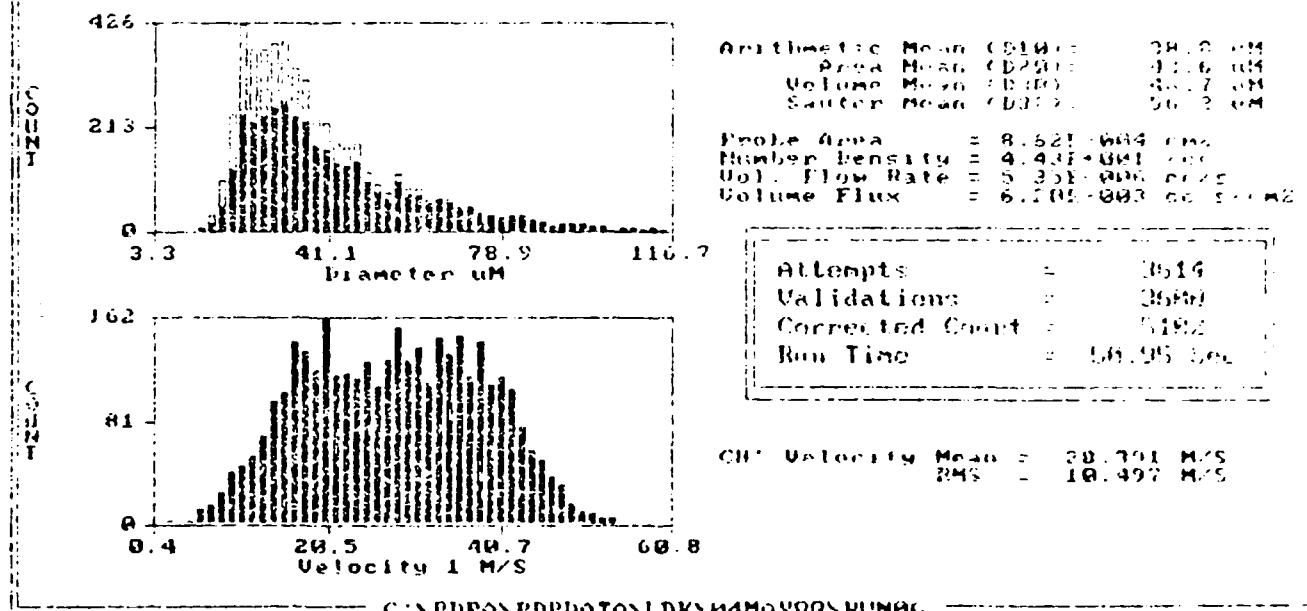
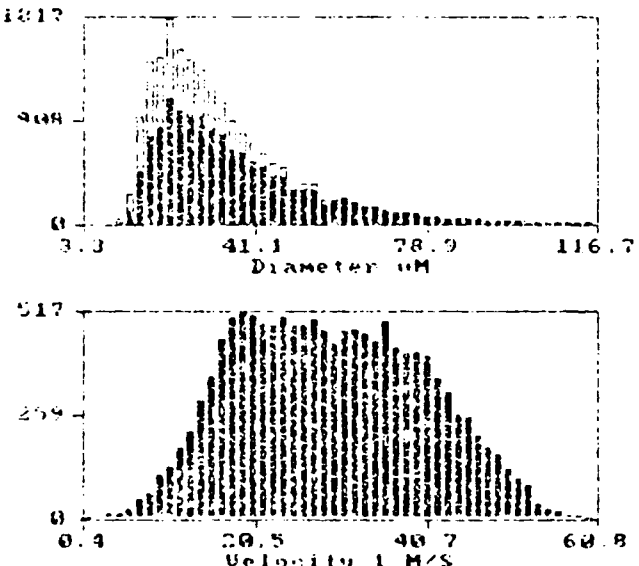


FIGURE D-3

* CHANNEL 1 SETUP ***** Date: 4 MAY 1988 ** Time: 2:46:49
 ***** USER VARIABLES ***** ***** INSTRUMENT SETUP *****
 A1 Pressure (psi) = 5.000 L1 Collimating Lens Select = 300 mm
 B1 Axial distance (cm) = 2.000 M1 Transmit Lens = 495 mm
 C1 Radial distance (cm) = 0.000 N1 Receiver Aperture = 100 m
 D1 Water(distilled) = 0.000 O1 Collection Angle = +/- 30
 ***** Velocity Settings ***** P1 High Voltage = 327 V
 ***** Experiment Status *****
 E1 Velocity Offset = 5.00 m/s Q1 Diameter Collection = On
 F1 Velocity Range = 0.39 - 60.81 m/s
 G1 Velocity Minimum = -3.00 m/s
 H1 Velocity Maximum = 70.00 m/s
 Measurement Range = 0.39 - 60.81 m/s Data Drive = C:
 ***** Diameter Settings ***** Experiment = LDK
 I1 Refractive Index = 1.330 Test = 04MAY88
 Run Number = 03
 J1 Diameter Range = 0.8 - 116.7 m T1 Time Out = 0 Seconds
 K1 Diameter Maximum = 120 m U1 Stop Mode = Samples
 Measurement Range = 3.3 - 116.7 m V1 Stop After = 60000 Samples
 ***** ***** ***** ***** ***** ***** ***** ***** ***** *****
 ***** DATA ACQUISITION ***** Date: 4 MAY 1988 Time: 2:46:49
 1813



Arithmetic Mean (D1R1) = 33.42 μm
 Area Mean (D2R2) = 36.16 μm
 Volume Mean (D3R3) = 36.12 μm
 Sauter Mean (D3S3) = 43.1 μm
 Probe Area = 8.90E-004 cm^2
 Net Density = 9.75E-002 cm^{-3}
 Volume Flow Rate = 8.12E-006 cm^3/s
 Volume Flux = 9.13E-007 cm^3/s

Attempts	= 13497
Validations	= 12445
Corrected Count	= 19486
Run Time	= 01.23 Sec

C1 Velocity Mean = 29.502 m/s
 RMS = 11.092 m/s

C:\SPDP\PPDP\DATA\LDK\04MAY03N\RUN03

FIGURE D-4

Appendix H. Letters of Confirmation



AEROSOL SCIENCE AND TECHNOLOGY

THE JOURNAL OF THE AMERICAN ASSOCIATION FOR AEROSOL RESEARCH

Editors-in-Chief

BENJAMIN Y. H. LIU
Mechanical Engineering Department
University of Minnesota
111 Church Street S.E.
Minneapolis, MN 55455

DAVID T. SHAW
Laboratory for Power and Environmental Studies
State University of New York at Buffalo
330 Bonner Hall
Buffalo, NY 14260

DAVID S. ENSOR
Center for Aerosol Technology
Research Triangle Institute
P.O. Box 12194
Research Triangle Park, NC 27709

December 28, 1988

Dr. S. P. Lin
Mechanical and Industrial Engineering Dept.
Clarkson University
Potsdam, NY 13676

Dear Dr. Lin:

- We have received your paper, and we thank you for your contribution. The manuscript is being forwarded to our reviewers.
- The Editors are pleased to accept your paper for publication. It is being forwarded to the publisher and is currently planned to appear in Volume 11/#3 publication scheduled in
December 1989.

Your paper is lacking

- original drawings or reproducible (glossy) prints of the illustrations.
 an abstract.
 —additional copies.
 other:

Please forward these items to the Editors directly to the publisher, to the attention of Desk Editorial .

Thank you.

Yours sincerely,

David T. Shaw/br>

JOURNAL OF COLLOID AND INTERFACE SCIENCE

EDITOR: **MILTON KERKER** ASSOCIATE EDITOR: **JOSIP P. KRATOVIL**
CLARKSON UNIVERSITY
POTSDAM, NEW YORK 13676
(315) 268-2390

PUBLISHER:
ACADEMIC PRESS, INC.
MARCOURT BRACE JOVANOVICH BUILDING
1250 SIXTH AVENUE
SAN DIEGO, CALIFORNIA 92101

March 17, 1989

Dr. S. P. Lin
Departmet of Mechanical and Industrial
Engineering
Clarkson University
Potsdam, N Y

RE: MS#7808KR-Navier-Stokes flow for the initial stage of
atomization-Kang and Lin.

Dear Dr. Lin:

This will acknowledge acceptance of the above paper for publication
in the JOURNAL OF COLLOID AND INTERFACE SCIENCE.

Galley proofs will be sent in due course of time.

In order to facilitate the preparation of the index, please complete
the enclosed form and return it to Academic Press in San Diego.
Academic Press will also need a copy of the enclosed copyright form.

Sincerely yours,


Milton Kerker

MK:ld
enc.

PENNSTATE



(814) 865-2519

College of Engineering
Department of Mechanical Engineering

208 Mechanical Engineering
The Pennsylvania State University
University Park, PA 16802

February 3, 1989

Mr. William O'Connor
American Institute
of Aeronautics and Astronautics
370 L'Enfant Promenade, SW
Washington, DC 20024-2518

Dear Mr. O'Connor:

Yesterday, I sent you the entire file and the final revised manuscript for Professor S. P. Lin's paper (J17146) with a recommendation for publication as a full paper. Today, I received a corrected version of page 14 with some necessary changes in the ACKNOWLEDGMENT section. Please replace page 14 of the earlier version that was sent to you on February 2 with the attached corrected page 14. I hope this does not cause too much inconvenience for you. Thank you very much.

Sincerely yours,

Kenneth K. Kuo
Associate Editor
Distinguished Alumni Professor
of Mechanical Engineering

KKK/mjc

Attachments

cc: ✓ Professor S. P. Lin, Clarkson University



OFFICE OF THE UNDER SECRETARY OF DEFENSE

WASHINGTON, D.C. 20301

RESEARCH AND
ENGINEERING

15 April 1986

Professor Sung P. Lin
Dept. of Mechnl & Industrial Eng.
Clarkson University
Potsdam, NY 13676

Dear Professor Lin:

I am pleased to inform you that we have selected your proposal as a basis for support under the Department of Defense-University Research Instrumentation Program for FY 87. Final acceptance of your proposal for participation in this program is contingent on execution of a written agreement with the Army Research Office contracting office which will contact your business office to negotiate an agreement about the costs, starting date, and terms and conditions for the acquisition of the research instrumentation.

Congratulations on your successful proposal and thank you for your interest in the research program of the Department of Defense.

Sincerely,

Leo Young
Leo Young
Director, Research and
Laboratory Management